JPL Quarterly Technical Review

Volume 3 April 1973 Number 1

Papers on:

Chemistry
Electric Fields
Mariner Jupiter/Saturn 1977 Project
Orbits and Trajectories
Planetary Exploration
Solar Cells
Solid-State Physics
Spacecraft Environments
Test Facilities

Abstracts of:

Technical Reports
Technical Memorandums
JPL Quarterly Technical Review
Open Literature Reporting

Jet Propulsion Laboratory/California Institute of Technology

JPL Quarterly Technical Review

Volume 3 April 1973 Number 1

Contents

Bibliography of Current Reporting

JPL Quarterly Technical Review Volume 3, Number 1 April 1973

Index: fluid mechanics, liquid propulsion, test facilities

Operation of Small Rocket Engines in the JPL High-Vacuum Molecular Space Simulator (Molsink)

J. E. Chirivella

Propulsion Division

The feasibility of operating small rocket engines in the JPL Molsink facility has been demonstrated. A 0.44-N (0.1-lbf) hydrazine engine and a 0.18-N (0.04-lbf) thruster using cold gas from a hydrazine plenum system were operated for both flight duty cycles and off-nominal conditions. The exhaust gases from these thrusters contain NH_3, N_2, and H_2. The chamber was also calibrated for larger bipropellant engines using nitrogen tetroxide/monomethyl hydrazine (NTO/MMH). The exhaust products of these engines contain CO_2, CO, N_2, H_2O, and H_2. A mixture of cold gases simulating the engine exhaust was injected through a nozzle under conditions simulating thrust levels up to 26.7 N (6 lbf). Pulsing and continuous operations were investigated. The chamber background pressure traces were compared with the traces obtained for the same thrusters operated with pure nitrogen at approximately equivalent thrust. Satisfactory recuperation times were encountered in all the pulsing modes. Test times greater than 20 s were obtained in steady state operation before the vacuum chamber back pressure climbed to prohibitive values.

Introduction

There are many altitude chambers for small rocket engine testing that are able to maintain a sufficiently low pressure to make meaningful measurements of engine vacuum performance parameters. However, the pumping capability of these facilities is not adequate to maintain a sufficiently low vacuum to allow a rocket exhaust plume to expand as it would in space, thus allowing the study of plume behavior. The JPL Molsink facility, because of its characteristic design and cryosorption pumping features, provides an extremely low recirculation of gases, along with background pressures as low as 10^{-10} N/m^2 (10^{-12} torr). The chamber has demonstrated the capability to maintain 1.33×10^{-4} N/m^2 (10^{-6} torr) during firings of catalytic hydrazine thrusters up to 0.44 N (0.1 lbf). The promising results obtained in various plume tests using these types of engines in the Molsink led JPL personnel to consider the operation of small bipropellant engines in the Molsink. In order to obtain an estimate of the response of the chamber parameters to such a

test, the chamber was calibrated for monomethylhydrazine (CN_2H_6) and nitrogen tetroxide (N_2O_4) bipropellant systems for thrust levels as high as 26.7 N (6 lbf). The calibration was brought about by simulating the exhaust with a cold gas mixture and injecting it through a nozzle located inside the chamber. The chamber was provided with a pressure ionization gauge, and the trace of the gauge was recorded and compared with the trace obtained when pure nitrogen was substituted for the cold gas mixture.

This article describes some of the features of the facility pertinent to the type of operation described above, the hydrazine engine tests, some peculiarities observed during the firing, and the calibration of small bipropellant engines. No problems were encountered during the pulsing mode calibration, and test times of about 20 s were encountered for steady state operation, before the Molsink chamber back-pressure diverged from nominal operating conditions.

Cryosorption Pumping in the Molsink Facility

The Molsink is an ultra-high-vacuum facility constructed of three concentric chambers. The innermost chamber is a sphere approximately 3 m (10 ft) in diameter and during normal operations is maintained at a temperature between 10 and 150 K with gaseous helium. The inner walls are wedge-shaped, resembling an anechoic chamber with a total surface area of 200 m^2 (2000 ft^2), and are made of aluminum. The gases are trapped by condensation on this cold wall, the "molecular trap," except for hydrogen and helium, which have a condensation point below the wall temperature. The cryopumping capacity of the chamber is limited to its helium refrigerator reserve capacity of 500 W. Hydrogen and helium can, however, be cryopumped by sorption. The technique of cryosorption pumping (see Refs. 1 and 2) consists of coating a surface with a layer of a material with a great affinity for hydrogen and helium. These gases are absorbed on the coating material. The phenomenon of cryosorption may take place also if the coating material is injected into the chamber simultaneously and/or in the same mixture with hydrogen and helium.

During rocket engine operation, the thruster is located near the top of the chamber on the chamber axis and is firing downward. In this manner, a greater cryotrapping efficiency is obtained, and all the chamber maintains axial symmetry. A view of the Molsink chamber is shown in Fig. 1, and further details on its operation can be found in Refs. 3–5.

Instrumentation

The instrumentation pertinent to this article consists of a Varian Milli-Torr Gauge. The current obtained in this gauge is amplified in the electrometer and the signal displayed on a standard oscilloscope. The response of the electronics is much faster than any significant transient involved in any plume pressure measurement. The gauge is located at the bottom door and is exposed directly to the exhaust gases of the plume (see Fig. 1).

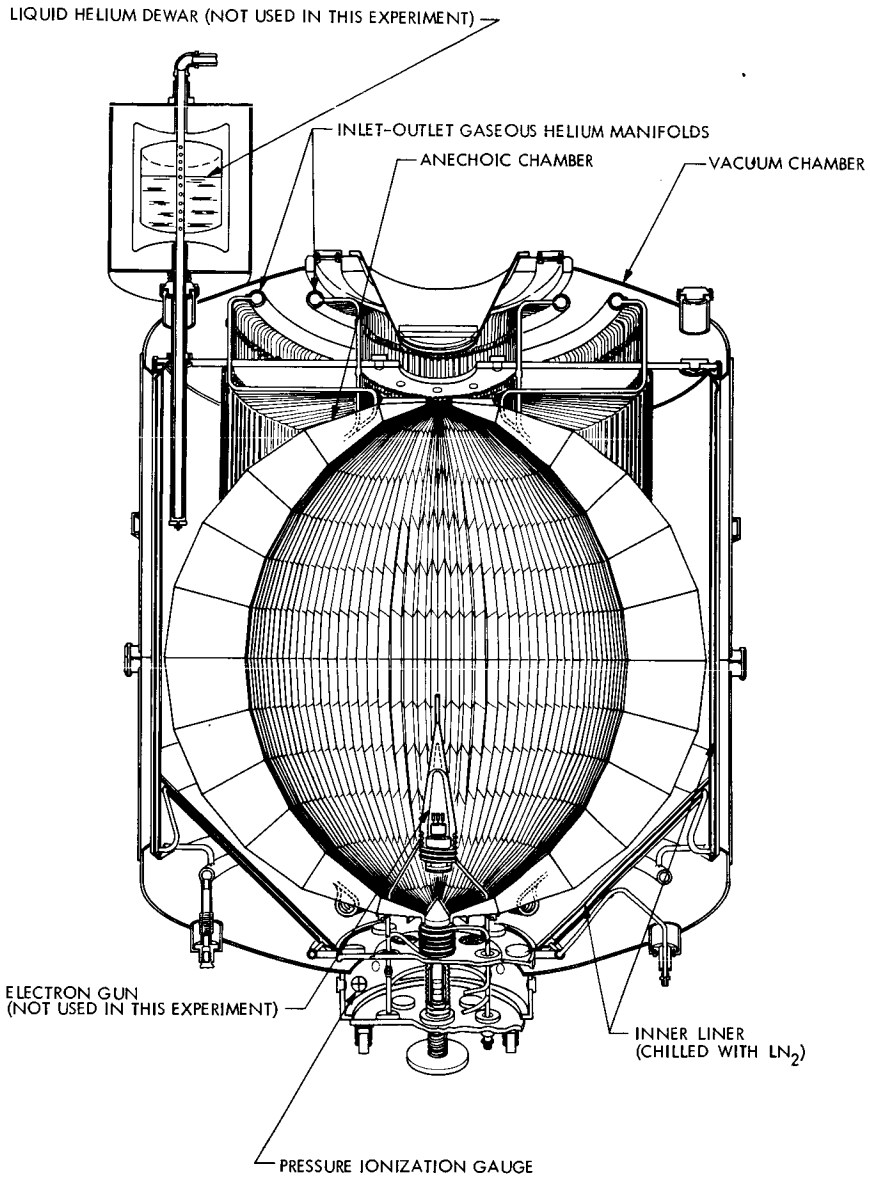

Fig. 1. Molecular sink ultra-high-vacuum chamber

Hydrazine System Tests

Cold Gas Thruster System

The module shown in Fig. 2 was coupled to a gas generator located underneath the module (not shown in the figure) and the cold gas was fed

into the chamber through a thruster TRW Model 35, described in Ref. 2. The thruster was operated at an accelerated duty cycle of 3 pulses of 20 ms/min at a thrust level of 0.18 N (0.04 lbf). The ammonia present in the cold gas cryopumped the hydrogen quite effectively, but after several hours of operation, some small injections of CO_2 through a separate nozzle were necessary to bring the Molsink pressure level back to nominal. After days of operation, the Molsink chamber pressure level was still in the 1.33×10^{-4} N/m^2 (10^{-6} torr) range. The Molsink chamber background pressure recuperation time was determined from a calibration firing conducted at the nominal gas generator conditions of 21°C (70°F) and 23.9×10^4 N/m^2 (34.7 psia), which yields a nominal flow rate of 1.8×10^{-4} kg/s (4×10^{-4} lb/s). This burst was conducted with a mixture simulating the cold gas generator gases. A trace of the pressure recorded on the oscilloscope is given in Fig. 3, together with the trace of the current through the solenoid valve. It can be seen that a recuperation time of less than 20 ms is obtained, if one takes into account some additional delay in the flight time of the gas molecules from the valve to the pressure gauge.

Catalytic Thruster System

The module shown in Fig. 2 injected hydrazine through a 3.17-mm (0.125-in.) tube into a Rocket Research Corporation MR-47, S/N 02, valve–thruster unit. The thrust level of the engine was maintained at 0.44 N (0.1 lbf). Flow control was accomplished by an all-titanium, three-stage Lee Company Viscojet. The thruster was fired in trains of 25 pulses spaced 10 s apart and of 200 ms duration. This was the first time that a hydrazine catalytic thruster was tested in such a high-vacuum space simulator. Figure 4a shows a view of the thruster, and Fig. 4b provides an overall view of the engine and its location with respect to the hardware tested. Visible in the figures are the heaters, insulation, and other components of thermal control. Figure 5 shows a trace from the pressure gauge. The recuperation time appears to be of the order of 2 s; however, in this case the gauge was not directly exposed to the exhaust gases. This could account for the long delay in recuperation. To reinforce the argument, the same figure shows another pressure gauge trace taken immediately after a fresh CO_2 injection in the chamber. As can be seen, the response is about the same as the one that was taken after the CO_2 of the chamber had been saturated with absorbed hydrogen. The chamber background pressure increased after 25 pulses, as Fig. 6 shows, and some injection of CO_2 was necessary to bring the chamber pressure back to normal. A background pressure of 1.33×10^{-4} N/m^2 (10^{-6} torr) was maintained during the test.

Nitrogen Tetroxide/Monomethyl Hydrazine System Tests

Nitrogen tetroxide/monomethyl hydrazine system exhaust products contain CO_2, CO, N_2, H_2, and H_2O. At a combustion chamber pressure of 6.89×10^4 N/m^2 (100 psia) and propellant preinjection temperature about 20°C (68°F), the molar concentration of gases in the plume is approximately 6% CO, 27% H_2O, 11% CO_2, 25% H_2 and 31% N_2. The heat release for this

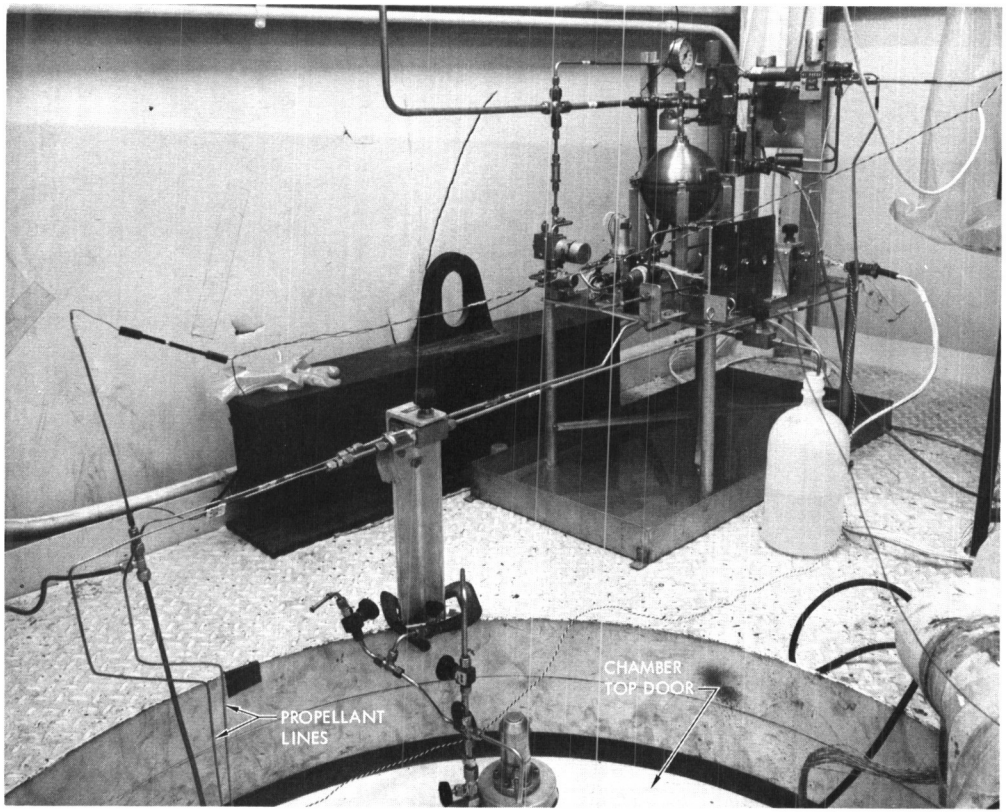

Fig. 2. Propellant feed module (note the compact construction because of limited space available)

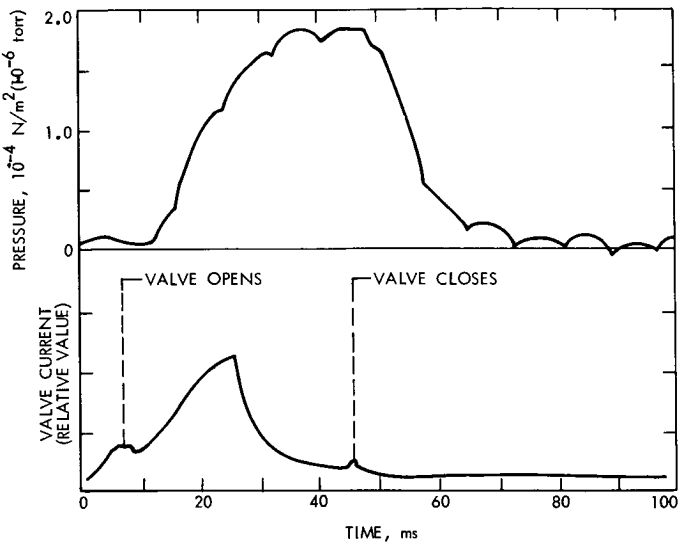

Fig. 3. Molsink chamber pressure gauge trace and solenoid valve current trace

process is about 3.13×10^5 J/kg, and, if a typical 22.19-N (5-lbf) engine is operated under this condition, a flow rate of 72 g/s (0.016 lb/s) may be necessary. Thus if t_1 stands for real time and t_2 for engine *on*-time, and the reserve capacity of the refrigerator is taken at 500 W,

$$\frac{t_1}{t_2} = \frac{75 \times 72 \times 4.18}{500} \approx 45$$

that is, if the *on*-time is a pulse of 100 ms, an *off*-time of 4.5 s is necessary to maintain the temperature of the wall constant. However, if one takes into account (1) the total mass of the aluminum molecular trap, 226.5 kg (500 lb), (2) the fact that the wall temperature can depart 2°C from the nominal one before the facility enters into the divergence condition (operations have to be stopped), and (3) the fact that the heat capacity of the aluminum at cryogenic temperatures as given by the Debye Theory for $T = 8$ K is $c_p = 0.624$ J/kg/K, then it can be seen that the walls can take as much as 280 J from the engine; that is, the *on*-time can be elongated, resulting in

$$\frac{t_1}{t_2} \approx 29$$

This ratio can still be improved, since considerable delays in heat conduction are encountered because of the thermal inertia of the facility.

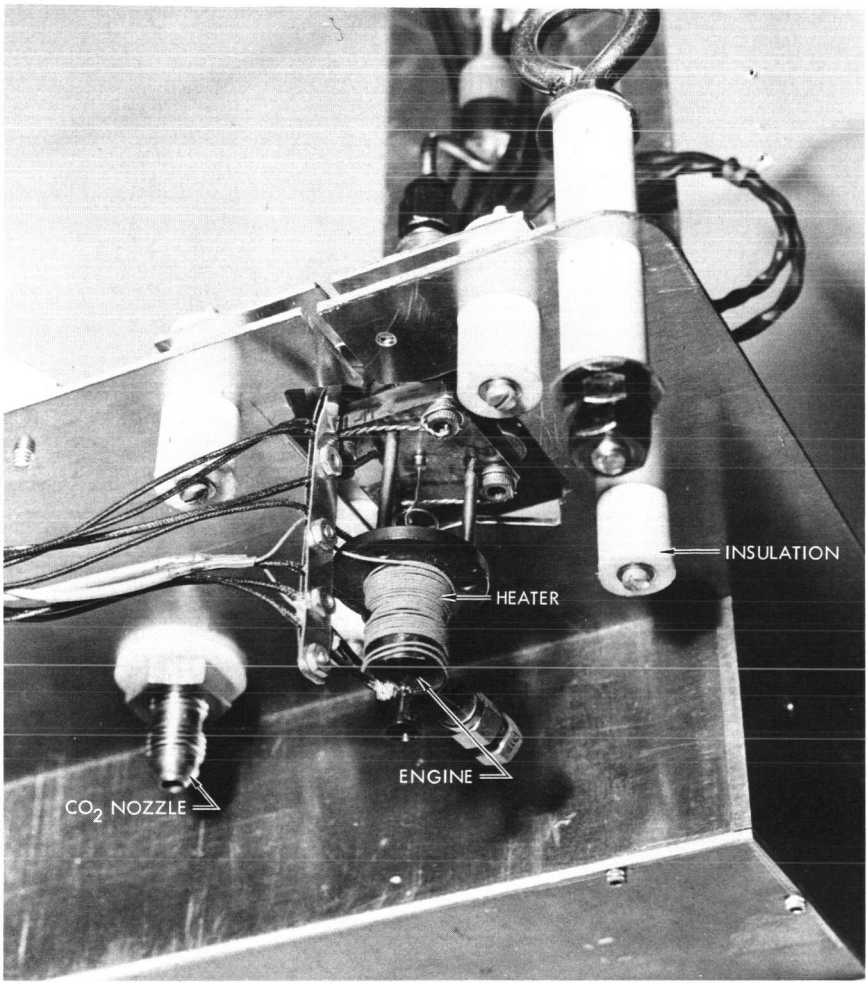

Fig. 4a. The 0.44-N (0.1-lbf) hydrazine thruster and thermal instrumentation

In order to evaluate the Molsink hydrogen pumping performance for larger bipropellant engines, the chamber was equipped with a nozzle. Table 1 indicates the characteristics of this nozzle, and Figs. 7a and 7b illustrate the manner in which it was arranged in the Molsink. An upstream plenum with a volume of 63.5 cm^3 was prepared by trapping the gas between valves A and B. Molsink vacuum was applied as far as valve A. The valve was suddenly opened, and the pressurized gas injected in the chamber through the nozzle.

A gas mixture was prepared with molar concentrations of 9.4% CO, 48.4% N_2, 17.2% CO_2, and 25% H_2. This mixture has an adiabatic index of $\gamma = 1.38$ and a molecular weight of $M = 24.26$, compared with a NTO/MMH system

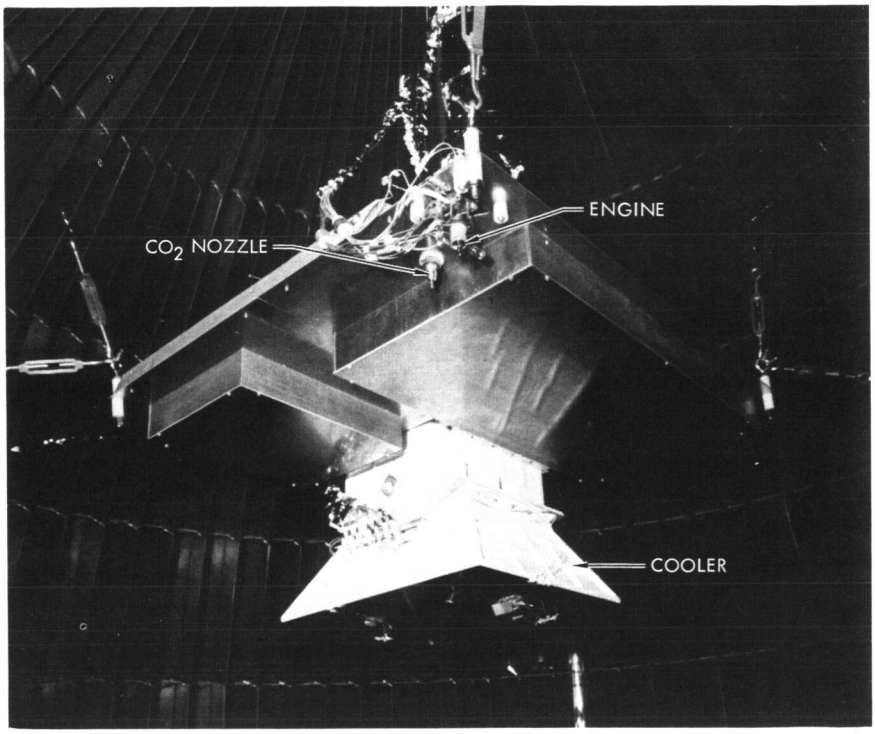

Fig. 4b. General view of engine and other tested hardware in Molsink chamber

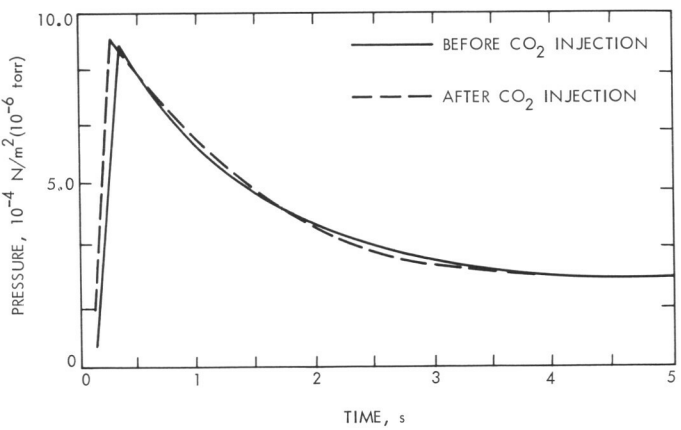

Fig. 5. Molsink chamber pressure traces for 0.44-N (0.1-lbf) hydrazine thruster

Table 1. Characteristics of nozzle used to inject the gas mixture

Nozzle parameter	Value or type
Convergent section half-angle	30 deg
Throat diameter	0.508 cm (0.2 in.)
Radius of wall curvature at throat	0.508 cm (0.2 in.)
Wall contour	Conical
Cone half-angle	25 deg
Exit diameter	1.97 cm (0.775 in.)
Expansion ratio	15
Throat area	0.202 cm^2 (0.031 $in.^2$)
Exit area	3.043 cm^2 (0.471 $in.^2$)

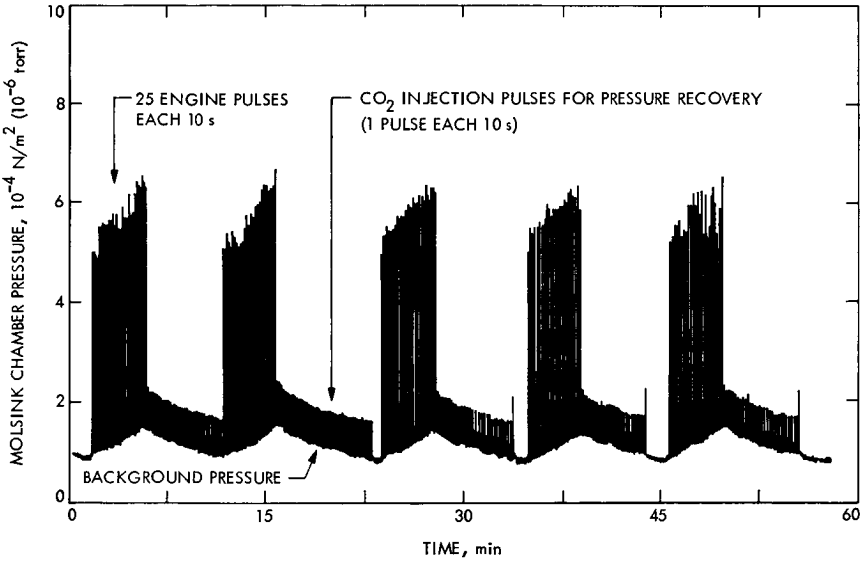

Fig. 6. Molsink chamber pressure recording during engine firing and CO_2 injection

having a γ value of 1.15 and a molecular weight of 20.15. Notice also that although the hydrogen contained is the same (25%), the proportion of nitrogen is higher (48.4% versus 31%). Thus, the results obtained in this mixture will be conservative, since nitrogen frost acts as sorption spoiler.

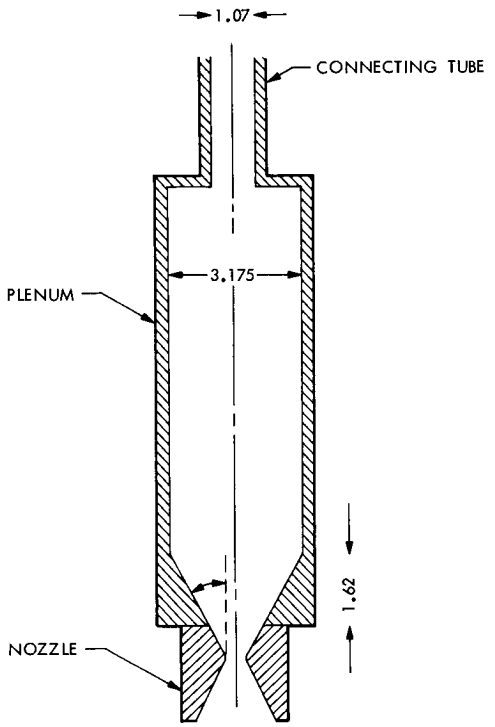

Fig. 7a. Nozzle-plenum assembly installed in the Molsink (all dimensions in centimeters)

The system shown in Figs. 7a and b was pressurized with this mixture, which was injected into the Molsink. The bursts were repeated with pure nitrogen substituted for the mixture at the same upstream plenum pressures. The ionization gauge signals were recorded and compared. A plenum pressure range from 2.39×10^5 N/m^2 (34.7 psia) to 7.9×10^5 N/m^2 (114.7 psia) was explored, which corresponds to thrust levels ranking from 8.87 N (2 lbf) to 27.05 N (6.1 lbf). The chamber could take higher pressure bursts, but the upstream plenum pressure gauge limit was reached and the range explored was considered sufficient. Table 2 summarizes the runs and Fig. 8 shows a comparison of the traces obtained for the mixture and for nitrogen for plenum pressures of 6.78×10^5 N/m^2 (100.1 psia): that is, thrusts of 23.33 N (5.27 lbf) and 24.8 N (5.6 lbf). One can see that both traces are very similar and that the influence on the chamber recuperation time of the presence of hydrogen in the mixture is very small. For the volume tested, the theoretical *on*-time is of the order of 52 ms; however, larger pulses are encountered because of the valve opening history and plenum pressure decay effects.

The chamber was then tested for a steady-state rocket firing. A mixture was prepared in a large plenum and the gases were injected into the

Table 2. Summary of results from engine pulsing mode calibrations

Gas	Upstream plenum pressure, N/m^2 (psia)	Ideal thrust, N (lbf)	Pulse width, ms	Peak of pressure gauge reading, N/m^2	torr
N_2	2.36×10^5 (34.7)	8.66 (1.95)	300	7.3×10^{-3}	5.5×10^{-5}
N_2	4.4×10^5 (64.7)	16.13 (3.63)	300	1.66×10^{-2}	1.25×10^{-4}
N_2	6.8×10^5 (100.1)	24.88 (5.6)	340	2.65×10^{-2}	2.00×10^{-4}
Mixture	2.36×10^5 (34.7)	9.1 (2.05)	280	5.3×10^{-3}	4.0×10^{-5}
Mixture	4.4×10^5 (64.7)	16.97 (3.82)	350	7.95×10^{-3}	6.0×10^{-5}
Mixture	6.78×10^5 (99.7)	23.44 (5.275)	300	1.06×10^{-2}	8.0×10^{-5}
Mixture	7.80×10^5 (114.7)	26.96 (6.068)	300	1.13×10^{-2}	8.6×10^{-5}

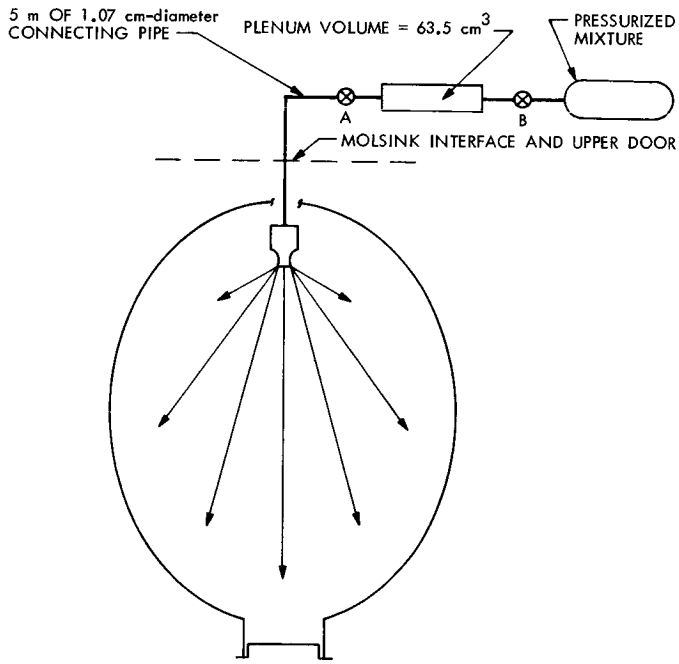

Fig. 7b. General arrangement of the cold gas injection system in the Molsink

chamber in much the same way as before but by maintaining steady flow. The temperature of nozzle, plenum, and gases was around 280 K. Table 3 summarizes the test conditions and the results. It can be seen that the test time is weakly dependent on pressure level, and that, for the worst case, it is larger than 20 s.

Table 3. Summary of results from engine steady-state mode calibrations

Plenum pressure, N/m^2 (psia)	Thrust, N (lbf)	Test time, s	Comments
1.01×10^5 (14.70)	3.42 (0.77)	32	Chamber very enriched in H_2 from previous firings
1.36×10^5 (19.70)	4.62 (1.04)	42	
1.70×10^5 (24.70)	5.77 (1.30)	40	
4.46×10^5 (64.70)	15.19 (3.42)	20	

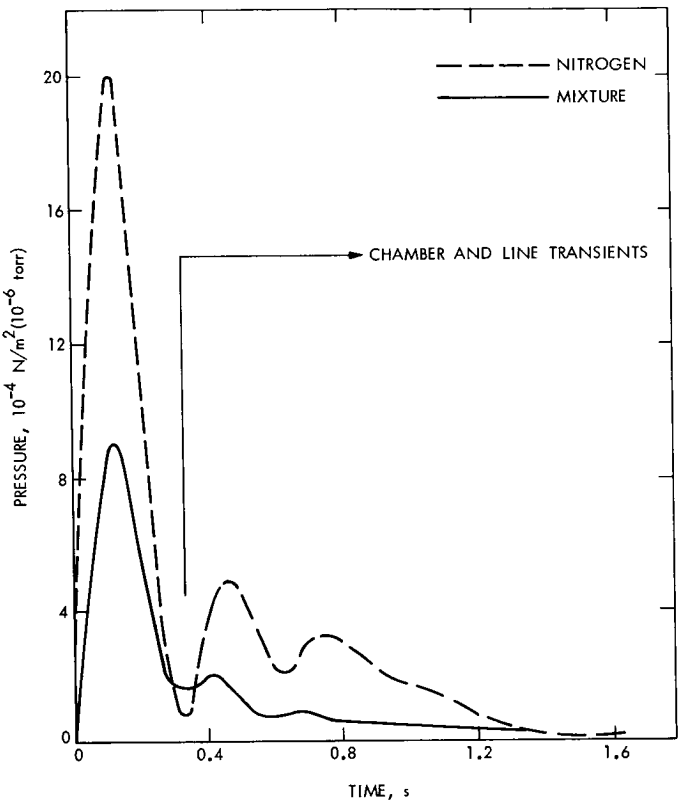

Fig. 8. Comparison of the pressure gauge traces obtained for nitrogen and the calibrating mixture. The plenum pressure for these bursts was 6.78×10^5 N/m^2 (99.7 psia)

Conclusions

The capability of the chamber to maintain space vacuum simulation for nominal flight duty cycles of hydrazine engines up to 0.44 N (0.1 lbf) has been demonstrated. Further, the behavior of the chamber indicated spare capability which may permit testing of still larger engines.

The NTO/MMH engine exhausts, possessing a higher concentration of condensables, provide the chamber with larger cryopumping rates than does the hydrazine engine. Although somewhat smaller sizes would be used with hot NTO/MMH systems, the chamber was able to cope with thrust levels as high as 25.9 N (6 lbf) in the pulsing mode, and as high as 15.19 N (3.5 lbf) in steady-state firings of 20 s.

Acknowledgement

The author wishes to extend his gratitude to Mr. James B. Stephens of the JPL Space Simulation Section and Mr. Philip I. Moynihan of the Liquid Propulsion Section for their continuous and efficient support in the Molsink operations.

References

1. Simon, W., "Nozzle Exhaust Backscatter Experiment Using the JPL Molsink Facility," in *JPL Quarterly Technical Review*, Vol. 1, No. 4, Jet Propulsion Laboratory, Pasadena, Calif., Jan. 1972.

2. Chirivella, J. E., Moynihan, P. I., and Simon W., "Small Rocket Plume Data," in *JPL Quarterly Technical Review*, Vol. 2, No. 2, Jet Propulsion Laboratory, Pasadena, Calif., July 1972.

3. Stephens, J. B., "Spacecraft Mechanism Testing in the Molsink," in *Proceedings of the 4th Aerospace Mechanisms Symposium*, Technical Memorandum 33-425, Jet Propulsion Laboratory, Pasadena, Calif., Jan. 15, 1970.

4. Stephens, J. B., "Molecular Sink," *Research/Development*, July 1967.

5. Stephens, J. B., "Space Molecular Sink Simulator Facility Design," *Journal of Spacecraft and Rockets*, June 1966.

6. Barron, R., *Cryogenic Systems*, McGraw-Hill Book Co., 1966, pp. 27–28.

Index: Mariner Jupiter/Saturn 1977 Project, orbits and trajectories, spacecraft environments and shielding

Saturn Satellite Encounter Opportunities for Mariner Jupiter–Saturn 1977

R. A. Wallace

Mission Analysis Division

The Mariner Jupiter–Saturn mission will allow scientists to collect data from a sophisticated spacecraft flying through the Saturn system some time between November 1980 and September 1981. This opportunity to explore one of our solar system's most complex planet and satellite systems must be planned and designed for, if the mission is to take full advantage of the science value return that is possible. Part of optimizing the Saturn encounter design for science value return will be the search for close satellite encounters. This article investigates the opportunities for close satellite encounters which meet the planetary constraints at Saturn that are imposed by science value return and environmental conditions. Since the satellites travel at various speeds in their orbits, Saturn arrival time is critical and has been chosen as the design parameter. Arrival times are recommended which afford close satellite encounters and also meet important mission constraints. A design chart illustrates the satellite opportunities as a function of Saturn arrival date. Through the use of such a design chart, the Saturn encounter design process, which will take place according to recommendations by the selected science investigators over the next several years, will be considerably streamlined. Potential applications are given to illustrate the use of the Saturn satellite opportunity chart in encounter design.

Introduction

The Mariner Jupiter–Saturn mission to be launched in 1977 will allow scientists to collect data from a sophisticated spacecraft flying through the Saturn system some time between November 1980 and September 1981. This opportunity to explore one of our solar system's most complex planet and satellite systems must be planned and designed for, if the mission is to take advantage of the science value return that is possible. Part of optimizing the Saturn encounter design for science value return will be the search for close satellite encounters. Investigated in this article are the opportunities for close satellite encounters which meet planetary constraints at Saturn imposed by environmental conditions and science value return.

Saturn Encounter Constraints

Encounter constraints considered in this study are:

(1) The range of Saturn arrival dates.

(2) The closest approach radius to Saturn.

(3) Flight outside Saturn's rings.

(4) Earth occultation.

(5) Solar system escape.

These are considered primary constraints, and their application will allow a search for the most favorable satellite encounters. Each of the constraints listed above is discussed below.

Saturn Arrival Date

Since the arrival conditions at Saturn vary with time for Jupiter–Saturn trajectories, a reasonable Saturn arrival date range should be chosen for study. One factor reasonably determines the latest Saturn arrival date: the Project-imposed end-of-funding date for mission operations. The end-of-funding date currently in use is July 1, 1981. Thirty days past encounter has been a generally accepted end-of-mission date. Other factors, such as Saturn solar conjunction (Saturn behind the Sun as viewed from Earth), dictate that Saturn arrival after September 1, 1981, is not probable.

The earliest considered Saturn arrival date is determined by allowable spacecraft mass and the availability of a launch pad. Launch energy requirements and a 30-day launch period impose a 3.5- to 4.0-year flight time to Saturn for the first launched spacecraft of mass near 750 kg. Since only one launch pad will be available, a delay of 11 days is required to prepare for the second launch. To assure launch of the second spacecraft, 12 to 14 possible launch days are required. Coupling this short launch period to the first possible launch date after the first launch results in an earliest Saturn arrival date near November 1, 1980. A reasonable range of Saturn arrival dates to consider, then, is from November 1, 1980, to September 1, 1981.

Closest Approach Radius to Saturn

A fairly arbitrary constraint is chosen for highest acceptable closest approach radius to Saturn, 10 Saturn radii (R_s) or about 600,000 km measured from the center of Saturn.[1] It is not expected that this constraint will be relaxed in the future; any change will probably be in restricting the closest approach radius further. It would seem inefficient to travel for 4 years through hostile space to pass more than twice the Earth–Moon distance from a major target. Of course, consideration for possible multiple satellite encounters at large Saturn distances might be weighed against having received a large and satisfying amount of data from the first arriving

[1] One R_s equals 60,400 km.

spacecraft. For this study, however, a closest approach radius upper limit of $10R_s$ is felt to be reasonable.

Flight Outside Saturn's Rings

A constraint of not flying through the rings of Saturn has been arrived at after discussion among Project personnel and scientific investigators, the hazard of possible catastrophic impact with ring material being the deciding factor. Controversy on the extent of the outer rings dictates the consideration of two ring limits, one conservative, the other standard. Studies conducted in the Environmental Hazards Group at the Jet Propulsion Laboratory indicate that particles large enough for catastrophic impact may exist in the ring plane to a distance of $4R_s$ from the center of Saturn. This estimate is considered conservative and may be relaxed in the future (two Saturn satellites, Janus and Mimas, orbit within this region, commonly designated as the D′ Ring—a hypothesized ring beyond the last visible ring, Ring A). A standard ring limit can be taken as the outer edge of Ring A, given in Ref. 1 as being at $2.28R_s$ (136,450 km).

Earth Occultation

Designing the Saturn encounter in such a way that the spacecraft travels through Saturn's Earth shadow (occultation of the spacecraft by Saturn from the Earth) will allow the study of several important scientific features. For example, radio waves sent from the spacecraft back to Earth and traveling through Saturn's atmosphere just before and after Earth occultation will aid immeasurably in determining the characteristics of the atmosphere of Saturn.

Solar System Escape

If the spacecraft continues to function and can be tracked after Saturn encounter, solar system escape has been listed as a desirable feature in the Saturn encounter design. This characteristic can be assured if the spacecraft's orbit is direct (if its momentum vector is in the same sense as the North ecliptic pole vector) and is in the same sense as the orbits of Saturn's satellites which also follow direct orbits around Saturn.[2]

Method of Analysis

Since Saturn is the last planet to be encountered, no aiming point requirements at Saturn are required for the trajectory to proceed to another planet. Thus if no constraints were imposed on the Saturn encounter design, finding close satellite flybys would be relatively simple, as there would be no Saturn arrival time constraint. The satellites could be encountered at any time during their orbits. The constraints just discussed, however, limit the possible satellite opportunities. Not only is a close satellite flyby desired, but planetary and environmental constraints must also be satisified. Saturn

[2] Phoebe is an exception and travels in a direction opposite to that of the other satellites.

arrival times which provide close satellite flybys and simultaneously satisfy the constraints discussed earlier are the object of this study. Discussed below is a tool which allows consideration of the satellite encounter and constraints imposed by the planetary encounter on the trajectory. After this discussion, the application of the tool is illustrated and simulation used in the analysis is discussed.

B-Plane Discussion

The B-plane is a useful mathematical tool borrowed from nuclear scattering theory. The B-plane itself is the plane perpendicular to the incoming hyperbolic trajectory asymptote, with the **B**-vector being the vector in the B-plane from the planet center to the intersection of the asymptote vector with the B-plane. Figure 1 illustrates this concept. The usefulness of the B-plane concept for the present study is that the encounter constraints discussed can all be represented in the B-plane, along with all possible encounter trajectories. When a B-plane mapping is viewed, every point represents an encounter trajectory, and constraint regions associated with these encounter trajectories can be shown. By mapping the satellite orbits onto the B-plane with their time-positions,[3] close satellite encounter opportunities which also satisfy the encounter constraints can be found.

Application of Constraints to B-plane

Figure 2 illustrates the application of constraints 2 through 5, discussed previously, to a typical Jupiter–Saturn trajectory. Constraint 1, the Saturn arrival date, changes the form of the constraint regions slowly; very little change occurs within a week or two of the arrival date for which the B-plane plot was generated. Changes warranting additional B-plane plots occur, however, within 45 to 60 days of the arrival date.

Each point (an aiming point) on the B-plane of Fig. 2 represents an encounter trajectory. If a particular aiming point lies within a constraint region, then the trajectory associated with the aiming point will satisfy that region's constraint. Several observations concerning Fig. 2 should be noted:

(1) By the application of the constraints discussed, a closed preferred aiming point zone becomes evident and is indicated on Fig. 2.

(2) The satellite orbits map onto the B-plane in, at first glance, an unexpected manner. If we note that the points in the B-plane each represent encounter trajectories, the situation will become clearer. Associated with each satellite orbit are two closed aiming point loci, an upper, mushroomed-shaped locus and a lower, elliptically shaped locus. These come about because there are two ways to reach the satellite when it is behind the planet from the approach. These twc ways utilize the gravity-bending of Saturn. Thus trajectories whicl

[3] Satellite ephemerides used in this study were derived from elliptical orbit elements given i Ref. 2.

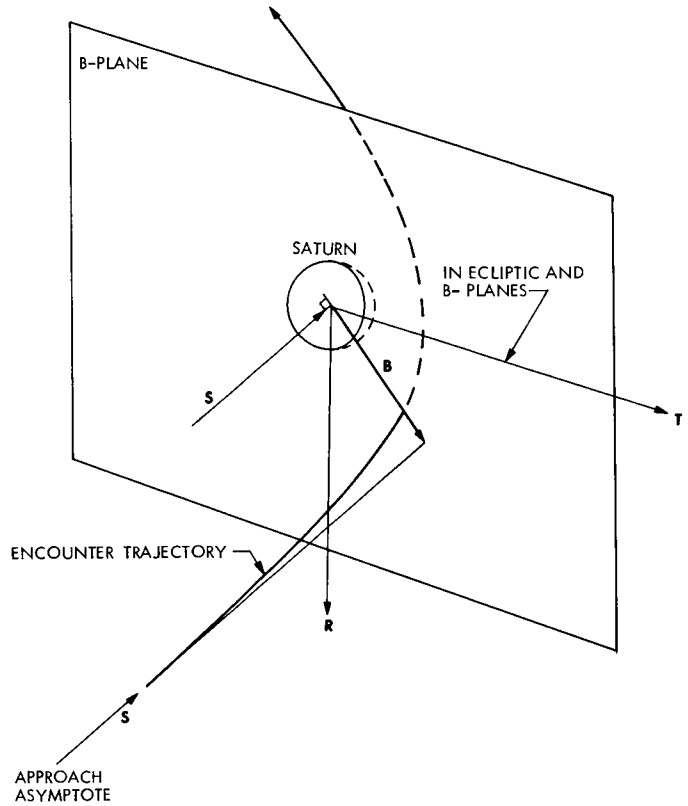

Fig. 1. Illustration of B-plane

encounter a satellite can do so by encountering the satellite before the closest approach to Saturn or by passing over Saturn, bending down, and catching the satellite after closest approach to Saturn. Passing over Saturn to encounter the satellite or catching the satellite prior to closest approach to Saturn are methods that provide trajectories whose aiming points describe the upper, mushroom-shaped locus. Trajectories passing under Saturn and encountering the satellite after closest approach to Saturn have aiming points which describe the lower, elliptically shaped locus (see the explanatory diagrams in Fig. 2).

(3) The satellite aiming points move through the preferred aiming point zone with time in a nonlinear manner, but do so predictably, as shown in such figures as Fig. 2. Thus one can see that because the satellite aiming points move through the preferred aiming point zone quickly, the Saturn arrival time is critical in determining a satellite encounter opportunity. The trajectory should be designed so that the spacecraft arrives at Saturn when the satellite can be encountered

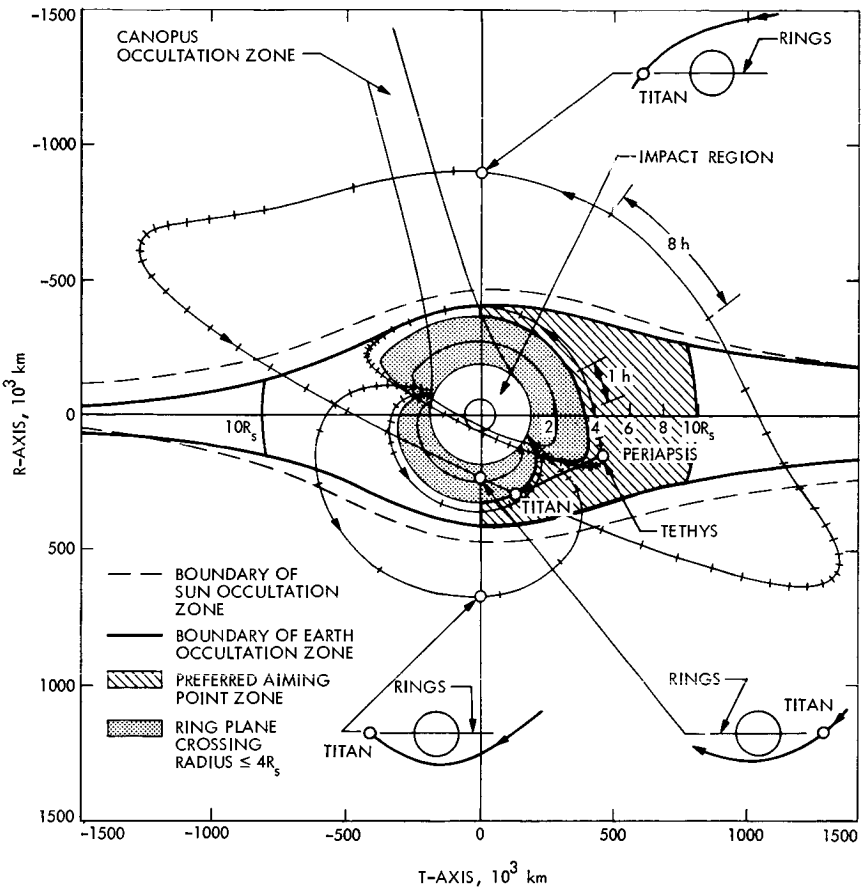

Fig. 2. Saturn B-plane mapping for Saturn arrival date of April 21, 1981

and the mission can still meet the planetary and environmental constraints.

Simulation

By generating B-plane mappings for the Jupiter–Saturn trajectories of interest, one can determine the satellite encounter trajectories which also satisfy the planetary and environmental constraints. The goal of the present study is to provide Saturn arrival dates which allow satellite encounters. Only trajectories from Earth to Jupiter to Saturn, with Saturn arrival dates between November 1980 and September 1981, were considered, this being consistent with the first constraint previously discussed. The trajectory conditions on the approach asymptote were taken from precision-integrated trajectory simulations. Rather than generate a multitude of B-plane plots for each satellite for intervals of every week, a computer program was

produced to fit a number of B-plane plots (six or more for each satellite) covering the Saturn arrival date range. Using this computer program, the arrival times were found when the satellite encounter resulted in satisfying the desired planetary and environmental constraints. The data thus generated were then spot-checked with additional B-plane plots. Encounter times when the aiming point left or entered a constraint region were found to agree with the fitted data to within an hour or less, and time durations within the preferred aiming point regions agreed to within 3%. This sort of accuracy is quite satisfactory for the preliminary searching that the resulting data will be used for.

One Earth launch date—August 25, 1977—was used for all simulations. No noticeable difference in the B-plane mappings could be discerned when they were checked with simulations using August 17, 1977, or September 21, 1977, as launch dates.

Saturn has ten major satellites; all but three were studied for encounter opportunities. Janus and Mimas (both within the D′ Ring region) and Phoebe (the farthest from Saturn at $215R_s$ with a period of 550 Earth days and a retrograde inclination of 150 deg) were not chosen for study.

Throughout this study the satellites were assumed to be massless. When a particular satellite opportunity is chosen for more detailed study, the effect of satellite mass should be considered—especially for a multiple satellite encounter.

Mariner Jupiter–Saturn 1977 Satellite Opportunities

By following the procedure just outlined, Saturn satellite opportunities as a function of Saturn arrival time have been generated for Saturn arrival dates between November 1980 and September 1981. Figure 3 is an example of a 30-day Saturn arrival date period when satellite encounters that satisfy the planetary and environmental constraints are available. The darkened periods denote the arrival times when the aiming points lie in the preferred aiming point region. The outlined, but undarkened, associated periods are the arrival times when the satellite aiming points result in encounter trajectories that extend through the D′ Ring region. The lower periods are for the lower, elliptically shaped satellite locus in the B-plane, and the upper periods, for the upper, mushroom-shaped satellite aiming point locus.

Potential applications of Saturn satellite opportunity charts such as Fig. 3 can be significant to mission design. Four such applications will be discussed below, and Saturn encounter designs will be shown to illustrate them.

Integration of Jupiter and Saturn Satellite Opportunities

Because one arrival date at either Jupiter or Saturn fixes the arrival date at the other planet for ballistic trajectories, satellite opportunity charts for

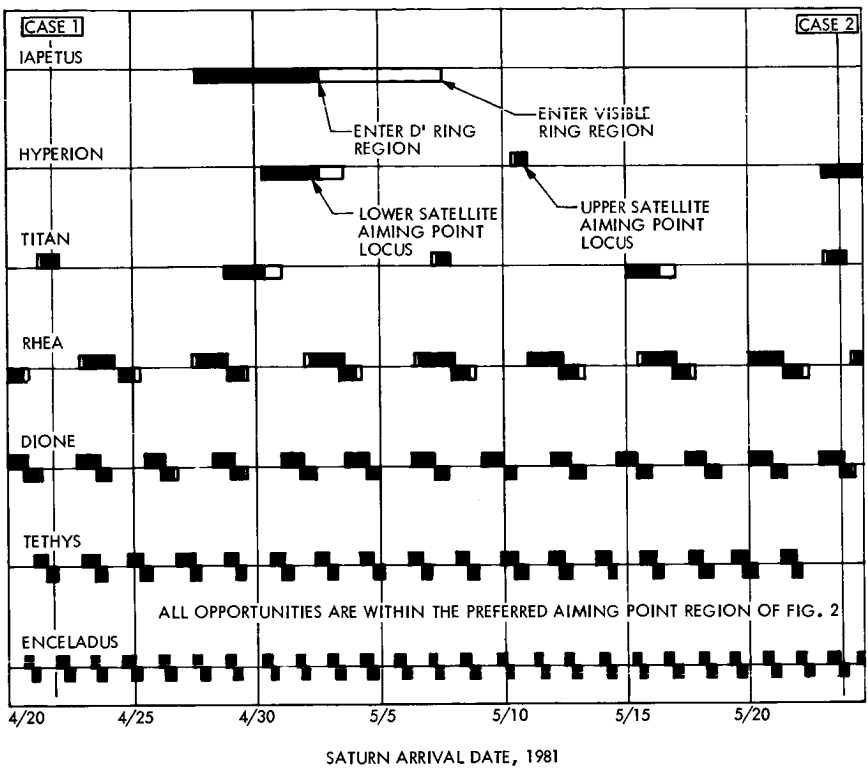

Fig. 3. Saturn satellite encounter opportunities for Saturn arrival dates between April 20, 1981, and May 20, 1981

both planets are required for satellite tradeoff purposes. Charts such as Fig. 3 fulfill this purpose for satellite opportunities at Saturn.

Single Satellite Encounter

The Saturn arrival times given in Fig. 3 can be used to design an encounter that can be tailored to planetary science. The satellite can be encountered by flying over or under the rings, encountered before encountering Saturn, encountered with a grazing Earth occultation, etc.

Retargeting

The Mariner Jupiter-Saturn Project will launch two spacecraft on Jupiter-Saturn trajectories. One of the spacecraft will arrive at Saturn some 60 to 90 days prior to the second spacecraft. If the information sent back to Earth from the first arriving spacecraft warrants it, a retargeting of the second arriving spacecraft would be possible.

If a satellite other than those originally selected were desired for encounter, then a satellite which satisfied encounter constraints and had a similar Saturn arrival date would have to be chosen[4] (see Case 1 (April 21, 1981) on Fig. 3). For this case, it is possible to arrive at Saturn on April 21, 1981, and target either to Titan (arriving at Titan before Saturn) or Tethys (arriving at Tethys just after Saturn, flying over the rings). This possibility is illustrated in the B-plane mapping shown in Fig. 2, where the change in **B** magnitude is about 375,000 km. Such a retargeting (changing the aiming point by the difference in the **B** magnitudes) would require about 70 m/s if the maneuver were performed 60 days before Saturn encounter.

Multiple Satellite Encounters

Case 2 on Fig. 3 indicates that on May 23, 1981, the aiming points for five Saturn satellites are in the preferred aiming zone: Hyperion, Titan, Dione, Tethys, and Enceladus. Through the use of computer programs based on conic simulations, trajectories which pass close to these satellites on May 23, 1981, can be analyzed. Figure 4 shows the closest approach distances (measured to the satellite's center) to Dione, Tethys, and Enceladus as a function of Saturn arrival time. The closest approach radius to Hyperion is very high and off the chart. For each time point, the encounter trajectory was constrained to a 10,000-km approach to Titan, with the trajectory passing through the center of Titan's Earth occultation zone. The resulting closest approaches to the other three satellites are plotted on Fig. 4. Thus the encountering of four Saturn satellites with one trajectory, which also satisfies the planetary and environmental constraints, is a possibility.

From Fig. 4, a Saturn arrival time of May 23, 1981, $16^h04.8^m$ was chosen for further study. Figures 5 and 6 show the encounter trajectory as seen from the north trajectory pole and from the Earth, respectively. Note that an Earth occultation of Saturn and, separately, of Saturn's rings occurs (see Fig. 6). Some encounter characteristics are given in Table 1 for this example. It should be stressed that the satellites were considered massless, and approximate analyses show that the closest approach distances in Table 1 could be in error by as much as ±40,000 km.

Future Plans

In summary, potential Saturn satellite opportunities have been determined as a function of Saturn arrival time. Future encounter design studies will be carried out which examine promising satellite encounters in detail and consider the effect of satellite masses on encounter trajectories. These future studies should provide candidates for the final Saturn encounter design.

---

[4] Arrival time changes of more than a few hours require excessive use of propulsion fuel on a weight-limited spacecraft.

Table 1. An example of multiple satellite encounter characteristics[a]

Satellite	Satellite closest approach		Time from Saturn encounter for closest approach to satellite, h
	distance, km	angular radius, deg	
Titan[b]	10,000	13.6 ± 0.9	E − 21.19
Dione	94,400	0.2 ± 0.1	E + 4.77
Tethys	44,800	1.5 ± 0.3	E + 3.67
Enceladus	75,400	0.2 ± 0.1	E + 2.75

[a]Saturn arrival time = May 23, 1981, $16^h04.8^m$. Saturn closest approach radius = $4.5R_s$ (267,000 km).

[b]Earth occultation occurs.

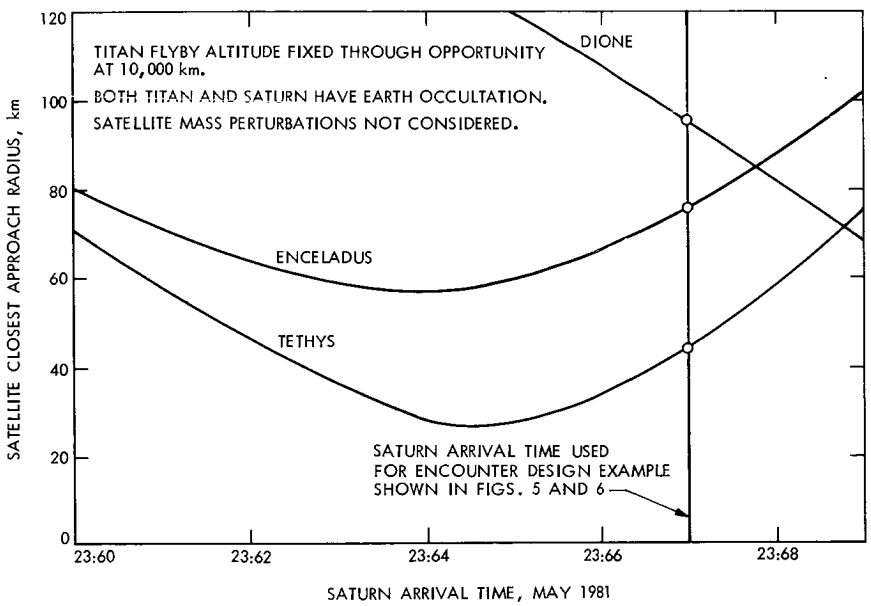

Fig. 4. Example of multiple Saturn satellite encounter opportunities, Saturn arrival date of May 23, 1981

Acknowledgment

The author wishes to acknowledge the following people for the design of computer programs which supported this study: P. A. Penzo, P. H. Roberts, and M. B. Simes. Saturn approach data were derived from precision integrated trajectory data generated by J. G. Beerer.

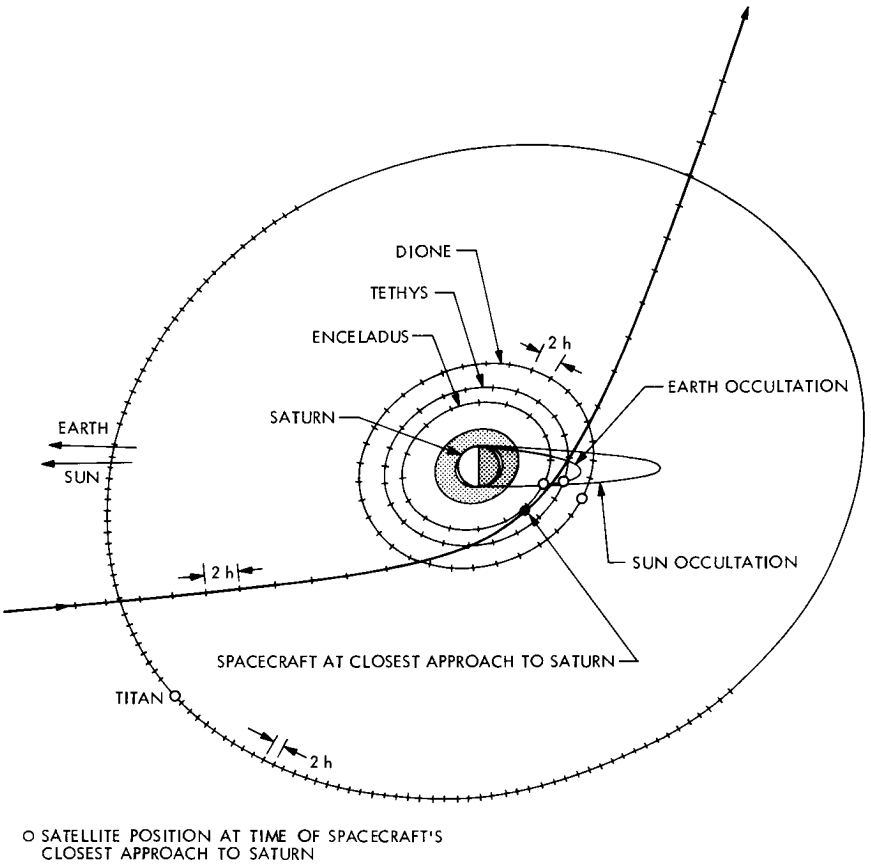

Fig. 5. Multiple Saturn satellite encounter viewed from north trajectory pole (Saturn arrival time: May 23, 1981, $16^h04.8^m$ GMT)

References

1. Newburn, R. L., Jr. and Gulkis, S., *A Brief Survey of the Outer Planets: Jupiter, Saturn, Uranus, Neptune, Pluto, and Their Satellites*, Technical Report 32-1529, Jet Propulsion Laboratory, Pasadena, California, April 15, 1971, p. 29.

2. *Explanatory Supplement to the Astronomical Ephemeris and the American Ephemeris and Nautical Almanac*, H. M. Stationery Office, London, 1961.

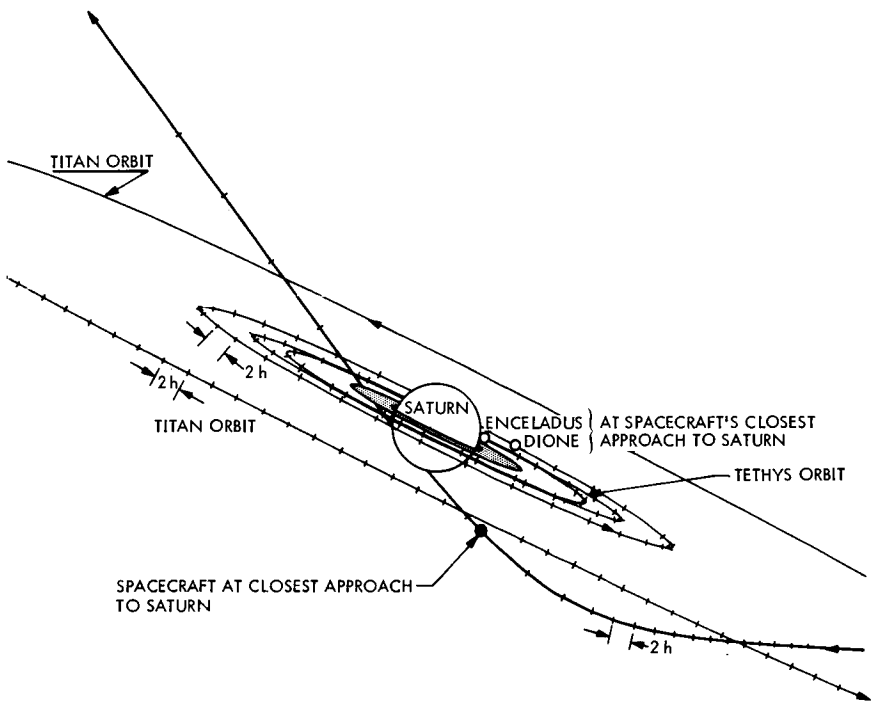

Fig. 6. Multiple Saturn satellite encounter viewed from Earth (Saturn arrival time: May 23, 1981, $16^h04.8^m$ GMT)

Index: electricity and magnetism, plasma physics, spacecraft environments and shielding

The Electric Field in the Vicinity of a Photo-Emitting Plate in a Plasma

J. Barengoltz and C. Bauerle

Project Engineering Division

Knowledge of the electric field in the vicinity of a spacecraft provides necessary corrections to measurements of ambient fields and charged particle fluxes and a required parameter to understand the motion of dust particles and grains around the spacecraft. Although the surface potential is sufficient to correct field and particle values, the more complex problem of the entire electric field, needed for grain transport calculations, is treated here for the one-dimensional case.

By approximations to the analysis of a photo-emitting plate immersed in a dilute plasma, performed by Guernsey and Fu, explicit expressions for the potential and the electric field have been derived. The two classes of implicit solutions for the potential reported by them are shown to yield essentially identical results for the electric field within the Debye length for photoelectrons from the plate, under the conditions in our solar system. The values were obtained following assumptions of a later paper by Guernsey and Fu, in which the emitted photoelectron distribution is taken as Maxwellian. These results are compared with a simple model due to Grard and Tunaley, wherein the effect of the dilute plasma is neglected entirely.

Introduction

A spacecraft in the interplanetary medium is subjected to a variety of electrical effects. In addition to its interactions with the solar plasma of protons and electrons, the solar illumination of parts of the spacecraft surface causes the emission of photoelectrons. It is expected that the positive charging due to the photoelectric effect will dominate the negative charging due to plasma electron accretion and that an electrically connected, conducting spacecraft will have a positive equilibrium surface potential (Ref. 1). Prior to equilibration, currents will flow as the various charge species tend toward their steady-state distributions. Although the charging rates and hence the time to reach equilibrium depend on the heliocentric distance of the spacecraft, the dependence is similar for all of the mechanisms. Therefore the equilibrium condition is not dependent on heliocentric distance to a good approximation.

While the surface potential of a spacecraft is important to measurements of ambient fields and charged particle environments, the potential (or the electric field) everywhere in the vicinity of the spacecraft is of interest here. Knowledge of the field permits probabilistic calculations of the likelihood of a charged grain (e.g., a dust particle) dislodged from the spacecraft migrating back to it. This matter is of extreme importance to a mission in which the relocation of particles on an experiment could degrade the life detection sensitivity.

The exact solution for the potential problem in even a simple three-dimensional geometry is formidable. Recently the one-dimensional solution has been obtained in an implicit form by Guernsey and Fu (Refs. 2 and 3). Their solution is strictly valid only for a spacecraft with characteristic dimensions large compared to the Debye length for the photoelectrons (Ref. 2). However, for positions within the Debye length, the solution will be approximately correct in all cases and may be made even more realistic by comparing the nonilluminated (i.e., no photoelectric effect) one-dimensional problem to the analogous spherical geometry problem. Guernsey and Fu also proved the existence of two classes of potentials: the usual monotonic solution and a solution with a sign change and a minimum. This second form of potential has a major bearing on the interpretation of the apparently long-lived grains orbiting spacecraft. Only a nonmonotonic potential has the ability to trap a charged grain of the same sign as the spacecraft surface.

Formulation of the Problem

In the following discussion, the nonmonotonic potential solution will be developed as in Ref. 2. The extension to the monotonic solution may be obtained by setting ϕ_m, the minimum value, to zero and x_m, the position corresponding to ϕ_m, to infinity.

Following Ref. 2, one may write Poisson's equation in the form:

$$\frac{d^2\phi}{dx^2} = \begin{cases} -\dfrac{\partial}{\partial\phi} V_1(\phi) & x \leq x_m \\ -\dfrac{\partial}{\partial\phi} V_2(\phi) & x \geq x_m \end{cases} \tag{1}$$

where $V_1(\phi)$ and $V_2(\phi)$ are complicated functions of the velocity distributions of the various charge species and the parameters of the potential as well as their argument ϕ. Formally, Eq. (1) may be solved in quadrature:

$$\int_{\phi_m}^{\phi} \frac{d\phi'}{[-V_1(\phi')]^{1/2}} = -\sqrt{2}(x - x_m) \qquad x \leq x_m$$

$$\int_{\phi_m}^{\phi} \frac{d\phi'}{[-V_2(\phi')]^{1/2}} = \sqrt{2}(x - x_m) \qquad x \leq x_m \tag{2}$$

The boundary conditions may then be imposed on $V_1(\phi)$ and $V_2(\phi)$ through Eq. (2). The relevant conditions are charge neutrality at infinity, no electric field at infinity, and zero total current at steady-state. There are also conditions to be imposed on the velocity distributions of the charged species. One of Fu's significant results is that for a uniform plasma proton distribution and Maxwellian plasma electron and photoelectron distributions, both types of solutions for the potential exist if and only if

$$1 < T_e/T_v < n_v/n_e \tag{3}$$

where n_e and T_e are the plasma electron density and temperature (at infinity) and n_v and T_v are the photoelectron density and temperature (at the surface) (Ref. 3). The relevant plasma electron quantities are known to be about n_e = 5 cm^{-3} and kT_e = 12.9 eV. For the photoelectron distribution, recent data by Feuerbacher and Fitton for air-exposed silica and aluminum as actually found in spacecraft provide yield functions and current densities for photoemission (Ref. 4). Although the energy distributions are not well characterized by a Maxwellian velocity distribution, this assumption should provide reasonable results. We have derived n_v = 1000 cm^{-3} and kT_v = 3 eV for aluminum and n_v = 100 cm^{-3} and kT_v = 2 eV for silica. Thus the requirements of Eq. (3) are met for the situation under consideration.

Approximation to the Solution of Guernsey and Fu

As mentioned previously, the expressions for $V_1(\phi)$ and $V_2(\phi)$ are complicated and involve integrals including the distribution functions. Guernsey and Fu provided systems of equations which allow ϕ_m, the minimum potential, and ϕ_0, the surface potential, to be calculated. However, because $V_1(\phi)$ and $V_2(\phi)$ cannot be expressed in a closed form so that the integral required in Eq. (2) may be performed, their solution is implicit. Starting from their expression for $V_1(\phi)$, we have attempted to approximate it so that the potential (and the electric field) may be written in an approximate explicit form. We have obtained

$$V_1(\phi) \simeq 4\pi n_i\, e(\phi - \phi_m) + \frac{8\sqrt{\pi}}{3}\, e^{3/2}\, (\phi - \phi_m)^{3/2} \left(\frac{n_v}{\sqrt{kT_v}} - \frac{n_e}{\sqrt{kT_e}} \right) \tag{4}$$

where n_i is the proton density, which may be determined by an equation in Ref. 3, and all other quantities have been previously defined.

Upon substitution of Eq. (4) into Eq. (2), a potential of the form

$$\phi = \phi_m + \{-c_1 + [(\sqrt{\phi_0 - \phi_m} + c_1)^{1/2} - c_2 x]^2\}^2 \tag{5}$$

is obtained for the region

$$x < \frac{[(\sqrt{\phi_0 - \phi_m} + c_1)^{1/2} - c_1^{1/2}]}{c_2} \tag{6}$$

where c_1 and c_2 are known constants. Since the electric field is the negative gradient of the potential, the electric field for the same region may be obtained by differentiation:

$$E = 4\,c_2\{-c_1 + [(\sqrt{\phi_0 - \phi_m} + c_1)^{1/2} - c_2 x]^2\}\,[(\sqrt{\phi_0 - \phi_m} + c_1)^{1/2} - c_2 x] \tag{7}$$

Note that Eqs. (5) and (7) are appropriate for either the monotonic or nonmonotonic solutions, provided that the proper values of ϕ_0, ϕ_m, and n_i are employed.

Results and Conclusions

Substitution of the photoelectron number density n_v and the temperature kT_v previously developed for aluminum (Al) and silica (SiO_2) provides the potential parameters summarized in Table 1. The plasma electron parameters are also included for completeness. Note that Guernsey and Fu have also provided a formula for the proton density n_i (Ref. 2). Since the proton density is a known parameter, required in the unperturbed state to be equal to the plasma electron density n_e, their system of equations may overspecify the problem. However, the values for n_i derived, especially for nonmonotonic potential, agree closely with n_e.

Table 1. Potential parameters

Material	n_e, cm^{-3}	kT_e, eV	n_v, cm^{-3}	kT_v, eV	n_i, cm^{-3}	ϕ_0, V	ϕ_m, V
Al (monotonic)	5	12.9	1000	3	7.7	13.7	0
Al (non-monotonic)	5	12.9	1000	3	5.7	12.0	−2.2
SiO_2 (monotonic)	5	12.9	100	2	8.9	4.1	0
SiO_2 (non-monotonic)	5	12.9	100	2	5.5	1.8	−2.8

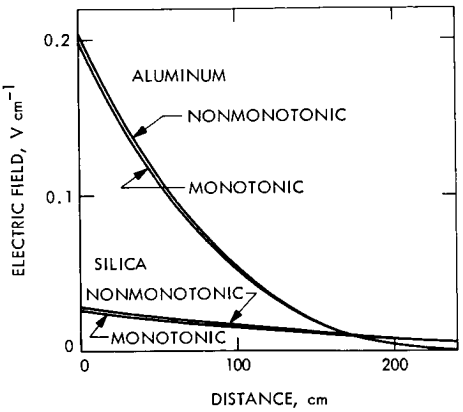

Fig. 1. Electric field in present model

From the values for the surface potential ϕ_0 and the minimum potential ϕ_m, we see that the two solutions for the potential are quite different. On the other hand, the electric field (Fig. 1) differs little for the monotonic and nonmonotonic solutions in the region shown. Of course, at larger distances from the plate, the nonmonotonic electric field will change sign, level off, and then asymptotically approach zero from the negative side. Although this behavior has a profound effect on the trapping of charged grains in orbit, the small absolute value of the field in either model for such distances indicates little effect on the migration of charged grains to the surface.

Finally, we have compared the results of our calculation with the electric field derived in Ref. 5. The normalized electric field in this work is given by

$$\frac{E(x)}{E_0} = \left(1 - \frac{1}{3\sqrt{2}} \frac{x}{\lambda_0}\right)^3 \tag{8}$$

where E_0 is the electric field at the surface and λ_0 is the photoelectron Debye length, defined in terms of the mean velocity. Since Grard and Tunaley (Ref. 5) disregard the ambient plasma in the first approximation, a photoelectron velocity distribution with a tail extending to infinity leads to an infinitely thick plasma sheath in their formulation. Thus we have used their formula (Eq. 8), which corresponds to a rectangular velocity distribution rather than a Maxwellian distribution. It is hoped that this choice will approximately compensate for the ambient plasma. With E_0 from our calculations, a comparison expressed as the fractional difference between our nonmonotonic results (noted as E_F) and the values given by Eq. (8) from Ref. 5 (noted as E_{GT}), is illustrated in Figs. 2 and 3. For silica the agreement is very good for the region of interest (Fig. 2). Figure 3 shows a poorer comparison for aluminum. However, the two models agree to within 20% for

distances of less than 95 cm of the plate, where the field in our calculations has reduced from about 0.2 V cm^{-1} to 0.06 V cm^{-1}.

To summarize, we have developed an approximate explicit expression for the electric potential and field in the vicinity of an illuminated plate immersed in the solar wind plasma. The results for the surface potential for

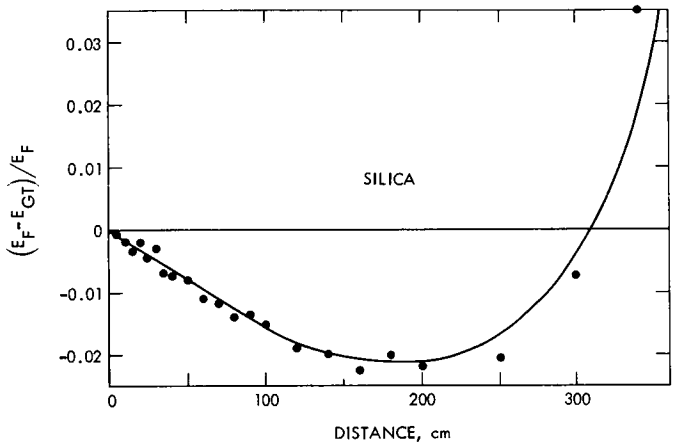

Fig. 2. Comparison of electric field: present model vs Grard and Tunaley model for silica

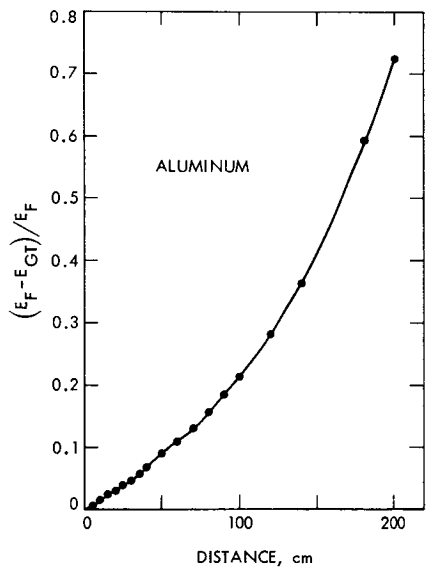

Fig. 3. Comparison of electric field: present model vs Grard and Tunaley model for aluminum

aluminum and silica seem reasonable (Refs. 1, 5, and 6). The spatial dependence of the electric field is similar to that derived from a less complicated treatment (Ref. 5). Most importantly, however, the electric field is shown to fall off owing to the photoelectron shielding in the case of a metal such as aluminum. In any case, the field will decrease more rapidly than an exponential characterized by the plasma electron Debye length, which is 1200 cm for our plasma values. Exponential fits to the curves in Fig. 1 yield effective lengths of 80 cm for aluminum and 200 cm for silica.

References

1. Whipple, E. C., Jr., *The Equilibrium Electric Potential of a Body in the Upper Atmosphere and in Interplanetary Space*, NASA X-615-65-296, 1965.

2. Guernsey, R. L., and Fu, J. H. M., "Potential Distribution Surrounding a Photo-Emitting Plate in a Dilute Plasma," *J. Geophys. Res.*, Vol. 75, No. 16, 1970.

3. Fu, J. H. M., "Surface Potential of a Photoemitting Plate," *J. Geophys. Res.*, Vol. 76, No. 10, 1971.

4. Feuerbacher, B., and Fitton, B., "Experimental Investigation of Photoemission from Satellite Surface Materials," *J. Appl. Phys.*, Vol. 43, 1972.

5. Grard, R. J. L., and Tunaley, J. K. E., "Photoelectron Sheath Near a Planar Probe in Interplanetary Space," *J. Geophys. Res.*, Vol. 76, No. 10, 1971.

6. Chopra, K. P., "Thermionic and Photoelectric Screening of Objects Moving in an Ionized Medium," *Astronautica Acta*, Vol. 11, No. 3, 1965.

Index: industrial processes and equipment, power sources, quality assurance and reliability, solid-state physics, spacecraft environments and shielding

Study of Interaction Among Silicon, Lithium, Oxygen and Radiation-Induced Defects for Radiation-Hardened Solar Cells

P. A. Berman

Guidance and Control Division

In order to improve reliability and the useful lifetime of solar cell arrays for space use, a program was undertaken at JPL for development of radiation-hardened lithium-doped silicon solar cells. These cells have been shown to be significantly more resistant to degradation by ionized particles than the presently used n–p non-lithium-doped silicon solar cells. This paper describes the results of various analyses performed to develop a more complete understanding of the physics of the interaction among lithium, silicon, oxygen, and radiation-induced defects. A discussion is given of those portions of the previous model of radiation damage annealing which were found to be in error and those portions which were upheld by these extensive investigations.

Introduction

The objectives of this program and the reasons for JPL's interest have been discussed in a previous issue of the JPL Quarterly Technical Review (Ref. 1) but will be reiterated here briefly for sake of completeness. State-of-the-art silicon solar cells used in spacecraft solar array power systems degrade with electron and proton irradiation which occurs in near-Earth space as a result of the Van Allen belts and in deep space as a result of solar proton flares. The amount of degradation is dependent upon the irradiation spectrum and fluence. This problem is presently circumvented by overdesigning the panels with respect to the initial power output so that the degraded output will meet or exceed mission requirements. This approach is oftentimes used in conjunction with thick coverglasses which attenuate some of the radiation. Thus tradeoffs must be made between the power and useful lifetime of a solar array and its allowable size, weight, and cost. Effort has therefore been directed to develop an improved radiation-hardened solar cell. Tests have shown that lithium-doped p–n solar cells can be designed and fabricated to be significantly more radiation-resistant than conventional silicon n–p solar cells at temperatures above 30°C. They can also be made

reproducibly with initial conversion efficiencies better than those of the state-of-the-art cells. The present data indicate that these lithium-doped solar cells, when properly optimized for a particular mission environment, can be effectively three times more radiation-resistant to electrons and 10 times more radiation-resistant to protons and neutrons than present-day conventional 10-Ω-cm n–p solar cells.

The JPL lithium-doped cell program has been in existence for about 5 years and has involved subcontracts to industrial organizations and universities as shown in Table 1.

Reference 1 discussed the pragmatic aspects associated with the fabrication of lithium-doped silicon solar cells. This report deals with the investigation carried out to determine the physical processes associated with the interaction among silicon, lithium, oxygen and radiation-induced defects. The objective of this portion of the program was to develop an understanding of the physics of the system and to develop a model which would allow a more sophisticated approach to design of lithium-doped silicon solar cells.

A number of analytical tools were utilized in order to gain understanding of the effects of lithium doping on both the fundamental physical properties and the device characteristics of silicon solar cells. Some of the major analytical tools used were:

(1) Irradiation primarily by 1-MeV electrons, but also Sr^{90} β-sources, neutrons, protons, and high-energy (28–30 MeV) electrons.

(2) Solar cell electrical characteristics measurement (primarily current-voltage characteristics).

(3) Minority carrier diffusion length and lifetime measurements.

(4) Junction capacitance measurements to determine the concentration and concentration gradient of ionized lithium near the junction.

(5) Electrical resistivity measurements.

(6) Hall-effect measurements to determine carrier removal rates and mobility changes.

(7) Electron spin resonance (ESR) to determine the energy level and structure of radiation-induced defects.

(8) Infrared absorption spectroscopy to determine radiation-induced defect levels.

The measurements shown in (2) through (8) above were generally monitored before and after irradiation and as a function of environmental conditions such as time and temperature. Of the analytical techniques discussed above, the most valuable technique (aside from the solar cell electrical characteristics measurements) was found to be the capacitance vs voltage measurement, which provided quantitative correlations with the cell radiation recovery characteristics.

Table 1. Organization summary

Organization	Function
Heliotek Division of Textron Inc., Sylmar, Calif. Centralab Division of Globe Union, El Monte, Calif.	Lithium-doped cell development, analysis, and fabrication.
Naval Research Laboratory, Washington, D. C. Philco-Ford Corp., Palo Alto, Calif. Lockheed Georgia Corp., Marietta, Ga.	Investigation of behavior and operating characteristics of lithium-doped silicon cells in a simulated space environment
RCA, Princeton, N. J. TRW Systems, Redondo Beach, Calif.	Evaluation and analysis of lithium-doped silicon, silicon diodes, and silicon solar cells. Investigation of radiation damage model and annealing kinetics
Gulf Radiation Technology, San Diego, Calif. Naval Research Laboratory, Washington, D. C.	Evaluation of lithium-doped silicon. Investigation of radiation damage model and annealing kinetics
University of Illinois, Urbana, Ill.	Study of luminescent and tunneling phenomena in irradiated silicon
MIT, Cambridge, Mass. University of Utah, Salt Lake City, Utah	Study of radiation kinetics in electronic material
Rensselaer Polytechnic Institute, Troy, N. Y.	Investigation of structure of radiation damage in lithium-diffused silicon solar cells
University of Denver, Denver, Colo.	Study of effects of space particle bombardment on solar cell materials
University of Kentucky, Lexington, Ky.	Study of structural damage in lithium-doped solar cells by neutrons
Brown University, Providence, R. I.	Study of effects of subthreshold electron irradiation on silicon
Jet Propulsion Laboratory, Pasadena, Calif.	Direction and coordination of all above programs

The results of measurements of carrier removal, diffusion length, and other such physical properties were often very strongly affected by the amount of lithium doping in the silicon. For example, the behavior of lightly lithium-doped silicon can be significantly different from that of heavily lithium-doped silicon because of masking effects or competing mechanisms.

Thus great care must be taken in extrapolating the results of one level of doping to those of a different level of doping.

In some types of measurements, such as ESR and absorption spectroscopy, there is an inherent requirement for a particular concentration of defects in order that the structure be observed. Other techniques such as Hall-effect, minority carrier diffusion length, and minority carrier lifetime measurements allow a wider latitude of lithium concentrations and can therefore be used to correlate results between low and high lithium concentrations.

Results

Characteristics of Lithium-Doped Silicon as a Function of Lithium-Dopant Concentration

The Hall-effect measurements performed on heavily doped float-zone (oxygen-lean) silicon indicated that all carrier removal occurred nearly instantaneously during irradiation by 1-MeV electrons. In the lightly lithium-doped float-zone samples, however, it appears that some carrier removal occurred during irradiation, but carrier removal continued to occur for a long time after termination of the irradiation, the loss during irradiation being related to the initial lithium concentration and the electron fluence. Capacitance vs voltage measurements indicated that more lithium was consumed during recovery than during irradiation, which is not consistent with a model which assumes formation of a lithium-vacancy defect during irradiation with subsequent association with a second lithium donor during recovery. Hall mobility values increased in a manner that indicates loss of lithium donors and no acceptor formation in the final state.

The carrier removal rate during recovery appears to be directly proportional to the lithium donor concentration at that point in the cell. At a distance of 5 μm from the junction, 5 times as many lithium donors are removed as there are oxygen-vacancy centers at that distance. Since the oxygen-vacancy centers are introduced relatively uniformly throughout the N region by 1-MeV electrons, the amount of lithium reacting is not proportional to the concentration of the oxygen-vacancy centers but the concentration of the lithium itself. It is possible that the oxygen-vacancy centers act as nucleation sites for precipitation of lithium in the silicon. For lithium-doped oxygen-rich silicon, 5 times as many lithium donors react per induced defect center during recovery from exposure to 3×10^{14} 1 MeV e/cm^2 as from 3×10^{15} 1 MeV e/cm^2. This again indicates that the number of lithium atoms interacting with the radiation-induced defects is a function of the number of lithium atoms which are available for interaction. (Although fewer lithium donors reacted per defect at the higher fluence, the fractional recovery, as measured by short-circuit current was the same for both fluences.)

A similar effect was observed with respect to the removal rates of lithium-doped cells fabricated from oxygen-lean silicon. The ratio of carriers

removed during irradiation to carriers removed during recovery decreased from 4 to 2 when the fluence was increased by an order of magnitude. That is, at 3×10^{14} e/cm^2 four carriers were removed during recovery for each carrier removed during irradiation. For irradiation to a fluence of 3×10^{15} e/cm^2, only two carriers were removed during recovery for each carrier removed during irradiation. Again, it appears that the number of lithium donors interacting during recovery is dependent upon the number available for interaction.

In lithium-doped oxygen-lean silicon it was observed that higher carrier removal rates during the recovery phase promotes more complete recovery and that for good recovery the carrier removal during recovery should be at least 1.5 times the removal which occurred during the irradiation. The fact that during satisfactory recovery from similar fluences of 1-MeV electrons the removal rate during recovery has been observed to vary between 1.5 and 4 times that observed during irradiation indicates that no discrete quantity of lithium appears to react with the radiation products. This is further evidenced by the observation that lower concentrations of lithium in oxygen-lean silicon Hall bar samples produced lower carrier removal rates than did higher concentrations of lithium.

The carrier removal studies indicate that the model used in the past, which simply assumed that two lithium donors were removed for each annealed damage center, must be severely modified. It now appears that the irradiation-induced defects can act as nucleation sites for precipitation of lithium donors. In highly lithium-doped oxygen-lean silicon, the carrier removal reached equilibrium shortly after irradiation. In lightly lithium-doped oxygen-lean silicon and highly lithium-doped oxygen-rich silicon, carrier removal reached equilibrium approximately 1 to 2 years after irradiation. Thus the precipitation process does not go on indefinitely but reaches a state of equilibrium, and if sufficient lithium is present, about 25% of the donors appear to remain active. It should be noted that the carrier removal has not resulted in degradation of cell electrical characteristics after recovery of highly lithium-doped cells exposed to 1-MeV electron fluences up to 3×10^{15} e/cm^2.

Lightly lithium-doped float-zone material irradiated with 1-MeV electrons indicated the formation of radiation-induced defects with a level 0.17-eV below the conduction band as well as a second defect with a level deeper in the energy gap. The removal of both defects was seen during annealing. The introduction of the deeper level appeared to increase with increasing lithium concentration, indicating that lithium is probably associated with the structure of this defect. In contrast to this, the 0.17-eV-level introduction rate appeared to be independent of the lithium concentration. The introduction rate of the 0.17-eV level in lightly lithium-doped float-zone silicon, moderately lithium-doped crucible silicon, and non-lithium-doped crucible solar cells was of the order of 0.2-cm^{-1} for all cases.

A distinct dependence of annealing properties of lithium-doped silicon on lithium concentration was observed in float-zone silicon with lithium

densities between $2 \times 10^{14}/cm^3$ and $2 \times 10^{16}/cm^3$. The carrier density and mobility of lightly lithium-doped silicon changed very slowly with time at room temperature, in contrast to the very fast changes observed in heavily lithium-doped silicon. The lightly lithium-doped float-zone silicon exhibited annealing characteristics which are very similar to heavily lithium-doped crucible-grown (oxygen-rich) silicon. The mobility increased slowly at room temperature and more rapidly at 373 K, while the carrier density decreased. Increases in carrier density during room temperature anneal, which possibly indicate disassociation of lithium from defects, have been observed previously in heavily lithium-doped float-zone silicon but were not observed for the lightly lithium-doped float-zone silicon or heavily lithium-doped crucible silicon. It thus appears that the ratio of lithium concentration to the oxygen concentration has a major effect in determining the annealing properties of lithium in silicon. From this point of view, low-oxygen-content silicon can be made to behave in a manner similar to high-oxygen-content silicon if the ratio of lithium to oxygen remains relatively constant.

Electron Spin Resonance Investigation of Oxygen-Vacancy Center Production

Electron spin resonance (ESR) measurements were used to investigate the formation of radiation-induced oxygen-vacancy defect centers, commonly referred to as A-centers, in lithium-containing crucible-grown silicon (with phosphorus background doping). Prior to irradiation a resonance line attributed to the lithium-oxygen donor was observed, the density of which was proportional to the lithium concentration. No resonance due to the phosphorus donor was found, even though the phosphorus doping density was of the order of $10^{16}/cm^3$. After 300 K irradiation by 30-MeV electrons to fluences of the order of 10^{16}–10^{17} electrons/cm^2, the lithium-oxygen resonance line decreased while the oxygen-vacancy resonance line increased. The introduction rate of oxygen-vacancy centers for lightly lithium-doped samples was similar to that obtained for non-lithium-doped samples, while for heavily lithium-doped samples the introduction rate was lower by about an order of magnitude, indicating that lithium is acting in such a manner as to inhibit the stable formation of this type of defect. Upon annealing the heavily lithium-doped sample between 300 and 600 K, the annealing was found to be centered near 325 K as contrasted with results on non-lithium-doped silicon, which indicated an anneal of the oxygen-vacancy center near 550 K. This again indicates that the presence of lithium reduces the stability of this defect.

Activation Energy Associated with Annealing

The activation energy for annealing of lithium-doped float-zone silicon after irradiation by 1-MeV electrons was found to be of the order of 0.66 eV by RCA on the basis of the relationship between reciprocal temperature and unannealed fraction. Gulf Radiation Technology, on the basis of τ measurements as a function of isothermal annealing times after irradiation by 30-MeV electrons, has found a similar activation energy of the order of 0.75 eV

for lightly, moderately, and heavily lithium-doped float-zone silicon. On the basis of isothermal and isochronal annealing studies on lithium-doped float-zone silicon after irradiation by neutrons, Gulf Radiation Technology has determined an activation energy of approximately 0.69 eV.

Annealing rate studies at various temperatures have been conducted by TRW on lithium-doped solar cells fabricated from crucible (oxygen-rich) silicon after irradiation by 1-MeV electrons by utilizing the I_{sc} parameter to determine reciprocal half-time for recovery as a function of reciprocal annealing temperature. The apparent activation energy was found to be of the order of 1.10 eV. Studies performed by RCA on the annealing characteristics of lithium-doped cells fabricated from crucible silicon indicated an activation energy of approximately 1.07 eV on the basis of the relationship of reciprocal fraction of damage remaining as a function of annealing time. RCA has also made measurements of the lithium diffusion constant near room temperature for an unirradiated lithium-doped cell fabricated from crucible silicon and has determined an activation energy of 1.03 eV utilizing measurements of lithium drift capacitance.

The accepted activation energy of lithium in oxygen-lean silicon as determined by Pell (Refs. 2–4) is of the order of 0.65 eV, and thus the activation energies determined from annealing studies of irradiated lithium-doped oxygen-lean silicon are in very good agreement with this value. It should be emphasized that the agreement is reasonable for all types of radiation investigated (i.e., 1-MeV electrons, 30-MeV electrons, and neutrons) and is surprisingly consistent in view of Pell's observation that the activation energy increases with increasing oxygen concentration and the fact that the amount of oxygen in oxygen-lean silicon is not a controlled or measured parameter. Pell determined the dissociation constant (activation energy) of lithium-O^+ to be approximately 0.42 eV, so that when this activation energy is added to the 0.65-eV activation energy for diffusion of lithium in silicon, an activation energy of 1.07 eV appears to be reasonable for high-oxygen-content lithium-doped silicon. The activation energy, indeed, is quite consistent with the activation energies determined through annealing studies on irradiated lithium-doped crucible-grown silicon and with the activation energy determined for unirradiated lithium-doped crucible silicon.

Thus a very good agreement is obtained among results of annealing studies done independently by TRW, RCA, and Gulf Radiation Technology, among results of annealing studies done after different types of irradiation, among results of annealing studies done on oxygen-lean and oxygen-rich lithium-doped silicon, and among the results of studies done on diffusion of lithium in unirradiated silicon and annealing characteristics of irradiated lithium-doped silicon. These studies show that the activation energy associated with neutralization of radiation-induced defects in lithium-doped silicon, whether point defects or cluster defects, is well in agreement with the activation energy associated with diffusion of lithium in silicon and lends very strong

support to the theory that the neutralization of radiation-induced defects is dependent upon diffusion of lithium to the defect sites.

Lithium Surface Concentration

Measurement of the lithium surface concentration in silicon as a function of lithium diffusion time indicated the occurrence of a peak in surface concentration with a subsequent falloff as the time was increased. The occurrence of lower lithium concentrations for longer diffusion times is indicative of diffusion from a limited source. The peak occurred more rapidly and was of greater magnitude as the diffusion temperature was increased. Furthermore, the lithium concentration measured near the junction by capacitance vs voltage techniques was found to be as high as 7 times that calculated from the surface concentration measurements. This might be due to the effect of the space charge region near the junction. As the diffusion times were increased, the surface concentration not only decreased but exhibited larger sample-to-sample variations in lithium density as measured at the junction. This is probably due to the fact that there is a limited lithium source.

Lithium Density Gradient

The time-temperature schedule of lithium diffusion determines the distribution of the lithium within the body of the cell. A very convenient method for determining the lithium concentration near the junction is measurement of capacitance vs voltage as the cell is reverse biased. This technique is applicable to a distance of up to 10 μm from the junction, depending upon the silicon resistivity, after which the cell goes into "reverse breakdown." As a result of very thorough and extensive analysis, it now appears that nature has been extremely kind in that it is possible to predict quantitatively the lithium-doped cell radiation recovery characteristics by measurement of the lithium concentration gradient within this narrow region adjacent to the p–n junction by means of the nondestructive and relatively convenient capacitance vs voltage measurement. (It should be noted that the modifying "relatively convenient" is used because the measurement does take some time to make, and while it is possible to measure small quantities of cells on a 100% basis, it would be impractical for large production lots except on a sampling basis.)

Once the applicability of the capacitance vs voltage relationship was fully realized and utilized, many of the results which previously appeared to be anomalous became readily explainable. The most important of these was the different recovery behavior among cells from the same lot (which were supposedly identical). It was found that, in fact, the cells were not identical, but that the lithium density gradient could vary by a factor of more than 70. This was not at all obvious from the resultant cell electrical characteristics. For example, 10 cells from each of 10 experimental groups with diffusion times ranging between 3 and 7 hours and temperatures ranging between 330 and 370°C were measured in a solar simulator and were also measured with

respect to lithium concentration. While the total spread of all cells was about 5% in open-circuit voltage, the spread in lithium concentration was of the order of 400%. The open-circuit voltage has been found in almost all cases to vary directly with the lithium density; however, this experiment showed that rather large changes are required in lithium concentration to effect small changes in open-circuit voltage. The short-circuit current of these cells also varied about 5%, but in this case the higher the lithium density the smaller the short-circuit current. This resulted in a smaller spread in the maximum power among all cells than in either the short-circuit current or open-circuit voltage, since cells having high short-circuit current generally would have lower open-circuit voltage and vice versa. Thus the spread in power is even less affected by a spread in lithium concentration than either short-circuit current or open-circuit voltage.

When cells were reordered to correspond to their lithium density gradient rather than the lithium diffusion schedule, the results were found to be entirely predictable. This led to the selection of lithium diffusion schedules which not only gave cells with high initial efficiencies but also with similarly high radiation recovery capabilities, because for optimal lithium diffusion schedules, the lithium density gradient was found to vary by only a factor of 2 rather than 70 as for the worst-case diffusions. The best uniformity in lithium density gradient was found for shorter diffusion times. The lithium concentration at the junction appears to decrease with increasing lithium diffusion time, which indicates diffusion from a starved source. This correlates well with lithium surface concentration measurements discussed in a previous section, which also indicated decreases with longer lithium diffusion times. Further evidence for the starved source theory was the observation that in one small lot of cells which compared evaporated lithium source vs paint-on lithium source for a lithium diffusion schedule of 8 hours at 325°C, the spread in cell maximum power and lithium density gradient at the junction was lower for the evaporated lithium cells than for the paint-on lithium cells. Thus it appears that the nonuniformity in lithium density gradient generally observed for long time diffusions is not inherent in the long time diffusions but rather is technique-dependent. This indicates that by properly controlling the method of lithium source introduction and lithium diffusion schedule, very good uniformity in lithium density gradient can be achieved and, with it, very good uniformity of cell radiation recovery characteristics.

For a given fluence, the lithium-doped solar cell short-circuit current appears to be a linear function of the logarithm of the lithium density gradient as measured with the capacitance-voltage technique and a linear function of a logarithm of the minority carrier diffusion length.

The radiation damage coefficient of lithium-containing cells immediately after irradiation appears to be a function of the fluence and exhibits a square root dependence on the lithium density gradient. Time to half recovery is linearly dependent upon the logarithm of the lithium density gradient as is the dependence of the recovered open-circuit voltage. While the damage

coefficient immediately after irradiation is proportional to the square root of the lithium density gradient, after recovery, cells irradiated to 3×10^{13} 1 MeV e/cm^2 maintain this dependence; recovered cells after an irradiation of 3×10^{14} 1 MeV e/cm^2 exhibit a smaller dependence of lithium density gradient; and cells recovered from exposure to 3×10^{15} 1 MeV e/cm^2 exhibit almost no discernible dependence of damage coefficient on lithium density gradient. Furthermore, the scatter in results increases as the fluence increases.

Short-circuit current values after recovery from exposure to 3×10^{15} 1 MeV e/cm^2 also show very little dependence on lithium density gradient, while cells recovered from lower fluences exhibit higher short-circuit currents with lower lithium density gradients. For lithium-doped cells having lithium density gradient of 10^{18} cm^{-4} exposed to 3×10^{14} 1 MeV e/cm^2, the ratio between the damage coefficient after recovery to the damage coefficient before recovery is less than 0.1. That is to say, 90% of the effective damage centers were annealed out during recovery. When cells were exposed to a fluence of 1 MeV electrons of 3×10^{15} e/cm^2, the same 90% recovery was found to occur only for high lithium gradient cells, that is, of the order of 10^{19} cm^{-4}, while in cells having a lithium density gradient of 10^{18} cm^{-4}, only 70% recovery was found to occur.

As the fluence of 1-MeV electrons is increased, the dependence of recovered open-circuit voltage on lithium density gradient becomes increasingly more pronounced. This is to be contrasted with the results of the short-circuit current parameter, which showed a decreasing dependence on lithium density gradient as the fluence was increased. After recovery from 1-MeV electron irradiations to 3×10^{13} and 3×10^{14} e/cm^2, the open-circuit voltage of lithium-doped cells fabricated according to the previously discussed JPL-designed lithium diffusion schedule matrix averaged about 40 mV above that of 10 ohm-cm n–p cells. After exposure to a 1-MeV electron fluence of 3×10^{15} e/cm^2, however, only the lithium cells having a lithium density gradient greater than 10^{19} cm^{-4} maintained this 40-mV open-circuit voltage advantage. For each order-of-magnitude increase in the lithium density gradient, there appears to be an increase of 20 and 25 mV in open-circuit voltage after recovery from exposure to 1-MeV electron fluences of 3×10^{13} and 3×10^{14} e/cm^2, respectively.

After recovery from a 1-MeV fluence of 3×10^{15} e/cm^2, however, there appears to be an increase of 50-mV open-circuit voltage for each order-of-magnitude increase in the lithium density gradient.

After exposure to 1-MeV electron fluences of 3×10^{13} and 3×10^{14} e/cm^2, there was no strong trend in recovered power with respect to the lithium density gradient. However, cells with a lithium density gradient above 5×10^{18} cm^{-4} appeared to exhibit slightly lower recovered power. This is believed to be at least in part a result of the higher damage coefficients after recovery associated with the higher gradient cells. In contrast to this, after exposure to 1-MeV electrons at a fluence of 3×10^{15} e/cm^2, a very decided trend towards higher recovered power with higher

lithium density gradients is observed up to a lithium density gradient of about 4×10^{18} cm^{-4}. For lithium density gradients greater than this, there is not much improvement in recovered power, probably because of the lower initial power associated with the high lithium density gradient cells. At the high fluence, cells with gradients less than 4×10^{18} cm^{-4} exhibit significantly lower power outputs. Thus it appears that cells having a lithium density gradient between 4×10^{18} and 2×10^{19} cm^{-4} are optimal for a moderate to heavy radiation environment.

Conclusions

The investigations described have resulted in a significantly greater understanding with respect to the action of lithium in irradiated silicon and have corrected some major misconceptions previously held with respect to the model of radiation damage and annealing of lithium-doped silicon. Specifically the previous model involved association of lithium-vacancy or lithium-oxygen-vacancy (the vacancy occurring as a result of radiation-induced lattice atom displacement) during irradiation, resulting in a negatively charged defect center which could act as a recombination center for light-generated electron-hole pairs. Annealing was believed to take place when a second lithium ion (positively charged) associated with the defect to yield a neutralized center which no longer acted as a recombination center. The investigations described above have clearly shown that this is not a realistic model, but rather that the radiation-induced defect can act as a nucleation site for precipitation of lithium so that the number of lithium atoms which eventually associate with a radiation-induced defect is dependent upon the number available for interaction. Furthermore, the recovery characteristics of lithium-doped silicon are dependent upon the lithium-to-oxygen ratio in the silicon.

Previously it was qualitatively believed that the annealing behavior was predicated on diffusion of lithium ions through the silicon to the radiation-induced defect site. This has now been clearly *quantitatively* demonstrated by a number of techniques for determining the activation energy associated with annealing. The lithium diffusion model has been upheld for both oxygen-rich and oxygen-lean silicon and for a variety of irradiating particle species and energies.

Measurement of the lithium density gradient near the p–n junction has been developed as the most powerful tool for predicting the radiation recovery characteristics of lithium-doped solar cells fabricated from both oxygen-lean and oxygen-rich silicon. This has led to the development of significantly improved lithium-doped solar cells.

References

1. Berman, P. A., "JPL Lithium-Doped Solar Cell Development Program," in *JPL Quarterly Technical Review*, Vol. 2, No. 1, pp. 29–36, Jet Propulsion Laboratory, Pasadena, Calif., Apr. 1972.

2. Pell, E. M., "Ion Drift in an N/P Junction," *J. Appl. Phys.*, Vol. 31, p. 291, 1960.

3. Pell, E. M., "Study of an Li-O Interaction in Si by Ion Drift," *J. Appl. Phys.*, Vol. 32, p. 1048, 1961.

4. Pell, E. M., "Diffusion Rate of Li in Si at Low Temperatures," *Phys. Rev.*, Vol. 119, p. 1222, 1960.

JPL Quarterly Technical Review Volume 3, Number 1 April 1973

Index: chemistry, thermodynamics

A Method for Estimating Both the Solubility Parameters and Molar Volumes of Liquids

R. F. Fedors

Propulsion Division

The solubility parameters and molar volumes of substances can be used, in conjunction with suitable theory, to provide estimates of the thermodynamic properties of solutions. The solubility characteristics of polymer/solvent systems and the estimation of the equilibrium uptake of liquids by polymers are examples of the types of practical problems that are amenable to treatment. For low-molecular-weight liquids, the solubility parameter δ is conveniently calculated using the expression $\delta = (\Delta E_v/V)^{1/2}$, where ΔE_v is the energy of vaporization at a given temperature and V is the corresponding molar volume which is calculated from the known values of molecular weight and density. For high-molecular-weight polymers, the volatility is much too low for ΔE_v to be obtained directly, and hence recourse must be made to indirect methods for estimating δ for these materials. One such widely used method is based on Small's additive group "molar-attraction constants," which when summed allow the estimation of δ from a knowledge of the structural formula of the material. However, the density must still be determined experimentally.

The proposed method of estimating δ, also based on group additive constants, is believed to be superior to Small's method for two reasons: (1) the contribution of a much larger number of functional groups has been evaluated, and (2) the method requires only a knowledge of the structural formula of the compound.

Introduction

The solubility parameter of a liquid δ, defined as the square root of the cohesive energy density, is a quantity which, in conjunction with suitable theory, allows one to estimate several thermodynamic properties of solutions. The cohesive energy density itself is defined as the ratio of the energy of vaporization to the molar volume, both referred to the same temperature.

The concept of the solubility parameter was developed by Scatchard (Ref. 1), subsequently greatly extended by Hildebrand (Ref. 2), and had as its origin the attempt to formulate an expression for the partial molar energy of mixing, or for the special case of zero volume change, for the heat of mixing

of two liquids. The theory has been particularly successful in describing, at least semiquantitatively, the thermodynamic properties of dilute solutions and especially so when the component liquids are nonpolar.

The ability to estimate the solubility parameter of both liquids and polymers can often be an extremely useful tool, applicable to the solution of a diverse number of practical problems. For example, the solubility parameter has been used to predict the lipid uptake by prosthetic heart valve poppets (Ref. 3) and to predict the permeability of polymeric propellant expulsion bladders to both hydrazine and nitrogen tetroxide (Ref. 4). It is also a necessary quantity for the determination of crosslink density, a key parameter that determines elastomeric behavior (Ref. 5).

Although several methods exist for the estimation of δ, these generally require some kind of experimental input such as vapor pressure vs temperature data, heat capacity vs temperature data, the normal boiling point, or the measurement of colligative properties of solutions (Ref. 2). Consequently the experimental evaluation of δ may be time-consuming as well as tedious.

The method reported here, based on additive atomic and group increments, permits the estimation of both δ and the molar volume for both liquids and high-molecular-weight polymers, and requires only a knowledge of the chemical structure of the compound. Other methods which have been put forward (Refs. 6–9) require that the density of the compound be determined experimentally. In addition, the number of atoms or groups for which the increments have been evaluated is rather limited in extent.

Discussion

Based upon an examination of a vast amount of data on simple liquids, it was found that a general system for estimating both ΔE_v and V could be set up by assuming

$$\Delta E_v = \sum_i \Delta e_i \tag{1}$$

and

$$V = \sum_i \Delta v_i \tag{2}$$

where the Δe_i and Δv_i are the additive atomic and group contribution for the energy of vaporization and molar volume respectively. These contributions, applicable at a temperature of 25°C, are listed in Table 1.

Of special interest is the large number of atoms and groups for which the additive increments have been evaluated, including several metals which contain only metal-carbon bonds, i.e., for organometallic compounds. Furthermore, it has been found that both ΔE_v and V for cyclic compounds can be estimated from the properties of a linear compound having the same

Table 1. Atomic and group contributions to the energy of vaporization and the molar volume at 25°C

Atom or group	Δe_i, cal/mole	Δv_i, cm³/mole
CH_3	1125	33.5
CH_2	1180	16.1
CH	820	−1.0
C	350	−19.2
$H_2C=$	1030	28.5
$-CH=$	1030	13.5
$C=$	1030	−5.5
$HC\equiv$	920	27.4
$-C\equiv$	1690	6.5
Phenyl[a]	7630	71.4
Phenylene (o,m,p)[a]	7630	52.4
Phenyl (trisubstituted)[a]	7630	33.4
Phenyl (tetrasubstituted)[a]	7630	14.4
Phenyl (pentasubstituted)[a]	7630	−4.6
Phenyl (hexasubstituted)[a]	7630	−23.6
Ring closure 5 or more atoms	250	16
Ring closure 3 or 4 atoms	750	18
Conjugation in ring for each double bond	400	−2.2
Halogen attached to carbon atom with double bond	−20% of Δe_i of halogen	4.0
CO_3 (carbonate)	4200	22.0
COOH	6600	28.5
CO_2	4300	18.0
CO	4150	10.8
CHO (aldehyde)	5100	22.3
CO_2CO_2 (oxalate)	6400	37.3
C_2O_3 (anhydride)	7300	30.0
HCOO (formate)	4300	32.5
$CONH_2$	10000	17.5
CONH	8000	9.5
CON	7050	−7.7
HCON	6600	11.3
HCONH	10500	27.0
COCl	5000	38.0
NH_2	3000	19.2
NH	2000	4.5
N	1000	−9.0
$-N=$	2800	5.0
CN	6100	24.0
NO_2 (aliphatic)	7000	24.0
NO_2 (aromatic)	3670	32.0
NO_3	5000	33.5

[a]These values are listed for convenience. The values reported for Δe_i and Δv_i can be evaluated from the appropriate entries in the table.

Table 1 (contd)

Atom or group	Δe_i, cal/mole	Δv_i, cm³/mole
NO_2 (nitrite)	2800	33.5
SCN	4800	37.0
NCO	6800	35.0
NF_2	1830	33.1
NF	1210	24.5
O	800	3.8
OH	7120	10.0
OH (disubstituted or on adjacent C atoms)	5220	13.0
PO_4	5000	28.0
PO_3	3400	22.7
SH	3450	28.0
S	3380	12
S_2	5700	23.0
SO_3	4500	27.6
SO_4	6800	31.6
F	1000	18.0
F (disubstituted)	850	20.0
F (trisubstituted)	550	22.0
CF_2 (for perfluoro compounds)	1020	23.0
CF_3 (for perfluoro compounds)	1020	57.5
Cl	2760	24.0
Cl (disubstituted)	2300	26.0
Cl (trisubstituted)	1800	27.3
Br	3700	30.0
Br (disubstituted)	2950	31.0
Br (trisubstituted)	2550	32.4
I	4550	31.5
I (disubstituted)	4000	33.3
I (trisubstituted)	3900	37.0
B	3300	−2.0
Al	3300	−2.0
Ga	3300	−2.0
In	3300	−2.0
Tl	3300	−2.0
Si	810	0
Ge	1930	−1.5
Sn	2700	1.5
Pb	4100	2.5
P	2250	−1.0
As	3100	7.0
Sb	3900	8.9
Bi	5100	9.5
Se	4100	16.0
Te	4800	17.4
Zn	3460	2.5
Cd	4250	6.5
Hg	5450	7.5

chemical structure; this is accomplished by adding a cyclization increment to both ΔE_v and V of the linear compound.

For example, suppose one wanted to estimate both δ and V for a liquid such as *N*-phenyl piperazine (I). The linear compound which is

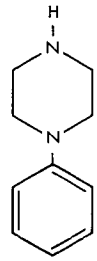

(I)

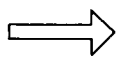

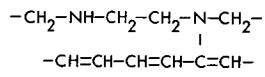

(II)

used for estimating these properties is formed by cutting bonds in the ring compound in such a manner that any functional group listed in Table 1 and present in the ring itself remains intact; the reason for this provision is the fact that the increments listed in the table for some groups are not simply the sum of the atomic contributions; i.e., the values for a carboxylate group, COO, are not obtained by summing the values of carbon and two ether oxygen atoms. Considering the linear compound II, we can set up Table 2. Hence for the cyclic compound the estimates for δ and V are 10.3 and 147.4. The values obtained experimentally and listed by Hoy (Ref. 10) are 10.55 and 152.1.

Experience using this method has shown that deviations between the experimentally measured ΔE_v and V and the estimated values are generally

Table 2. Estimation of Δ and V for compound (I)

Group	Δe_i, cal/mole	Δv_i, cm³/mole
4 CH_2	4720	64.4
1 NH	2000	4.5
1 N	1000	−9.0
5 CH=	5150	67.5
1 C=	1030	−5.5
3 conjugated double bonds	1200	−6.6
2 6-membered rings	500	32.0
	15,600	147.3

Table 3. Volume calculation for crystalline polymer

Group	Δv_i, cm³/mole
10 CH_2	161
2 NHCO	19
14 main chain skeletal atoms	28
	208

less than about 5–10%. Major deviations, when they occur, are usually limited to the first few members of a homologous series.

A problem occurs when the compound in question has either a T_g (glass transition temperature) or a T_m (melting temperature) above room temperature in that the estimates for both V and δ refer to the supercooled liquid rather than to the glass or to the crystalline phase. It can be shown that the estimates obtained using the increments from Table 1 for V would be smaller than the experimentally obtained values for both a glass or a crystal. On the other hand, the estimates for ΔE_v obtained using the increments would be greater than the experimental values.

For high-molecular-weight polymers which have a T_g greater than 25°C, this divergence in the V values can be taken into account by the introduction of small correction factors, namely,

$$\Delta v_i = 4n, n < 3$$
$$\Delta v_i = 2n, n \geq 3 \qquad (3)$$

where n is the number of main chain skeletal atoms in the smallest repeating unit of the polymer. This includes all the skeletal atoms in a ring system which may be part of the main chain; i.e., for the phenylene group in poly(ethylene terephthalate), n is taken equal to 6 and n has the value 12 for the repeating unit.

As an example, consider poly(hexanethylene adipamide), which has a T_g of 50°C (Ref. 1), an average density of the amorphous material equal to 1.08 gm/cm³, and a smallest repeating unit of $(CH_2)_6NHCO(CH_2)_4NHCO$. The V value calculated using the increments from Table 1 is given in Table 3.

Hence, the predicted V is 208 cm³/mole, which is close to the experimental value of 209 cm³/mole.

As an approximate rule of thumb, the relationship between the molar volume of the liquid and crystalline phase V_c can be taken as

$$V = (1 + 0.13x)V_c \tag{4}$$

where x is the degree of crystallization. Applied to poly(hexamethylene adipamide) and taking V equal to 208 cm^3/mole, this expression predicts V_c to have the value 184 cm^3/mole compared to the measured value of 185 cm^3/mole (Ref. 11).

From the very limited data available, it does not seem that the estimates for ΔE_v for a glass vary appreciably from that calculated for the liquid. Hence, provisionally and as an unavoidable approximation, one can assume that ΔE_v for the glass and the liquid are the same.

Using Eqs. (1) and (2), we can write the solubility parameter for liquids at 25°C

$$\delta = \left(\frac{\sum_i \Delta e_i}{\sum_i \Delta v_i}\right)^{1/2} \tag{5}$$

and the limiting form for liquids of high molecular weight is

$$\delta = \left(\frac{\Delta e_{ir}}{\Delta v_{ir}}\right)^{1/2} \tag{6}$$

where Δe_{ir} and Δv_{ir} are the contributions for the energy of vaporization and molar volume of the repeating unit, respectively.

Equations (5) and (6) require only a knowledge of the chemical structure in order to estimate δ. A limitation here is that the increments reported in Table 1 have been evaluated at 25°C and hence the δ value can be estimated only for this temperature. However, as will now be demonstrated, it is possible to circumvent this difficulty.

When values of the heat of vaporization ΔH_v are known at one temperature, T_1, these can be converted to the appropriate values at another temperature, T_2, using the following empirical relationship first proposed by Watson (Ref. 12).

$$\frac{\Delta H_{v,T_2}}{\Delta H_{v,T_1}} = \left(\frac{T_c - T_2}{T_c - T_1}\right)^{0.38} \tag{7}$$

where T_c is the critical temperature. Since the heat and energy of vaporization are related by $\Delta H_v = \Delta E_v + RT$, where T is the temperature and R is the gas constant in the appropriate units, it is evident that Eq. (7) may be used to estimate the temperature dependence of ΔE_v and hence δ as

well. However, for high-molecular-weight polymers, the critical temperatures are generally unknown, and consequently, for these materials, Eq. (7) cannot be directly used.

The difficulty can be eliminated by using Dugger's equation (Ref. 13). He has shown that for both polar and nonpolar liquids the dependence of the orthobaric density ($\rho_L - \rho_v$) on temperature is accurately given by

$$\frac{\rho_{L_2} - \rho_{v_2}}{\rho_{L_1} - \rho_{v_1}} = \left(\frac{T_c - T_2}{T_c - T_1}\right)^{0.3} \tag{8}$$

For temperatures at or below the normal boiling point, $\rho_L \gg \rho_v$ (for polymers, this condition will always be valid), and hence ρ_v can be neglected compared to ρ_L.

Using this expression and Eq. (7), the terms involving temperature can be eliminated, and hence,

$$\frac{\Delta H_{v,T_2}}{\Delta H_{v,T_1}} = \left(\frac{\rho_2}{\rho_1}\right)^{1.27} \tag{9}$$

Using the fact that $\Delta H_v = \Delta E_v + RT$, we can write Eq. (7) as

$$\delta_2^2 = \delta_1^2\left(\frac{V_1}{V_2}\right)^{2.27} + \frac{R}{V_2}\left[T_1\left(\frac{V_1}{V_2}\right)^{1.27} - T_2\right] \tag{10}$$

When the temperatures T_1 and T_2 do not differ by more than about 150°C and when both are at or below the normal boiling point of the liquid, then the second term on the right-hand side will be negligible compared to the first and hence

$$\delta_2 = \delta_1\left(\frac{V_1}{V_2}\right)^{1.13} = \delta_1\left(\frac{\rho_2}{\rho_1}\right)^{1.13} \tag{11}$$

This expression provides a means of estimating the temperature dependence of the solubility parameter from a knowledge of the temperature dependence of the density. Another convenient relationship can be developed which involves temperature directly. Over small ranges in temperature, the dependence of volume on temperature is given by

$$V_2 = V_1[1 + \alpha(T_2 - T_1)] \tag{12}$$

where α is the cubical coefficient of expansion. Substituting this relationship into Eq. (11) and expanding the term in parenthesis, we obtain

$$\delta_2 = \delta_1[1 + 1.13\alpha(T_1 - T_2)] \tag{13}$$

This particularly simple expression is valid to within about 2%, provided that $T_1 - T_2$ is less than about 50°C.

References

1. Scatchard, G., *Chem. Revs.* Vol. 8, p. 321, 1931.
2. Hildebrand, J. H., and Scott, R. L., *The Solubility of Nonelectrolytes*, Rheinhold Publishing Corp., New York, 1950.
3. Moacanin, J., et al., "Prediction of Lipid Uptake by Prosthetic Heart Valve Poppets From Solubility Parameters," in *JPL Quarterly Technical Review*, Vol. 1, No. 2, p. 54, Jet Propulsion Laboratory, Pasadena, Calif., July 1971.
4. Landel, R. F., "Permeability of Polymer Films and the Solubility Parameter," in *Supporting Research and Advanced Development*, Space Programs Summary 37-44, Vol. IV p. 104, Jet Propulsion Laboratory, Pasadena, Calif., Apr. 30, 1967.
5. Fedors, R. F., and Landel, R. F., "Mechanical Response of Elastomers Which Exhibit Weak to Moderate Viscoelastic Character," in *Supporting Research and Advanced Development*, Space Programs Summary, 37-55, Vol. III, p. 206, Jet Propulsion Laboratory, Pasadena, Calif., Feb. 28, 1969.
6. Small, P. A., *J. Appl. Chem.* Vol. 3, p. 71, 1953.
7. Dunkel, M., *Z Physik. Chem.* Vol. A138, p. 42, 1928.
8. Bowden, S. T., and Jones, W. J., *Phil. Mag.* Vol. 39, p. 155, 1948.
9. Rheineck, A. E., and Lin, K. F., *J. Paint Tech.* Vol. 40, p. 611, 1968.
10. Hoy, K. L., *J. Paint Tech.*, Vol. 42, p. 76, 1970.
11. Pickett, O. A., Jr., "Physical Constants of Poly(Hexamethylene Adipanide)," in *Polymer Handbook*, J. Brandnep and E. H. Immergut, eds., Interscience Publishers, New York, Sec. VI, p. 79, 1966.
12. Watson, K. M., *Ind. Eng. Chem.* Vol. 23, p. 360, 1931; Vol. 35, p. 398, 1943.
13. Duggar, J. F. Jr., *J. Phys. Chem.* Vol. 62, p. 634, 1958.

Bibliography of Current Reporting

Author Index With Abstracts

Technical Report 32-1526, Vol. XIII, pp. 139–153,
February 15, 1973

This article presents a three-state Markov chain as a model for the errors occurring on the Ground Communications Facility high-frequency wideband channel. An analytic expression for the capacity of the channel in terms of the model parameters is obtained, and comparison is made with the capacity of a binary symmetric channel with the same bit-error rate. For a better understanding of the channel's intrinsic behavior and for use in estimating the performances of different error-detecting and error-correcting codes, we obtain analytic expressions for three sets of channel parameters. These are the bit-error statistics, the block-error statistics, and the distribution of burst lengths and error-free (gap) intervals.

ANDERSON, J. D.

A03 Measurement of General Relativistic Time Delay With Mariners 6 and 7

J. D. Anderson, P. B. Esposito, W. Martin, and
D. O. Muhleman (California Institute of Technology)

Space Research XII, pp. 1623–1630, Akademie-Verlag,
Berlin, 1971

Range and doppler data extending over the interval from August 1969 to December 1970 have been obtained at S-band from Mariners 6 and 7. The range data possess an accuracy of 0.1 μs and constitute the basis of the experimental determination of the relativistic time delay. At superior conjunction, this effect reached a maximum of approximately 200 μs for Mariner 6 and 180 μs for Mariner 7. The prediction of Einstein's theory of general relativity that the propagation of electromagnetic radiation is delayed due to the solar gravitational field has been verified to at least 4%. Non-gravitational forces acting on the spacecraft limit the accuracy of this result. Furthermore, since the solar corona also contributes to a delay in the signal propagation it is important to separate this effect from the relativistic delay. Analysis of the Mariner data indicates a coronal model consistent with those deduced by other methods. Uncertainties in this model as well as the influence of non-modeled forces acting on the spacecraft limit the ultimate precision of the relativity experiment to at best 1%.

ANDERSON, T. O.

A04 DSN Progress Report for November–December 1972: Optimum Control Logic for Successive Approximation Analog-to-Digital Converters

T. O. Anderson

Technical Report 32-1526, Vol. XIII, pp. 168–176, February 15, 1973

Optimum control logic is a popular subject with designers and manufacturers of high-resolution, high-speed, low-cost, modular analog-to-digital converters of the successive-approximation type which are found in abundance in today's module market. With miniaturization being a strong consideration, it may not be long before the complete control logic will be available in a single medium-scale integrated-circuit chip. This article describes designs that may be strong contenders for such chips. One novelty of these designs is found in their optimum logic and minimum component count, considering presently available components. Another novelty is that they are modular or iterative, i.e., the logic structure is the same for all bits. A high-resolution converter logic is then simply an extension of the logic for a low-resolution converter.

BACK, L. H.

B01 Viscous Non-adiabatic Laminar Flow Through a Supersonic Nozzle: Experimental Results and Numerical Calculations

L. H. Back and P. F. Massier

Trans. ASME, Ser. C: J. Heat Transf., Vol. 94, No. 4, pp. 437–445, November 1972

Flow and thermal regimes found in relatively low Reynolds-number flows of high-temperature gases in cooled convergent–divergent nozzles used in propulsion systems and in research facilities are investigated by a combined experimental and numerical approach. The experiments were conducted with argon at temperatures up to 14,200°R, and the throat Reynolds number ranged from 2200 to 2800. The numerical calculations involved the laminar-flow equations in differential form. Taken together, the experiments and the numerical calculations provide information on the pressure, heat-flux, and shear-stress distributions along internal flows with heat transfer, and on the velocity and enthalpy distributions across the flow as well as along the flow. The influence of heat conduction and of the viscous shear extended to the centerline all along the nozzle.

B02 **Shear-Layer Flow Regimes and Wave Instabilities and Reattachment Lengths Downstream of an Abrupt Circular Channel Expansion**

L. H. Back and E. J. Roschke

Trans. ASME, Ser. E: J. Appl. Mech., Vol. 39, No. 3, pp. 677–681, September 1972

This article describes an experimental investigation of water flow through an abrupt circular-channel expansion over a Reynolds number range between 20 and 4200. The shear layer between the central jet and the reverse flow region along the wall downstream behaved differently in the various flow regimes that were observed. With increasing Reynolds number these regimes changed progressively from a laminar flow to an unstable vortex sheetlike flow and then to a more random fluctuating flow. The distance between the step and the reattachment location downstream correspondingly increased, reached a maximum, and then decreased. Of particular significance are the shear layer wave instabilities observed in the shear flow and their relationship to reattachment which apparently has not received much attention previously. Visual observations aided in understanding the results.

BAISLEY, R. L.

B03 **Helicopter Visual Aid System**

R. L. Baisley

JPL Quarterly Technical Review, Vol. 2, No. 4, pp. 72–86, January 1973

The results of an evaluation of police helicopter effectiveness revealed a need for improved visual capability. A JPL program developed a method that would enhance visual observation capability for both day and night usage and demonstrated the feasibility of the adopted approach. This approach made use of remote pointable optics, a display screen, a slaved covert searchlight, and a coupled camera. The approach was proved feasible through field testing and by judgment against evaluation criteria.

BAR-DAVID, I.

B04 **DSN Progress Report for November–December 1972: Performance of Coded, Noncoherent, Hard-Decision MFSK Systems**

I. Bar-David and S. Butman

Technical Report 32-1526, Vol. XIII, pp. 82–91, February 15, 1973

The capacity of noncoherent multifrequency shift-keying (MFSK) systems that use a hard-decision receiver is determined as a function of the predetection signal-to-noise ratio (ST/N_0). For any given predetection signal-to-noise ratio there is an optimum number of frequencies that maximize the system capacity. This optimum number decreases as the predetection signal-to-noise ratio decreases. However, this article shows that this number is never less than 7. This means that binary-frequency shift keying, a commonly used modulation technique at very low data rates, is suboptimum by at least 2.2 dB, compared to the performance obtainable with 7 signals. Similar results are obtained for the computational cut-off R_{comp} when convolutional coding with sequential decoding is used over such an MFSK channel. Use of MFSK channels is expected for entry missions into thick atmospheres, such as those of Venus and Jupiter.

BARATH, F. T.

B05 Microwave Radiometric Measurements of Atmospheric Temperature and Water From an Aircraft

P. W. Rosenkranz, F. T. Barath, J. C. Blinn III, and E. J. Johnston

J. Geophys. Res., Vol. 77, No. 30, pp. 5833–5844, October 20, 1972

For abstract, see Rosenkranz, P. W.

BARTOS, K.

B06 DSN Progress Report for November–December 1972: Hydrostatic Bearing Runner Damage at the Spain 64-m-Diameter Antenna

J. Chapman and K. Bartos

Technical Report 32-1526, Vol. XIII, pp. 219–226, February 15, 1973

For abstract, see Chapman, J.

BECKER, R. A.

B07 Mariner 9 Television Pictures: Microfiche Library User's Guide: MTC/MTVS Real-Time Pictures

R. A. Becker

Technical Memorandum 33-595, February 15, 1973

This memorandum describes the content and organization of the Mariner 9 Mission Test Computer/Mission Test Video System microfiche library. This 775-card library is intended to supply the user with a complete record of the images received from Mars orbit during the Mariner 9 mission operations, November 15, 1971 to November 1, 1972.

BERMAN, A. L.

B08 DSN Progress Report for November–December 1972: Mariner 9 Doppler Noise Study

A. L. Berman

Technical Report 32-1526, Vol. XIII, pp. 227–235, February 15, 1973

This article presents doppler-noise data, as calculated by and compiled from the near-real-time 360/75 pseudo-residual program during the Mariner Mars 1971 mission, as a function of uplink and downlink signal strength. Some observations are made about the nature of this relationship, as well as about the functional dependence of doppler noise on round-trip light time and ground frequency standards.

BERMAN, P. A.

B09 Development of a Thick-Film Silicon Ribbon Growth Technique for Application to Large-Area Solar Cells and Arrays

P. A. Berman

JPL Quarterly Technical Review, Vol. 2, No. 4, pp. 44–52, January 1973

This article describes a new technique for growth of large-area silicon ribbons. This technique is an edge-defined, film-fed growth process by which single crystals can be grown having a shape controlled by the *outside* dimensions of a shaping die, with growth taking place from an extremely thin film of liquid fed by capillary action from a crucible below. The material from which the die is fabricated is very critical to the process. The die must be wet by the silicon, but adverse impurities must not be introduced into the silicon, and the die must not become degraded by the molten silicon. A breakthrough in die fabrication that has allowed the growth of silicon ribbons having dimensions 1 × 30 cm with a thickness of 0.7 mm is described. The implications of

this significant advancement with respect to development of photovoltaic solar arrays for wide-scale terrestrial solar-to-electric energy conversion systems are discussed.

BLINN, J. C., III

B10 Microwave Radiometric Measurements of Atmospheric Temperature and Water From an Aircraft

P. W. Rosenkranz, F. T. Barath, J. C. Blinn III, and E. J. Johnston

J. Geophys. Res., Vol. 77, No. 30, pp. 5833–5844, October 20, 1972

For abstract, see Rosenkranz, P. W.

BOETTGER, H. G.

B11 Negative Ion Mass Spectrometry—A New Analytical Method for Detection of Trinitrotoluene

J. Yinon, H. G. Boettger, and W. P. Weber (University of Southern California)

Anal. Chem., Vol. 44, No. 13, pp. 2235–2237, November 1972

For abstract, see Yinon, J.

B12 Modification of an AEI/GEC MS9 High-Resolution Mass Spectrometer for Electron Impact/Chemical Ionization Studies

J. Yinon and H. G. Boettger

Chem. Instr., Vol. 4, No. 2, pp. 103–113, 1972

For abstract, see Yinon, J.

BOGNER, R. S.

B13 Mariner Mars 1971 Battery Design, Test, and Flight Performance

R. S. Bogner

Technical Memorandum 33-591, April 15, 1973

This memorandum presents the design, development, manufacture, test, and flight performance of the battery used in the Mariner Mars 1971 spacecraft. The 20-A-h nickel–cadmium bat-

tery, capable of delivering over 800 W-h, weighed 29.4 kg and contained 26 cells in series.

BOSE, T. K.

B14 Anode Heat Transfer for a Flowing Argon Plasma at Elevated Electron Temperature

T. K. Bose

Int. J. Heat Mass Transfer, Vol. 15, No. 10, pp. 1745–1763, October 1972

Heat transfer from a pre-ionized gaseous plasma flowing over an anode surface at an elevated electron temperature in the presence of an electric field normal to the surface is investigated theoretically. A laminar boundary layer is considered in which only the velocity profile is locally similar and fluid properties are assumed to change uniformly in the gas flow direction. Results obtained by an approximation method show that for moderate current densities $|j_e| < 10^6$ A/m^2, the velocity and temperature distributions are insensitive to current. In addition, the effect of elevated electron temperature is negligible on convective heat transfer, but is significant for the overall heat transfer due to the enthalpy transport by current. Total heat flux to the anode is obtained by evaluating the Nusselt number and adding terms due to the potential drop in the sheath and the surface work function.

BOURKE, R. D.

B15 Mariner Jupiter/Saturn 1977—The Mission Frame

R. D. Bourke, R. F. Miles, Jr., P. A. Penzo, S. L. Van Dillen, and R. A. Wallace

Astronaut. Aeronaut., Vol. 10, No. 11, pp. 42–49, November 1972

Following cancellation of the Outer Planet Grand Tour Project, NASA and JPL examined alternative missions for exploring the outer planets during the latter 1970s. The alternate mission that proved most attractive scientifically, yet fits within the projected NASA budget, embraces dual flights to Jupiter and Saturn, with launch in 1977. NASA has implemented this mission as the Mariner Jupiter/Saturn 1977 Project. This article presents an evaluation of the various alternative launch opportunities as well as the scientific objectives, technical approach, and description of the Mariner Jupiter/Saturn 1977 mission.

BURLAGE, H., JR.

B16 Unmanned Planetary Spacecraft Chemical Rocket Propulsion

H. Burlage, Jr., W. Gin, and R. W. Riebling

J. Spacecraft Rockets, Vol. 9, No. 10, pp. 729–737, October 1972

To optimize the performance and operational characteristics of an unmanned interplanetary spacecraft for a particular mission, and to achieve high cost effectiveness of the entire system (including launch vehicle), it is important that the type of spacecraft propulsion system to be used matches, as closely as possible, the various requirements and constraints. A universal chemical propulsion system that can do it all well does not seem possible. So a limited number of types that can satisfy the variety of needs anticipated for future interplanetary missions must be made available. Those that are discussed in this article are deemed to be the most promising candidates.

BUTMAN, S.

B17 DSN Progress Report for November–December 1972: Performance of Coded, Noncoherent, Hard-Decision MFSK Systems

I. Bar-David and S. Butman

Technical Report 32-1526, Vol. XIII, pp. 82–91, February 15, 1973

For abstract, see Bar-David, I.

B18 DSN Progress Report for November–December 1972: Efficient Signal Generation for High-Power Dual-Spacecraft Command

S. Butman

Technical Report 32-1526, Vol. XIII, pp. 130–132, February 15, 1973

The possibility of transmitting to two spacecraft simultaneously from a single antenna has arisen in the forthcoming Viking 1975 Project due to mission requirements that will place two orbiters and two landers at Mars. Two of the spacecraft will be simultaneously controlled from the ground. Therefore, there is a requirement that two command signals be sent (on two separate carrier frequencies) from a single transmitter comprised of a single klystron power amplifier and antenna.

This article describes a frequency multiplex scheme that would meet this requirement, and be potentially 1.6 times as efficient (+2 dB) as the one currently under consideration, without exceeding the peak voltage rating of the klystron.

CALLAHAN, P. S.

C01 Near Sun Observations of the Solar Wind

P. S. Callahan, P. F. MacDoran, and A. I. Zygielbaum

Space Research XII, pp. 1529–1533, Akademie-Verlag, Berlin, 1972

A radio technique which exploits the opposite changes of group and phase velocity in a dynamic plasma has been used to study the solar wind during May, June, and July 1970, using the Mariner 6 and 7 spacecraft after their superior conjunctions. The spectrum of the solar wind turbulence in the range 1.6×10^{-4} to 2×10^{-3} Hz has been estimated. The average spectrum falls as $f^{-1.6}$ from 1.6×10^{4} to 6×10^{-4} Hz and then becomes flat. The spectrum shows significant changes from day to day at the low frequencies.

CHANEY, W. D.

C02 DSN Progress Report for November–December 1972: DSN Tracking System: Conversion to High-Speed Radio Metric Data

W. D. Chaney and H. E. Nance

Technical Report 32-1526, Vol. XIII, pp. 5–6, February 15, 1973

At the present time, radio metric data are transmitted from the deep space stations via the teletype mode. To meet future requirements, and to update the transmission mode, the operational concept is scheduled to be changed to utilize the high-speed data transmission facilities. This article outlines the implementation schedule and the testing requirements for providing this new capability.

CHAPMAN, J.

C03 DSN Progress Report for November–December 1972: Hydrostatic Bearing Runner Damage at the Spain 64-m-Diameter Antenna

J. Chapman and K. Bartos

Technical Report 32-1526, Vol. XIII, pp. 219–226, February 15, 1973

On November 12, 1972 the rear pad of the 64-m-diameter antenna in Spain grounded upon a foreign object in the hydrostatic-bearing-runner oil trough. The rear pad and the runner were damaged. The antenna was being operated by the contractor, Collins Radio, Dallas, Texas, while conducting final analog pointing-accuracy tests. This article describes the damage incurred by the three hydrostatic-bearing pads and the runner surfaces and the methods of repair used by the contractor to return the antenna to testing status.

CHEN, C. J.

C04 Measurement of Electron Distribution Function in a Cesium Plasma

C. J. Chen, J. Wu (State University of New York), and F. T. Wu (State University of New York)

J. Appl. Phys., Vol. 43, No. 11, pp. 4570–4573, November 1972

A conventional plane Langmuir probe with dc superimposed on a small sinusoidal signal is used to measure the electron-energy distribution in a cesium discharge tube. The current–voltage characteristics and second-derivative characteristics are obtained for various discharge conditions. The electron-energy distribution at different gas-particle densities and electric fields in the positive column is calculated. The deviation from a Maxwellian distribution is observed for a low gas density and high electric field plasma. The calculation of the distribution function is also carried out by solving numerically the Boltzmann equation with electric field, including the effects of the elastic and inelastic collisions.

CHIRIVELLA, J. E.

C05 ATS-F Radiant Cooler Contamination Test in a Hydrazine Thruster Exhaust

J. E. Chirivella

Technical Memorandum 33-592, April 15, 1973

A test was conducted under simulated space conditions to determine the potential thermal degradation of the Applications Technology Satellite-F radiant cooler from contaminants generated by a 0.44-N (0.1-lbf) hydrazine thruster. The radiant cooler, an aluminum plate simulating the satellite interface, and a 0.44-N (0.1-lbf)

hydrazine engine were assembled to simulate their flight configuration. The cooler was provided with platinum sensors for measuring temperature, and its surfaces were instrumented with six quartz-crystal microbalance (QCM) units to measure contaminant mass deposits. The whole assembly was tested in the molecular-sink vacuum facility at JPL.

This was the first time that a radiant cooler and a hydrazine engine were tested together in a very-high-vacuum space simulator. The engine was subjected to an accelerated duty cycle of 1 pulse/min, and after 2 h of operation, the QCMs began to shift in frequency. The tests continued for several days and, although there was considerable activity in the QCMs, the cooler never experienced thermal degradation. Identification of the contaminants has not been completed to date, but considering the temperature of the radiant cooler surface (greater than 150 K), certain species of gases are immediately eliminated from consideration. Included among the remaining candidates are water, unreacted hydrazine, and ammonium hydrates. The test was the first successful measurement of detectable deposits from hydrazine-rocket-engine plumes in a high vacuum.

CLAY, D. R.

C06 Solar Wind Observations on the Lunar Surface With the Apollo-12 ALSEP

M. Neugebauer, C. W. Snyder, D. R. Clay, and B. E. Goldstein

Planet. Space Sci., Vol. 20, No. 20, pp. 1577–1591, October 1972

For abstract, see Neugebauer, M.

CROW, R. B.

C07 DSN Progress Report for November–December 1972: Block IV Subcarrier Demodulator Assembly Acquisition Problem

R. B. Crow, J. K. Holmes, and R. C. Tausworthe

Technical Report 32-1526, Vol. XIII, pp. 42–47, February 15, 1973

The Block IV subcarrier demodulator assembly (SDA) has been designed with four loop bandwidths. Two of these bandwidths are designed with unity damping, while the other two are achieved by increasing the loop gain. Any one of the four bandwidths can be used for normal tracking, and the "high-gain" bandwidths of

the set may be used for acquisition. The transition from acquisition to tracking mode should be accomplished by providing a slow reduction in gain in order to limit the peak phase error during the transition time. Excessive phase errors can lead to loss of lock or greatly diminished quality of data. This article documents the experiments and analysis that led to the bandwidth-reduction procedure used in the Block IV SDA so that acquisition is complete 80 s after phase lock for the 3.9- to 0.5-Hz configuration and 1300 s after phase lock for the 0.23- to 0.03-Hz configuration.

C08 Improvements in Deep-Space Tracking by Use of Third-Order Loops

R. C. Tausworthe and R. B. Crow

Proceedings of the 1972 International Telemetering Conference, Los Angeles, California, October 10–12, 1972, pp. 577–583

For abstract, see Tausworthe, R. C.

DAVIS, E. K.

D01 DSN Progress Report for November–December 1972: Mariner Venus–Mercury 1973 Mission Support

E. K. Davis

Technical Report 32-1526, Vol. XIII, pp. 26–28, February 15, 1973

During November and December 1972, DSN activities in support of Mariner Venus–Mercury 1973 have concentrated on finalizing ground-system test planning, spacecraft/DSN compatibility test planning, and on continuing implementation. This article summarizes the major accomplishments in the areas of planning, implementation, and testing.

DeMORE, W. B.

D02 Temperature and Pressure Dependence of CO_2 Extinction Coefficients

W. B. DeMore and M. Patapoff

J. Geophys. Res., Space Physics, Vol. 77, No. 31, pp. 6291–6293, November 1, 1972

The extinction coefficients of CO_2 are of particular interest in connection with the Mars atmosphere. This article describes the

measurement of CO_2 extinction coefficients under conditions of temperature and pressure somewhat different from those used for previous measurements. Room temperature data are reported for the wavelength range 1850–2200 Å at pressures of about 3–50 atm. Temperature dependence in the range of about −50 to +50°C was examined at wavelengths down to about 1750 Å. The results show that, whereas pressure effects are generally negligible, temperature dependence is strong enough to invalidate the use of room temperature data for the Mars atmosphere.

D03 **Pressure Dependence and Mechanism of the Reaction of Atomic Oxygen and Carbon Monoxide**

W. B. DeMore

J. Phys. Chem., Vol. 76, No. 24, pp. 3527–3532, November 23, 1972

The rate of the O + CO reaction has been measured at room temperature from 0.74 to 41.9 atm with CO_2 or N_2 as the major third body. The method was based on relative rate measurements, with the O + O_2 reaction as reference. The pressure dependence is more complex than that normally observed for simple atom association reactions. Below 1 atm the reaction appears to be intermediate between second and third order, in agreement with earlier results reported elsewhere. However, at higher pressures a further increase in rate constant is observed. This latter effect is attributed to a reaction path which is negligible at low pressures but which becomes dominant at higher pressures. Detailed mechanisms are suggested.

DIPPREY, D. F.

D04 **Liquid Propellant Rockets**

D. F. Dipprey

Chemistry in Space Research, pp. 465–597, American Elsevier Publishing Company, New York, 1972

Future space missions will require propulsion systems of higher performance, higher reliability for operations extending over periods of years in space, and gross reductions in system costs. Accomplishment of these goals will depend heavily on the efforts of chemists and chemical engineers to better understand the physicochemical processes involved in the production, storage, and combustion of existing and improved liquid propellants.

This article presents a brief overview of the state of knowledge in liquid rocket technology; examples of instances where some fundamental principles of chemistry, fluid mechanics, and mathemat-

ics can be applied; examples of current investigations where chemistry is being applied to this field; and indications of where advances are likely.

EDWARDS, J. N.

E01 DSN Progress Report for November–December 1972: Network Control System

J. N. Edwards

Technical Report 32-1526, Vol. XIII, pp. 209–218, February 15, 1973

A key function of the JPL DSN Network Control System (NCS) is to reduce DSN operating costs while providing the required fiscal year 1974/1975 mission support capability. The NCS Implementation Project Team has been established to fulfill these requirements. This article provides information regarding team responsibilities and activities, and describes both the final and interim NCS configurations and their interfaces.

EMERSON, R. F.

E02 DSN Progress Report for November–December 1972: Programmed Oscillator Software Development for High-Doppler-Rate Orbiting Spacecraft

R. F. Emerson

Technical Report 32-1526, Vol. XIII, pp. 48–53, February 15, 1973

The programmed oscillator can be used to track spacecraft signals. Orbiting spacecraft impose additional requirements upon the ephemeris used by the programmed oscillator; therefore, modifications to the existing programmed oscillator were made. Experience with the tracking of Mariner Mars 1971 during superior conjunction shows that a receiver, assisted by the signal from the programmed oscillator, permits the tracking of high-doppler-rate signals close to the threshold of the receiver. The advantages of programmed-oscillator-assisted receiver operation include the reduction of stress upon the loop voltage-controlled oscillator (VCO), obviating the need for more than one VCO per receiver, and the provision of an acquisition aid for the receiver operators. This was demonstrated during the recent Mariner 1971 solar occultation, where no other tracking method could maintain lock.

E03 DSN Progress Report for November–December 1972: Programmed Oscillator Tracking Accuracy Measurements

R. F. Emerson

Technical Report 32-1526, Vol. XIII, pp. 54–60,
February 15, 1973

The programmed oscillator has previously been shown to accurately track the low doppler rates encountered in cruise-phase spacecraft and planetary radar situations. To determine whether the programmed oscillator would be able to track the high doppler rates encountered with orbiting spacecraft such as Mariner Mars 1971, further tests were conducted which demonstrated that the programmed oscillator does have that capability. These tests further showed that the computations within the program used to drive the oscillator are so precise that no significant degradation in tracking ability is contributed by them.

ESCOBAL, P. R.

E04 3-D Multilateration: A Precision Geodetic Measurement System

P. R. Escobal, K. M. Ong, O. H. von Roos,
M. S. Shumate, R. M. Jaffe, H. F. Fliegel, and
P. M. Muller

Technical Memorandum 33-605, March 15, 1973

This report describes a new technique of satellite geodesy, called 3-D Multilateration, that can determine the relative three dimensional coordinates of ground stations within 1 cm over baselines of 20 to 10,000 km. With this high accuracy, several crucial geodetic applications become possible: earthquake-hazards assessment, precision surveying, plate tectonic s, and orbital applications.

Achievement of such accuracy can be attained through use of pulsed lasers to obtain simultaneous slant-ranges between an ensemble of ground stations and a moving retroreflector whose trajectory is known *a priori* only to the accuracy necessary for aiming the lasers. Numerical analysis has shown that suitably chosen multistation configurations result in well-conditioned solutions, with very small error magnification of the inherent ranging errors occasioned by the hardware subsystem. Laboratory tests have demonstrated that a laser hardware subsystem with a ranging accuracy of 3 cm can be built from commercially available components. By 1975, at the latest, an accuracy level of 1 cm can be achieved.

ESPOSITO, P. B.

E05 Measurement of General Relativistic Time Delay With Mariners 6 and 7

J. D. Anderson, P. B. Esposito, W. Martin, and D. O. Muhleman (California Institute of Technology)

Space Research XII, pp. 1623–1630, Akademie-Verlag, Berlin, 1971

For abstract, see Anderson, J. D.

FLEISCHER, G. E.

F01 Results of Solar Electric Thrust Vector Control System Design, Development, and Tests

G. E. Fleischer

Technical Report 32-1578, February 15, 1973

This report describes efforts recently undertaken to develop and test a thrust-vector control system (TVCS) for a solar-energy-powered ion-engine array. In particular, it summarizes the results of solar–electric propulsion-system technology (SEPST) III real-time tests of present versions of TVCS hardware in combination with computer-simulated attitude dynamics of a solar–electric multi-mission Phase A-type spacecraft configuration. In addition, current work on an improved solar–electric TVCS, based on the use of a state estimator, is described.

The report concludes that the results of SEPST III tests of TVCS hardware have generally proved successful, and the dynamic response of the system is close to predictions. Also, it appears that if TVCS electronic hardware can be effectively replaced by control computer software a significant advantage in control capability and flexibility can be gained in future developmental testing, with practical implications for flight systems as well. Finally, it is concluded from computer simulations that TVCS stabilization using rate estimation promises a substantial performance improvement over the present design.

FLIEGEL, H. F.

F02 3-D Multilateration: A Precision Geodetic Measurement System

P. R. Escobal, K. M. Ong, O. H. von Roos, M. S. Shumate, R. M. Jaffe, H. F. Fliegel, and P. M. Muller

Technical Memorandum 33-605, March 15, 1973

For abstract, see Escobal, P. R.

FRANK, H. A.

F03 Evaluation of New Plastic Compression (Ziegler) Type of Seals for Long-Life Planetary Batteries

H. A. Frank

Technical Memorandum 33-588, February 1, 1973

A program was initiated to develop improved types of terminal seals for aerospace Ni-Cd batteries. The approach used has not involved attempts, such as employed elsewhere, to improve the ceramic-to-metal seal that is now extensively employed for this application. Rather, the approach has been directed toward the development and evaluation of new types of seals. Of prime interest in this initial investigation has been the "Ziegler" type of compression seal and in particular the injection molded version developed by the Bell Telephone Laboratories (BTL).

A number of these units were designed, fabricated, and evaluated on an accelerated life test under a simulated battery environment. Results have shown that there are no major problems involved in scaling up the BTL small-size (5-A) seal to a larger-size (up to 50-A) seal suitable for most JPL flight batteries. Five out of five such seals successfully completed over 10 months of continuous thermal cycling (2-h cycle from -40°C to +71.1°C) without developing any leaks greater than 1.8×10^{-9} atm-cm^3/s of He.

FYMAT, A. L.

F04 Absorption Profile of a Planetary Atmosphere: A Proposal for a Scattering Independent Determination

A. L. Fymat and J. Lenoble (Université des Sciences et Techniques de Lille)

Appl. Opt., Vol. 11, No. 10, pp. 2249–2254, October 1972

The use of scattering theory to infer atmospheric optical parameters requires the separation of absorption and scattering. It is demonstrated that a gradient flux relation exists that would provide the absorption (altitude) profile independently of scattering and irrespective of the state of polarization of the light field. The relation is derived for an atmosphere of plane-parallel or spherical geometry and for broad (continuum) and narrow (spectral line) frequency bands. The results are shown to hold, in particular, for the polarizations induced by both Rayleigh and Mie scattering in

the field. Experimental setups are proposed for each of the cases considered of atmospheric geometry and frequency bandwidth. A final discussion considers the relevance of the present determination of the atmospheric absorption profile to the related problems of aerosol relative concentration, interpretation of radiometric and spectrometric data formed in the presence of scattering, clouds morphology, and radiative heat budget of the atmosphere.

F05 **Interferometric Spectropolarimetry: Alternate Experimental Methods**

A. L. Fymat

Appl. Opt., Vol. 11, No. 10, pp. 2255–2264, October 1972

Three alternate methods of obtaining spectra of the intensity and state of polarization of light are proposed. The methods make use of a two-beam amplitude division interferometer using the technique of Fourier spectroscopy, and can be applied to either emerging beam, source beam, or detector beam, or to both. They do not require the presence of polarizers in the arms of the instrument. In one method (Method 2) a single analyzer is used in front of the detector with three successive orientations of its transmission axis azimuth (0, 45, and 90 deg). In another method (Method 3) a linear polarizer assuming the same set of orientations is placed in the incident beam. A third method (Method 4), a hybrid of the former two methods, makes use of both a polarizer and an analyzer in the locations indicated. The latter method presents itself three alternate possibilities. Method 2 permits the determination of all four Stokes parameters of polarization, whereas Methods 3 and 4 cannot yield the ellipticity parameter.

All methods require the recording of three interferograms. However, two interferograms can provide the intensity and degree of polarization in any of the methods described. The theory of Method 1, reported earlier, is also established more rigorously concerning the proposed interferometric arrangements, the applicability of the method to the source beam, and the possibility of deriving the orientation of the plane of polarization and the ellipticity from a single interferogram.

GARDNER, J. A.

G01 **Solar Electric Propulsion System Integration Technology (SEPSIT) Final Report: Technical Summary**

J. A. Gardner

Technical Memorandum 33-583, Vol. I,
November 15, 1972

The use of solar–electric propulsion (SEP) as a means of exploring space beyond the reach of ballistic missions was investigated in 1972. The method used was to study the application of this new propulsion technology to a future flight project. A 1980 Encke rendezvous mission was chosen because a design successful for Encke could be used for less difficult, but scientifically rewarding, missions. Design points for the mission and for the thrust subsystem were specified, the baseline-vehicle design was defined, and a preliminary functional-description document for the thrust subsystem was originated. Analyses were performed in support of the design point selection for the SEP-module thrust subsystem to specify parameters, to clarify and optimize the interface requirements, and to assure feasibility of some of the more critical technological aspects of SEP application.

GEORGEVIC, R. M.

G02 Analytic Expressions for Perturbations and Partial Derivatives of Range and Range Rate of a Spacecraft With Respect to the Coefficient of the Second Harmonic

R. M. Georgevic

Technical Memorandum 33-594, March 15, 1973

Closed-form analytic expressions for the time variations of instantaneous orbital parameters and of the topocentric range and range rate of a spacecraft moving in the gravitational field of an oblate large body are derived using a first-order variation-of-parameters technique. In addition, the closed-form analytic expressions for the partial derivatives of the topocentric range and range rate are obtained with respect to the coefficient of the second harmonic (J_2) of the potential of the central body. The results are applied to the motion of a point-mass spacecraft moving in orbit around the equatorially elliptic, oblate Sun, with $J_2 \cong 2.7 \times 10^{-5}$.

GIFFIN, C. E.

G03 A Portable Self-Contained Gas Chromatograph

M. R. Stevens, C. E. Giffin, G. R. Shoemake, and
P. G. Simmonds

Rev. Sci. Instr., Vol. 43, No. 10, pp. 1530–1534, October 1972

For abstract, see Stevens, M. R.

GILVARRY, J. J.

G04 Possible Variation of the Gravitational Constant Over the Elements

J. J. Gilvarry and P. M. Muller

Phys. Rev. Lett., Vol. 28, No. 25, pp. 1665–1669, June 19, 1972

This article re-examines the theory and data of a previous experiment, which measured the relative difference $\Delta\kappa/\kappa$ in the gravitational constant κ between the two elements, and cites significant errors in the statistical analysis. The upper bound for F and Br from his experimental data correctly becomes $(\Delta\kappa/\kappa)_{max} = 2 \times 10^{-2}$, about 10 times the limit already set on the general variation of κ over the elements by direct use of a Cavendish balance.

GIN, W.

G05 Unmanned Planetary Spacecraft Chemical Rocket Propulsion

H. Burlage, Jr., W. Gin, and R. W. Riebling

J. Spacecraft Rockets, Vol. 9, No. 10, pp. 729–737, October 1972

For abstract, see Burlage, H., Jr.

GOLDSTEIN, B. E.

G06 Solar Wind Observations on the Lunar Surface With the Apollo-12 ALSEP

M. Neugebauer, C. W. Snyder, D. R. Clay, and B. E. Goldstein

Planet. Space Sci., Vol. 20, No. 20, pp. 1577–1591, October 1972

For abstract, see Neugebauer, M.

GOODWIN, P. S.

G07 DSN Progress Report for November–December 1972: Helios Mission Support

P. S. Goodwin

Technical Report 32-1526, Vol. XIII, pp. 7–20, February 15, 1973

Project Helios is a joint space endeavor between the United States and West Germany. Its objective is to place into heliocentric orbits two unmanned spacecraft which will come closer to the sun than any previously or presently planned Free-World deep-space undertaking. The West German government is designing and fabricating the spacecraft and will conduct mission operations. NASA will provide the launch vehicle, the launch facilities, and the major portion of the tracking and data acquisition. The launch of the first spacecraft is planned for mid-1974 and the second for late 1975.

To ensure proper technical coordination between the activities in West Germany and in the United States, the International Agreement provides for semiannual Helios Joint Working Group Meetings for the exchange of information and for the proper coordination of the activities leading toward launch and subsequent mission operations. This article reports the highlights, with respect to the DSN, of the subjects discussed during the Seventh Helios Joint Working Group Meeting which was held at Porz-Wahn (near Bonn), West Germany, October 25 to 31, 1972.

GREENHALL, C. A.

G08 DSN Progress Report for November–December 1972: Models for Flicker Noise in DSN Oscillators

C. A. Greenhall

Technical Report 32-1526, Vol. XIII, pp. 183–193, February 15, 1973

This article presents a mathematically tractable model for flicker noise. This model is not stationary but has stationary increments, and it is expressed as a limit of stationary processes. It behaves like flicker noise when subjected either to high-pass filtering or to direct spectral measurements, and the effects of a detrending operation on these measurements are investigated. The flicker-noise model of Barnes and Allan is reviewed, and the performances of the two models are compared.

GRENOBLE, D. E.

G09 Unified Approach to the Biomechanics of Dental Implantology

D. E. Grenoble (University of Southern California) and A. C. Knoell

JPL Quarterly Technical Review, Vol. 2, No. 4, pp. 7–17, January 1973

The human need for safe and effective dental implants is well-recognized. Although many implant designs have been tested and are in use today, a large number have resulted in clinical failure. These failures appear to be due to biomechanical effects, as well as biocompatibility and surgical factors.

This article proposes a unified approach, using multidisciplinary systems technology for the study of the biomechanical interactions between dental implants and host tissues. The approach progresses from biomechanical modeling and analysis, supported by experimental investigations, through implant design development, clinical verification, and education of the dental practitioner.

HANSON, R. J.

H01 Integral Equations of Immunology

R. J. Hanson

Commun. ACM, Vol. 15, No. 10, pp. 883–890, October 1972

The inversion of a particular integral equation of the first (Fredholm) kind is the basic problem considered. The strategy which yielded success consisted of three essential points: (1) fit the known experimental data by a curve with properties which derive from properties of the (as yet unknown) function; (2) stabilize the computation for the unknown function by using singular value decomposition; (3) constrain the unknown function approximation (since it represents a probability distribution) to be nonnegative. A number of test cases are presented. One set of actual experimental data is analyzed with the procedures presented.

HEALD, T. C.

H02 Information Management System for the California State Water Resources Control Board (SWRCB)

T. C. Heald and G. H. Redmann

JPL Quarterly Technical Review, Vol. 2, No. 4, pp. 53–61, January 1973

A study was made to establish the requirements for an integrated state-wide information management system for water-quality control and water-quality rights for the State of California. The data sources and end requirements were analyzed for the data collected and used by the numerous agencies, both State and Federal, as well as the nine Regional Boards under the jurisdiction of the State Board. This article details the data interfaces and outlines the system design. A program plan and statement of work for implementation of the project is included.

HOLMES, J. K.

H03 DSN Progress Report for November–December 1972: Block IV Subcarrier Demodulator Assembly Acquisition Problem

R. B. Crow, J. K. Holmes, and R. C. Tausworthe

Technical Report 32-1526, Vol. XIII, pp. 42–47, February 15, 1973

For abstract, see Crow, R. B.

HOTZ, G. M.

H04 A Survey of Actuator Shaft Sealing Techniques for Extended Space Missions

G. M. Hotz

Technical Memorandum 33-587, December 15, 1972

Actuators for control and articulation aboard Mariner spacecraft have employed output-shaft seals to maintain an internal gaseous atmosphere. This, combined with the limitation of temperature extremes through the use of electric heaters or the location of actuators in temperature controlled areas, has resulted in a favorable environment for actuator mechanisms. On future missions, considerably greater expected lifetimes, temperature ranges, and radiation exposures have led to a need to determine the limitations of the present O-ring output-shaft seal and to examine other candidate seals. Seals suited both to dynamic and static sealing were examined for potential use in three specific JPL actuator applications.

HOUSEMAN, J.

H05 Popping Phenomena With the Hydrazine Nitrogen-Tetroxide Propellant System

J. Houseman and A. Lee

J. Spacecraft Rockets, Vol. 9, No. 9, pp. 678–682, September 1972

The propellant spray resulting from the impingement of liquid jets of hydrazine and nitrogen tetroxide has been studied at atmospheric pressure by means of streak photography. The streak photographs show periodic small explosions that originate near the impingement point and propagate through the propellant spray at velocities of 3000 to 5000 ft/s, consuming all propellant droplets over a distance of up to 6 in. Typical streak photographs are presented. The frequency of the explosions or pops ranged up to several hundred per second, and could be controlled by varying the contact time in the liquid phase. Below a minimum threshold contact time, popping did not take place. At high values of contact time, the popping rate was controlled by the transit time of the free jet before impingement. Flashing of the oxidizer prior to impingement prevented popping under certain conditions. It is postulated that popping is initiated by liquid phase reactions. A mechanism for the occurrence of popping and its relation to reactive stream separation is suggested.

HOWE, T. W.

H06 DSN Progress Report for November–December 1972: DSN Support of the Mariner Mars 1971 Extended Mission

T. W. Howe and D. W. Johnson

Technical Report 32-1526, Vol. XIII, pp. 21–25, February 15, 1973

Each mission supported by the DSN is unique. Operations planning normally covers the standard mission only and does not include extended-mission operations. This article describes the innovations that had to be made to support the extended portion of the Mariner Mars 1971 mission.

HUTCHISON, J. J.

H07 Solid Propellants

H. E. Marsh, Jr., and J. J. Hutchison

Chemistry in Space Research, pp. 361–463, American Elsevier Publishing Company, New York, 1972

For abstract, see Marsh, H. E., Jr.

INGHAM, J. D.

I01 Thermoluminescence: Potential Applications in Forensic Science

J. D. Ingham and D. D. Lawson

JPL Quarterly Technical Review, Vol. 2, No. 4, pp. 18–28, January 1973

In crime laboratories one of the most difficult operations is to determine unequivocally whether or not two samples of evidence of the same type were originally part of the same thing or were from the same source. It has been found that high-temperature thermoluminescence (room temperature to 723 K) can be used for comparisons of this type, although work to date indicates that there is generally a finite probability for coincidental matching of glass or soil samples. Further work is required to determine and attempt to minimize these probabilities for different types of materials, and to define more clearly the scope of applicability of thermoluminescence to actual forensic situations.

JACKSON, E. B.

J01 DSN Progress Report for November–December 1972: Development Support Group

E. B. Jackson and A. L. Price

Technical Report 32-1526, Vol. XIII, pp. 127–129, February 15, 1973

This article presents the activities of the Development Support Group in operating the Venus Deep Space Station (DSS 13) and the Microwave Test Facility for the period October 16 through December 15, 1972. Major activities include an extensive test program of dual-uplink carrier generation and measurement of the resulting intermodulation products in the downlink band. A description of the progress of this test program, along with work required to minimize production of intermodulation products, is given. Progress in precision antenna-gain measurements, continuing planetary-radar experiments, and weak-source observations are other activities noted.

JACOBSON, R. A.

J02 Guidance Strategies and Analysis for Low-Thrust Navigation

R. A. Jacobson

Technical Memorandum 33-590, February 1, 1973

This memorandum presents a low-thrust guidance algorithm suitable for operational use. A constrained linear feedback-control law has been obtained using a minimum terminal-miss criterion and restricting control corrections to constant changes for specified time periods. Both fixed- and variable-time-of-arrival guidance were considered. The performance of the guidance law was evaluated by applying it to the approach phase of the 1980 rendezvous mission with the comet Encke.

JAFFE, R. M.

J03 3-D Multilateration: A Precision Geodetic Measurement System

P. R. Escobal, K. M. Ong, O. H. von Roos, M. S. Shumate, R. M. Jaffe, H. F. Fliegel, and P. M. Muller

Technical Memorandum 33-605, March 15, 1973

For abstract, see Escobal, P. R.

JET PROPULSION LABORATORY

J04 Mariner Mars 1971 Project Final Report: Project Development Through Launch and Trajectory Correction Maneuver

Jet Propulsion Laboratory

Technical Report 32-1550, Vol. I, April 1, 1973

The Mariner Mars 1971 mission was another step in the continuing program of planetary exploration in search of evidence of exobiological activity, information on the origin and evolution of the solar system, and basic science data related to the study of planetary physics, geology, planetology, and cosmology. The mission plan was designed for two spacecraft, each performing a separate but complementary mission. However, a single mission plan was actually used for the Mariner 9 due to the failure of the first launch spacecraft.

This report, the first of five volumes of the Mariner Mars 1971 Project Final Report, describes the major pre-operational project

activities, including planning, design, development, and system testing, and the operational activities from spacecraft launch through the Mariner 9 trajectory-correction maneuver.

JOHNSON, D. W.

J05 DSN Progress Report for November–December 1972: DSN Support of the Mariner Mars 1971 Extended Mission

T. W. Howe and D. W. Johnson

Technical Report 32-1526, Vol. XIII, pp. 21–25, February 15, 1973

For abstract, see Howe, T. W.

JOHNSTON, A. R.

J06 Evaluation of the Electro-optic Direction Sensor: Final Report

A. R. Johnston and P. M. Salomon

Technical Memorandum 33-598, February 1, 1973

This memorandum describes the evaluation of a no-moving-parts single-axis star tracker called an electro-optic direction sensor (EODS) and presents the results in detail. The work involved experimental evaluation of a breadboard sensor yielding results which would permit design of a prototype sensor for a specific application. The laboratory work included evaluation of the noise-equivalent input angle of the sensor, demonstration of a technique for producing an acquisition signal, constraints on the useful field-of-view, and a qualitative evaluation of the effects of stray light. In addition, the potential of the silicon avalanche-type photo diode for this application was investigated. No benefit in noise figure was found but the easily adjustable gain of the avalanche device was useful. The use of mechanical tuning of the modulating element to reduce voltage requirements was also explored. The predicted performance of EODS in both photomultiplier and solid-state detector configurations was compared to an existing state-of-the-art star tracker.

J07 An Electro-optic Direction Sensor

A. R. Johnston

J. Spacecraft Rockets, Vol. 9, No. 9, pp. 690–696, September 1972

This article describes a single-axis star sensor in which a wave plate having direction-dependent retardation, together with an

electro-optic modulator, provides the basis for indicating the direction of a distant point source of light. An alternating current photosignal is obtained, thus avoiding problems associated with detector drift. An analysis of the nominal sensor performance is compared with measurement and found to be in good agreement. The effect of varying the optical geometry on field of view is calculated; the effective noise input is evaluated; and satisfactory tracking of a +1 magnitude star with a 1-cm aperture and a photomultiplier detector is demonstrated, showing a signal-to-noise ratio of about 50 on an rms basis.

JOHNSTON, E. J.

J08 Microwave Radiometric Measurements of Atmospheric Temperature and Water From an Aircraft

P. W. Rosenkranz, F. T. Barath, J. C. Blinn III, and E. J. Johnston

J. Geophys. Res., Vol. 77, No. 30, pp. 5833–5844, October 20, 1972

For abstract, see Rosenkranz, P. W.

KATOW, M. S.

K01 DSN Progress Report for November–December 1972: Radial Extension Study of the 64-m-Diameter Antenna

M. S. Katow

Technical Report 32-1526, Vol. XIII, pp. 108–113, February 15, 1973

An increase in the paraboloidal RF capturing area of the 64-m-diameter antenna with minimal increase of the surface distortion may be attractive from the operations standpoint. This article describes a study of the problems involved in increasing an antenna from a 64-m to a 68-m diameter and the resulting distortion increase due to gravity loadings.

KIRSCHMAN, R. K.

K02 Weakly Superconducting, Thin-Film Structures as Radiation Detectors

R. K. Kirschman

Proceedings of the Fifth Applied Superconductivity Conference, Annapolis, Maryland, May 1–3, 1972, pp. 707–708

Weakly superconducting quantum structures are being investigated for use as detectors of microwave and far-infrared radiation in the 0.1–3.0 mm region. A program of experiments has been conducted to determine the sensitivity and frequency response of these structures. This article presents some of the results of the experiments.

KLIMASAUSKAS, C. C.

K03 DSN Progress Report for November–December 1972: A Myopic View of Computer-Based System Design

J. W. Layland and C. C. Klimasauskas

Technical Report 32-1526, Vol. XIII, pp. 154–167, February 15, 1973

For abstract, see Layland, J. W.

KNOELL, A. C.

K04 Unified Approach to the Biomechanics of Dental Implantology

D. E. Grenoble (University of Southern California) and A. C. Knoell

JPL Quarterly Technical Review, Vol. 2, No. 4, pp. 7–17, January 1973

For abstract, see Grenoble, D. E.

LANDEL, R. F.

L01 Thermomechanical Behavior of Rubberlike Materials

T. J. Peng and R. F. Landel

J. Polym. Sci., Pt. A-2: Polym. Phys., Vol. 10, No. 9, pp. 1681–1689, September 1972

For abstract, see Peng, T. J.

LAWSON, D. D.

L02 **Thermoluminescence: Potential Applications in Forensic Science**

J. D. Ingham and D. D. Lawson

JPL Quarterly Technical Review, Vol. 2, No. 4, pp. 18–28, January 1973

For abstract, see Ingham, J. D.

LAYLAND, J. W.

L03 **DSN Progress Report for November–December 1972: A Myopic View of Computer-Based System Design**

J. W. Layland and C. C. Klimasauskas

Technical Report 32-1526, Vol. XIII, pp. 154–167, February 15, 1973

This article presents one approach to the economical allocation of resources in a complex logical system. The main goal is the understanding of systems that may involve specialized digital hardware, a computer with software, and possibly a specialized microcode within the computer processor. These components are treated as uniformly characterizable options in the design of the system that will ultimately be used.

LEE, A.

L04 **Popping Phenomena With the Hydrazine Nitrogen–Tetroxide Propellant System**

J. Houseman and A. Lee

J. Spacecraft Rockets, Vol. 9, No. 9, pp. 678–682, September 1972

For abstract, see Houseman, J.

LENOBLE, J.

L05 **Absorption Profile of a Planetary Atmosphere: A Proposal for a Scattering Independent Determination**

A. L. Fymat and J. Lenoble (Université des Sciences et Techniques de Lille)

Appl. Opt., Vol. 11, No. 10, pp. 2249–2254, October 1972

For abstract, see Fymat, A. L.

LESH, J. R.

L06 DSN Progress Report for November–December 1972: Bandlimited Power of an Asynchronously Biphase-Modulated Squarewave

J. R. Lesh

Technical Report 32-1526, Vol. XIII, pp. 236–238, February 15, 1973

Expressions for the bandlimited power of a square wave which is biphase-modulated by an asynchronous binary data stream are determined by means of spectral integration. This article demonstrates the utility of these expressions through examples using typical Mariner Venus–Mercury 1973 mission parameters.

LINDSEY, W. C.

L07 L-Orthogonal Signal Transmission and Detection

W. C. Lindsey (University of Southern California) and M. K. Simon

IEEE Trans. Commun., Vol. COM-20, No. 5, pp. 953–960, October 1972

This paper investigates the detail capabilities and performance characterization of systems that employ L-orthogonal signaling techniques. L-orthogonal signals represent a unified set of signals wherein the polyphase and orthogonal (biorthogonal) signal sets are included as special cases. This fact is important since orthogonal (biorthogonal) and polyphase signaling sets represent opposing forces as far as tradeoffs between error probability, energy-to-noise ratio, and bandwidth requirements are concerned. Bounds on the performance of the optimum receiver and the performance of various suboptimum (practical) receiver structures are given. Coherent and differentially encoded signals are also pursued. Various comparisons and tradeoffs are made by means of numerical evaluation of the error-probability expressions.

L08 On the Detection of Differentially Encoded Polyphase Signals

W. C. Lindsey (University of Southern California) and M. K. Simon

IEEE Trans. Commun., Vol. COM-20, No. 6, pp. 1121–1128, December 1972

Any digital communication system that employs coherent detection requires coherent reference signals for proper operation. This article discusses the transmission and detection of differen-

tially encoded multiple phase-shift-keyed (MPSK) signals and the ambiguity resolution problem that results from suppression of the transmitted carrier. In particular, the analysis and performance of differentially encoded coherent MPSK systems that reconstruct coherent reference signals by means of generalized Costas or *N*th power loops are presented. The performance of such systems is then compared with that of ideal reception of MPSK signals and differentially coherent detection of differentially encoded MPSK signals. Emphasis is placed upon the special cases of quadriphase and octaphase signaling.

LINNES, K. W.

L09 DSN Progress Report for November–December 1972: Radio Science Support

K. W. Linnes

Technical Report 32-1526, Vol. XIII, pp. 37–41, February 15, 1973

Since 1967, radio scientists have used the DSN 26- and 64-m-diameter antenna stations to investigate pulsars, quasars, and radio galaxies, to study the effect of solar corona on radio signals, and to observe radio emissions from X-ray sources. Very-long-baseline-interferometry (VLBI) techniques have been used for high-resolution studies of quasars. During the reporting period, September–December 1972, VLBI observations of quasars and pulsars were made as part of the Quasar Patrol. Support was also provided by the 64-m-diameter antenna to search for interstellar molecules and to observe radiation from Jupiter.

MacDORAN, P. F.

M01 Near Sun Observations of the Solar Wind

P. S. Callahan, P. F. MacDoran, and A. I. Zygielbaum

Space Research XII, pp. 1529–1533, Akademie-Verlag, Berlin, 1972

For abstract, see Callahan, P. S.

MARKIEWICZ, B. R.

M02 Analysis of the Computed Torque Drive Method and Comparison With Conventional Position Servo for a Computer-Controlled Manipulator

B. R. Markiewicz

Technical Memorandum 33-601, March 15, 1973

A manipulator and its control system (modeled after a Stanford design) is being developed at JPL as part of an artificial intelligence project. The development includes an analytical study of the control system software. This report presents a comparison of the computed-torque method and the conventional position servo. No conclusion is made as to the preference of one system over the other, as this depends upon the application and the results of a sample data analysis.

MARSH, H. E., JR.

M03 Lipid-Absorbing Polymers

H. E. Marsh, Jr., and C. J. Wallace

JPL Quarterly Technical Review, Vol. 2, No. 4, pp. 1–6, January 1973

Present medicinal approaches to cholesterol reduction are indirect. They employ ion exchange to bind bile acids (which are derived from cholesterol by the liver) so that they will be eliminated instead of assimilated.

New polymers have been made that have the unusual property of being capable of absorbing both water and oils. As a result of this property, they are able to absorb lipids from micellar solutions. Lipid absorptions as high as 10% (based on dry polymer weight) in 5 min and 50% at equilibrium have been measured in model bile solutions. The presence of significant amounts of cholesterol, as well as of bile acid, in the absorbed lipids has been confirmed by thin-layer chromatography.

M04 Solid Propellants

H. E. Marsh, Jr., and J. J. Hutchison

Chemistry in Space Research, pp. 361–463, American Elsevier Publishing Company, New York, 1972

Before a new propellant is accepted for extensive use, it naturally must demonstrate advantages over existing propellants and that it can be applied practically at a cost commensurate with its advantages. A number of factors must be considered, such as the propellant energetics, propellant/motor mass fraction, and overall propellant performance. In addition, trade-offs must be evaluated and disadvantageous characteristics reduced, eliminated or compensated for by design. This article discusses the wide range of technological problems involved in the development of new and

improved solid propellants and describes some of the most promising approaches to these problems.

M05 Formulating Propellants for Fully Case-Bonded End-Burning Motors

H. E. Marsh, Jr., and D. E. Udlock

J. Spacecraft Rockets, Vol. 9, No. 9, pp. 625–626, September 1972

A new family of solid propellants is developed which makes possible high performance, fully case-bonded end-burning motors, resulting in an order-of-magnitude improvement in the thrust-to-mass capability of solid propellant rocket motors. This new capability is demanded of solid rocket motors by missions, such as planetary orbit insertion, requiring both low acceleration and large total impulse. Propellants having very high elongation and very low modules are made by means of a new formulating concept without sacrifice in performance and with improved quality control. Structural integrity tests in flight-weight motors have demonstrated this new technology.

MARTIN, W.

M06 Measurement of General Relativistic Time Delay With Mariners 6 and 7

J. D. Anderson, P. B. Esposito, W. Martin, and D. O. Muhleman (California Institute of Technology)

Space Research XII, pp. 1623–1630, Akademie-Verlag, Berlin, 1971

For abstract, see Anderson, J. D.

MASEK, T. D.

M07 Solar Electric Propulsion Thrust Subsystem Development

T. D. Masek

Technical Report 32-1579, March 15, 1973

This report presents the results of the third phase of the JPL Solar-Electric Propulsion System Technology (SEPST III) Program. This phase of the program included about three years of preparation and testing. Of this time, approximately six months were spent in testing a complete, automated thrust subsystem.

The system developed under this program was designed to demonstrate all the thrust subsystem functions thought to be necessary

on an unmanned planetary spacecraft. The demonstration included operation of the basic elements, power matching, input and output voltage regulation, three-axis thrust-vector control, subsystem automatic control including failure detection and correction capability (using a PDP-11 computer), operation of critical elements in thermal-vacuum, zero-gravity-type propellant storage, and data outputs from all subsystem elements. The subsystem elements, functions, unique features, and test setup are described. General features and capabilities of the test-support data system are also presented.

The test program culminated in a 1500-h, computer-controlled, system-functional demonstration that included simultaneous operation of two thruster/power conditioner sets. The results of this testing phase satisfied all the program goals. In particular, the subsystem performed all the expected functions, subsystem efficiency appears to be compatible with spacecraft requirements, projected specific mass is about 17 kg/kW of input power, and the major teletype-switching-system integration problems are understood. This work provides a base for the next phase of subsystem development (i.e., an engineering model).

MASSIER, P. F.

M08 Viscous Non-adiabatic Laminar Flow Through a Supersonic Nozzle: Experimental Results and Numerical Calculations

L. H. Back and P. F. Massier

Trans. ASME, Ser. C: J. Heat Transf., Vol. 94, No. 4, pp. 437–445, November 1972

For abstract, see Back, L. H.

MEDLEY, E. E.

M09 Thermal Decomposition of Aliphatic Monoamino-Monocarboxylic Acids

P. G. Simmonds, E. E. Medley, M. A. Ratcliff, Jr., and G. P. Shulman

Anal. Chem., Vol. 44, No. 12, pp. 2060–2066, October 1972

For abstract, see Simmonds, P. G.

MENICHELLI, V. J.

M10 A High-Efficiency, Small, Solid-State Laser for Pyrotechnic Ignition

L. C. Yang and V. J. Menichelli

JPL Quarterly Technical Review, Vol. 2, No. 4, pp. 29–37, January 1973

For abstract, see Yang, L. C.

M11 Generation of Narrow High Current Pulses

V. J. Menichelli and L. A. Rosenthal

JPL Quarterly Technical Review, Vol. 2, No. 4, pp. 38–43, January 1973

Many of the fundamental factors affecting the initiation of electroexplosive devices have not been satisfactorily explained. This article describes a narrow, high-current pulse generator capable of 94-A pulses 4 μs wide and which will be useful in the study of the initiation mechanism.

MENZIES, R. T.

M12 Remote Sensing With Infra-red Heterodyne Radiometers

R. T. Menzies

Opto-electronics, Vol. 4, No. 2, pp. 179–186, May 1972

The narrow spectral bandwidth capability of heterodyne radiometers can be utilized to construct highly selective pollutant sensing instruments. The infrared spectral region is favorable due to the availability of pollutant absorption lines and the wavelength dependence of heterodyne sensitivity. This article reviews the types of sensing systems that can make use of heterodyne techniques, including comments about the type of lasers that can serve as local oscillators. Sensitivity calculations of passive heterodyne radiometers to NO, CO_2, and SO_2 are then presented. The concluding discussion involves the use of a heterodyne receiver in an active NO sensing system which is based on infrared fluorescence.

MICCIO, J. A.

M13 DSN Progress Report for November–December 1972: The Traceability and Reporting Program: Mariner Mars 1971—Integration, Review, Evolution

J. A. Miccio

Technical Report 32-1526, Vol. XIII, pp. 239–243, February 15, 1973

The traceability and reporting program (TARP) is the basic support software utilized by the DSN Operational Data Center (ODC). It is used during mission operations to provide administrative control and selective dissemination of information concerning transferable DSN mission-data products. Significant qualitative information relative to data-record production, quality, logistics, and recycleability status are entered into the data base with respective operational data. Data records covered in TARP consist of original, system, and master magnetic tapes with supplemental microfilmed hard-copy records.

This article reviews the execution of this program in support of Mariner Mars 1971 operations. It also describes the evolution of the program through Mariner Mars 1971 and into its current status, and presents the planned configuration for Pioneer G and Mariner Venus–Mercury 1973 mission support. The program's current organization structure is adaptive to both mission-operation support and management-information support environments. Thus, concurrent efforts are being expended on the adaptability of the present system to data-management systems involved in hierarchical reporting relationships concerned with user–operations–management interfaces.

MILES, R. F., JR.

M14 Mariner Jupiter/Saturn 1977—The Mission Frame

R. D. Bourke, R. F. Miles, Jr., P. A. Penzo, S. L. Van Dillen, and R. A. Wallace

Astronaut. Aeronaut., Vol. 10, No. 11, pp. 42–49, November 1972

For abstract, see Bourke, R. D.

MINOVITCH, M. A.

M15 Gravity Thrust Jupiter Orbiter Trajectories Generated by Encountering the Galilean Satellites

M. A. Minovitch

J. Spacecraft Rockets, Vol. 9, No. 10, pp. 751–756, October 1972

A trajectory design philosophy is introduced for Jupiter orbiter missions that is based on the gravity thrust concept developed for interplanetary trajectories. This is accomplished by utilizing the

moving gravitational fields of the four Galilean satellites. A general theorem, applicable to any existing planetary satellite system, is developed to show how the effects of small satellite perturbations can be magnified by incorporating multiple revolutions between encounters.

MUDGWAY, D. J.

M16 DSN Progress Report for November–December 1972: Viking Mission Support

D. J. Mudgway

Technical Report 32-1526, Vol. XIII, pp. 29–36, February 15, 1973

DSN support for Viking remains in the transitional phase between planning and commitment and the early stages of implementation. Existing implementation schedules have been thoroughly reworked to reconcile desired operational-readiness dates with anticipated DSN manpower and funding resources. Investigation of downlink interference effects in a dual-carrier environment continued to make progress at the Venus Deep Space Station (DSS 13). The network configuration for the DSN Test and Training System is described.

MUHLEMAN, D. O.

M17 Measurement of General Relativistic Time Delay With Mariners 6 and 7

J. D. Anderson, P. B. Esposito, W. Martin, and D. O. Muhleman (California Institute of Technology)

Space Research XII, pp. 1623–1630, Akademie-Verlag, Berlin, 1971

For abstract, see Anderson, J. D.

MULLER, P. M.

M18 3-D Multilateration: A Precision Geodetic Measurement System

P. R. Escobal, K. M. Ong, O. H. von Roos, M. S. Shumate, R. M. Jaffe, H. F. Fliegel, and P. M. Muller

Technical Memorandum 33-605, March 15, 1973

For abstract, see Escobal, P. R.

M19 **Possible Variation of the Gravitational Constant Over the Elements**

J. J. Gilvarry and P. M. Muller

Phys. Rev. Lett., Vol. 28, No. 25, pp. 1665–1669, June 19, 1972

For abstract, see Gilvarry, J. J.

NANCE, H. E.

N01 **DSN Progress Report for November–December 1972: DSN Tracking System: Conversion to High-Speed Radio Metric Data**

W. D. Chaney and H. E. Nance

Technical Report 32-1526, Vol. XIII, pp. 5–6, February 15, 1973

For abstract, see Chaney, W. D.

NERHEIM, N. M.

N02 **Supersonic Electrical-Discharge Copper Vapor Laser**

G. R. Russell, N. M. Nerheim, and T. J. Pivirotto

Appl. Phys. Lett., Vol. 21, No. 12, pp. 565–567, December 15, 1972

For abstract, see Russell, G. R.

NEUGEBAUER, M.

N03 **Solar Wind Observations on the Lunar Surface With the Apollo-12 ALSEP**

M. Neugebauer, C. W. Snyder, D. R. Clay, and B. E. Goldstein

Planet. Space Sci., Vol. 20, No. 20, pp. 1577–1591, October 1972

The Apollo-12 ALSEP solar wind spectrometer obtained data from the lunar surface starting November 20, 1969. To a first approximation, the general features of the positive ion flux depend only on the instrument's orientation and location in space relative to the Sun–Earth system. However, there are some detectable effects of the interaction of the solar wind with the local magnetic field and surface, including the deceleration of incident positive ions and the enhancement of fluctuations in the plasma.

The expected asymmetry of sunset and sunrise times due to the motion of the Moon about the Sun is not observed. On one occasion, the solar wind was incident on the ALSEP site as early as 36 h (18°) before sunrise.

ONG, K. M.

001 3-D Multilateration: A Precision Geodetic Measurement System

P. R. Escobal, K. M. Ong, O. H. von Roos, M. S. Shumate, R. M. Jaffe, H. F. Fliegel, and P. M. Muller

Technical Memorandum 33-605, March 15, 1973

For abstract, see Escobal, P. R.

OTOSHI, T. Y.

002 DSN Progress Report for November–December 1972: S/X-Band Experiment: Development of Special Telecommunications Development Laboratory Support Test Equipment

T. Y. Otoshi and O. B. Parham

Technical Report 32-1526, Vol. XIII, pp. 72–81, February 15, 1973

This article documents the design of an X-band down converter and a doppler-extractor receiver that were specially developed and supplied to the Telecommunications Development Laboratory in July 1971. The special equipment enabled preliminary tests to be made on the performance of a combined S/X-band radio system similar to that which will be used for the Mariner Venus–Mercury 1973 mission.

003 Precision Reflectivity Loss Measurements of Perforated-Plate Mesh Materials by a Waveguide Technique

T. Y. Otoshi

IEEE Trans. Instr. Meas., Vol. IM-21, No. 4, pp. 451–457, November 1972

A waveguide method is described for improving the precision and accuracy of reflectivity loss measurements of perforated-plate mesh materials. Overall accuracies of the order of ±0.005 dB can be achieved through the use of a dual-channel tuned reflectometer system and high-precision insertion loss test set.

PARHAM, O. B.

P01 DSN Progress Report for November–December 1972: S/X-Band Experiment: Development of Special Telecommunications Development Laboratory Support Test Equipment

T. Y. Otoshi and O. B. Parham

Technical Report 32-1526, Vol. XIII, pp. 72–81, February 15, 1973

For abstract, see Otoshi, T. Y.

PARTHASARATHY, S. P.

P02 Evaluation of the Noise Autocorrelation Function of Stationary and Moving Noise Sources by a Cross Correlation Method

S. P. Parthasarathy

AIAA Preprint 73-186, AIAA Eleventh Aerospace Sciences Meeting, Washington, D.C., January 10–12, 1973

This article presents a theory for the evaluation of the autocorrelation function (or intensity and spectrum) in the frame of reference of motion of noise sources from known cross correlations. Stationary sources are considered first and then the theory is extended to moving sources such as those that occur in both subsonic and in supersonic jet flows. This method of obtaining the autocorrelation is illustrated by application to a high-temperature subsonic jet flow. The experimental values of the cross correlation obtained in the noise field are used together with a least squares method of inversion to determine the autocorrelation as a function of time and time delay.

PATAPOFF, M.

P03 Temperature and Pressure Dependence of CO_2 Extinction Coefficients

W. B. DeMore and M. Patapoff

J. Geophys. Res., Space Physics, Vol. 77, No. 31, pp. 6291–6293, November 1, 1972

For abstract, see DeMore, W. B.

PAUL, C. K.

P04 Theoretical Weighting of Photogrammetric Equations

C. K. Paul

J. Surveying Mapping Div., Proc. ASCE, Vol. 98, No. SU2, pp. 127–135, November 1972

The fundamental resection formulas of photogrammetry suggest a weighting scheme based on the standard deviations of the ratios of image coordinates to focal length. These ratios are functions of random variables having *a posteriori* means and variances. A theoretical development and formulation of the standard deviations of these ratios indicate that (1) the weights are maximum at the photo principal point and decrease toward the photoedges; and (2) the range of weight factors from center to edge is greater for smaller focal lengths. Weights vary by a factor of 2.00 for a camera focal length of 75 mm, 1.64 for a 100 mm focal length, 1.44 for 125 mm, 1.32 for 150 mm, 1.09 for 300 mm, 1.04 for 450 mm, and 1.02 for 600 mm.

PENG, T. J.

P05 Thermomechanical Behavior of Rubberlike Materials

T. J. Peng and R. F. Landel

J. Polym. Sci., Pt. A-2: Polym. Phys., Vol. 10, No. 9, pp. 1681–1689, September 1972

A simple form of nonisothermal free energy function $A(\lambda_1, \lambda_2, \lambda_3, T)$ for rubberlike materials results from postulating that the entropy is a separable symmetric function of the extension ratios λ_i along the principal strain directions and considering the fundamental properties of rubberlike materials, i.e., that rubber elasticity is associated primarily with changes in entropy and the variation of elastic tension with changes in temperature is linear. The explicit representation of A is reduced to the Valanis–Landel strain energy function for isothermal cases.

PENZO, P. A.

P06 Mariner Jupiter/Saturn 1977—The Mission Frame

R. D. Bourke, R. F. Miles, Jr., P. A. Penzo, S. L. Van Dillen, and R. A. Wallace

Astronaut. Aeronaut., Vol. 10, No. 11, pp. 42–49, November 1972

For abstract, see Bourke, R. D.

PHILLIPS, W. M.

P07 Postoperational Examination of an Externally Configured Thermionic Converter

W. M. Phillips

Technical Memorandum 33-597, March 15, 1973

An externally configured thermionic converter was operated for 200 h. The converter was disassembled and examined to determine internal changes as a result of operation. The metal/ceramic seals and all joints were unaffected by operation. Converter output voltage and operation time were sufficient to produce electrolysis of stabilized zirconia spacers used in the converter.

Surface analysis of the electrode surfaces indicated the presence of only oxygen, carbon, and silicon on the tungsten emitter. The niobium collector was, however, 25 to 40% covered with other elements. This coverage was composed of all elements present within the converter as construction materials except for silicon and tungsten, which were not detected on the collector, and carbon, which was detected only in small amounts.

P08 Uranium Nitride Behavior at Thermionic Temperatures

W. M. Phillips

Technical Memorandum 33-602, April 1, 1973

The feasibility of using uranium nitride for in-core thermionic applications was evaluated in electrically heated thermal-gradient tests and in flat-plate thermionic converters. These tests indicated that grain-boundary penetration of uranium nitride into both tungsten and rhenium will occur under thermal-gradient conditions. In the case of the tungsten thermionic converter, this led to grain-boundary rupture of the emitter and almost total loss of electrical output from the converter. It appears that uranium nitride is unsuitable for thermionic applications at the 2000 K temperatures used in these tests.

PICKERING, W. H.

P09 Some Practical Considerations in Technology Transfer

W. H. Pickering

AAS (American Astronautical Society) Science and Technology Book Series, Vol. 29, pp. 39–46, 1972

This article discusses the need for an effective transfer of the massive technological output of government science, resulting

from space exploration, to the nation's socio-economic structure. Large-scale recommendations are offered, including magnitude, scope, and levels of transfer. A stronger commitment to technological transfer at every level of government is urged, as well as a scientific, engineering, and technological evaluation of the total situation in a systems sense.

PIVIROTTO, T. J.

P10 Supersonic Electrical-Discharge Copper Vapor Laser

G. R. Russell, N. M. Nerheim, and T. J. Pivirotto

Appl. Phys. Lett., Vol. 21, No. 12, pp. 565–567, December 15, 1972

For abstract, see Russell, G. R.

POTTER, P. D.

P11 DSN Progress Report for November–December 1972: Efficient Antenna Systems: A New Computer Program for the Design and Analysis of High-Performance Conical Feedhorns

P. D. Potter

Technical Report 32-1526, Vol. XIII, pp. 92–107, February 15, 1973

It is well known that paraboloidal-antenna aperture efficiency is enhanced by providing aperture illumination which approaches uniformity in amplitude, phase, and polarization. For dual-reflector antenna systems, such as those used in the DSN, a high degree of uniformity is possible by use of specially shaped reflector surfaces. As a long-range solution to the problem of achieving high aperture efficiency, this approach is attractive because it is inherently broadband and requires only a simple feedhorn of the type presently being utilized in the DSN.

An alternate approach for achieving high aperture efficiency involves use of the existing antenna reflecting surfaces together with a more complex multimode feedhorn. This approach is attractive from an implementation standpoint. Preliminary experimental results are promising. The multimode technique does, however, suffer from bandwidth difficulties, at least with presently known mode-generation techniques. To assist and guide the multimode-feedhorn experimental effort, a new computer program has been developed which computes horn radiation patterns and bandwidth properties as a function of horn geometry. This article

describes the analytical technique utilized and the agreement with existing experimental data.

POWELL, W. B.

P12 Simplified Procedures for Correlation of Experimentally Measured and Predicted Thrust Chamber Performance

W. B. Powell

Technical Memorandum 33-548, April 1, 1973

Thrust-chamber performance should be evaluated in terms of an analytical model incorporating all the loss processes that occur in a real rocket motor. The Joint Army-Navy-NASA-Air Force (JANNAF) Performance Standardization Working Group has identified the important loss processes in the real thrust chamber, and has developed a methodology and a recommended procedure for predicting real thrust-chamber vacuum specific impulse.

Simplified equations, based on the JANNAF reference procedure for calculating vacuum specific impulse, are developed to relate the delivered performance (both vacuum specific impulse and characteristic velocity) to the ideal performance as degraded by the losses corresponding to a specified list of loss processes. These simplified equations enable the various performance loss components, and the corresponding efficiencies, to be quantified separately (except that interaction effects are necessarily arbitrarily assigned in the process).

The loss and efficiency expressions presented can be used to evaluate experimentally measured thrust-chamber performance, to direct development effort into the areas most likely to yield improvements in performance, and to predict performance of related thrust-chamber configurations.

PRICE, A. L.

P13 DSN Progress Report for November–December 1972: Development Support Group

E. B. Jackson and A. L. Price

Technical Report 32-1526, Vol. XIII, pp. 127–129, February 15, 1973

For abstract, see Jackson, E. B.

PURDUE, R. E.

P14 Tracking and Data System Support for the Pioneer Project: Pioneer 10—Prelaunch Planning Through Second Trajectory Correction: December 4, 1969 to April 1, 1972

A. J. Siegmeth, R. E. Purdue, and R. E. Ryan

Technical Memorandum 33-584, Vol. I, April 1, 1973

For abstract, see Siegmeth, A. J.

RANSFORD, G. A.

R01 Moon Model—An Offset Core

G. A. Ransford and W. L. Sjogren

Nature, Vol. 238, No. 5362, pp. 260–262, August 4, 1972

This article utilizes a lunar model with an asymmetric core to explain the Moon's offset center of gravity, moments of inertia, mascons, maria basins, igneous rocks, and remanent magnetism. A possible evolution theory is also presented.

RATCLIFF, M. A., JR.

R02 Thermal Decomposition of Aliphatic Monoamino-Monocarboxylic Acids

P. G. Simmonds, E. E. Medley, M. A. Ratcliff, Jr., and G. P. Shulman

Anal. Chem., Vol. 44, No. 12, pp. 2060–2066, October 1972

For abstract, see Simmonds, P. G.

REDMANN, G. H.

R03 Information Management System for the California State Water Resources Control Board (SWRCB)

T. C. Heald and G. H. Redmann

JPL Quarterly Technical Review, Vol. 2, No. 4, pp. 53–61, January 1973

For abstract, see Heald, T. C.

RENZETTI, N. A.

R04 DSN Progress Report for November–December 1972: DSN Functions and Facilities

N. A. Renzetti

Technical Report 32-1526, Vol. XIII, pp. 1–4, February 15, 1973

The Deep Space Network (DSN), established by the NASA Office of Tracking and Data Acquisition and under the system management and technical direction of JPL, is designed for two-way communications with unmanned spacecraft traveling approximately 16,000 km (10,000 mi) from Earth to planetary distances. The objectives, functions, and organization of the DSN are summarized, and the Deep Space Instrumentation Facility, the Ground Communications Facility, and the Network Control System are described.

RHOADS, J. W.

R05 A Technique for Computation of Star Magnitudes Relative to an Optical Sensor

J. W. Rhoads

Technical Memorandum 33-586, December 30, 1972

This memorandum describes the theory and techniques used to compute star magnitudes relative to any optical detector (such as the Mariner Mars 1971 Canopus star tracker). Results for various star detectors are presented.

RIEBLING, R. W.

R06 Unmanned Planetary Spacecraft Chemical Rocket Propulsion

H. Burlage, Jr., W. Gin, and R. W. Riebling

J. Spacecraft Rockets, Vol. 9, No. 10, pp. 729–737, October 1972

For abstract, see Burlage, H., Jr.

ROSCHKE, E. J.

R07 Shear-Layer Flow Regimes and Wave Instabilities and Reattachment Lengths Downstream of an Abrupt Circular Channel Expansion

L. H. Back and E. J. Roschke

Trans. ASME, Ser. E: J. Appl. Mech., Vol. 39, No. 3, pp. 677–681, September 1972

For abstract, see Back, L. H.

ROSENKRANZ, P. W.

R08 Microwave Radiometric Measurements of Atmospheric Temperature and Water From an Aircraft

P. W. Rosenkranz, F. T. Barath, J. C. Blinn III, and E. J. Johnston

J. Geophys. Res., Vol. 77, No. 30, pp. 5833–5844, October 20, 1972

A five-channel microwave spectrometer operating near the 1.35-cm wavelength water vapor and the 5-mm wavelength oxygen resonances was flown in the NASA Convair 990 aircraft at altitudes near 12 km and used to infer layer thicknesses, water vapor, and liquid water abundances in the troposphere. The calibration of the spectrometer and a multiple regression method of interpretation of the data obtained from the flights are described. Possible errors from clouds and from the terrestrial surface are discussed. Values of atmospheric layer thicknesses, water vapor content, and liquid water content inferred from microwave data obtained over two frontal systems are presented. The inferred values of 1000- to 500-mb and 500- to 250-mb thicknesses agree with directly measured values to within 15 m at the places where the direct measurements were made. This agreement is equivalent to errors $<1°K$ in mean temperature.

R09 Microwave Emissivity of Ocean Foam and Its Effect on Nadiral Radiometric Measurements

P. W. Rosenkranz and D. H. Staelin (Massachusetts Institute of Technology)

J. Geophys. Res., Vol. 77, No. 33, pp. 6528–6538, November 20, 1972

Emissivities at a normal look angle have been computed for two models of ocean foam: a porous dielectric and a series of thin water films. The two models give nearly the same results for low foam densities. They show an emissivity spectrum that is roughly constant from 20 to 60 GHz and that tends to decrease at lower frequencies, depending on the thickness and density of the foam. A whitecap model (with graded density) shows less change of emissivity with frequency. Radiometric measurements are described that show the increased emissivity of rough seas due to white water at frequencies of 10.7, 19.4, 22.2, and 31.4 GHz. The

effect of increased emissivity of the surface on radiometrically inferred values of atmospheric parameters such as water vapor and liquid water contents is discussed.

ROSENTHAL, L. A.

R10 Generation of Narrow High Current Pulses

V. J. Menichelli and L. A. Rosenthal

JPL Quarterly Technical Review, Vol. 2, No. 4, pp. 38–43, January 1973

For abstract, see Menichelli, V. J.

ROURKE, K. H.

R11 DSN Progress Report for November–December 1972: Filtering Dual-Frequency Radio Metric Data

K. H. Rourke

Technical Report 32-1526, Vol. XIII, pp. 66–71, February 15, 1973

This article introduces a technique for reducing the effect of ionospheric and space-plasma charged particles on radio metric measurements. Development of the method is motivated by the difficulty in obtaining complete, two-way range calibrations when dual-frequency measurements are available for only the radio downlink. Using least-squares theory, estimation techniques are derived that allow the downlink calibration to be "fed back" to correct unobserved uplink errors. Plausible numerical examples are presented, indicating that such techniques are applicable to precision range measurements of two-station tracking.

RUSCH, W. V. T.

R12 Net-Field Polarization in a Magnetically Biased Plasma

W. V. T. Rusch (University of Southern California) and C. T. Stelzried

Radio Sci., Vol. 7, No. 12, pp. 1131–1141, December 1972

The net-field polarization of a plane wave propagating in a magnetically biased cold plasma has been treated in a systematic fashion. Under quasi-longitudinal conditions the polarization transformations are particularly simple and as such have been treated in the literature. However, under more general conditions the polarization transformations are relatively complex. The axial

ratio, tilt angle, rotation rate, and polarization sense all become functions of the initial conditions and the constants of the medium. Under quasi-longitudinal conditions the polarization ellipse rocks between two extremes, while the axial ratio also changes periodically between a minimum and a maximum value. The wide variety of polarization transformations available suggests the usefulness of slabs of magnetically biased plasma to synthesize microwave polarizers and depolarizers. The theory of net-field polarization when applied to data obtained during the 1968 solar occultation of Pioneer 6 verified that the usual quasi-longitudinal approximation (Faraday rotation) is adequate to describe S-band polarization in the solar corona.

RUSSELL, G. R.

R13 Supersonic Electrical-Discharge Copper Vapor Laser

G. R. Russell, N. M. Nerheim, and T. J. Pivirotto

Appl. Phys. Lett., Vol. 21, No. 12, pp. 565–567, December 15, 1972

A copper vapor laser, utilizing a pulsed discharge transverse to a supersonic flow of copper vapor, argon, and helium and oscillating at 5106 and 5782 Å, has been built and tested. Laser energy densities per pulse of 2.5 μJ cm^{-3} have been achieved to date. Laser pulse widths of up to 185 ns have been obtained with delay times after initiation of the current pulse of 220–250 ns. Both the delay time and pulse width are in good agreement with theoretical predictions. Quenching of the laser pulse is shown to be due to a rapid increase in the differential pumping of the lasing levels from the ground state because of a decay in the electron temperature.

RYAN, R. E.

R14 Tracking and Data System Support for the Pioneer Project: Pioneer 10—Prelaunch Planning Through Second Trajectory Correction: December 4, 1969 to April 1, 1972

A. J. Siegmeth, R. E. Purdue, and R. E. Ryan

Technical Memorandum 33-584, Vol. I, April 1, 1973

For abstract, see Siegmeth, A. J.

SALOMON, P. M.

S01 Evaluation of the Electro-optic Direction Sensor: Final Report

A. R. Johnston and P. M. Salomon

Technical Memorandum 33-598, February 1, 1973

For abstract, see Johnston, A. R.

SAVAGE, J. E.

S02 DSN Progress Report for November–December 1972: Matrix Multiplication With Fixed Matrices and Polynomial Evaluation With Fixed Polynomials

J. E. Savage

Technical Report 32-1526, Vol. XIII, pp. 194–202, February 15, 1973

It has been shown that the conventional method for computing $m \times n$ matrix–vector products and Horner's rule for evaluating polynomials are optimal when matrix and vector elements as well as polynomial coefficients and polynomial variables are indeterminate. This article treats the calculation of matrix–vector products and the evaluation of polynomials when the matrix elements and polynomial coefficients are known and drawn from a set of size s. It is shown that the algorithms which are optimal for indeterminate matrix entries and polynomial coefficients are nonoptimal when s is fixed and the entries and coefficients are known. Good algorithms for this case are given and tight bounds are derived on the combinational complexity of the most complex matrix–vector function and the most complex polynomial-evaluation function.

SCHINDLER, R. A.

S03 An Interference Spectrometer for the Remote Sensing of Pollutants

R. A. Schindler

J. Spacecraft Rockets, Vol. 9, No. 9, pp. 714–715, September 1972

A small, high-resolution interference spectrometer for sensing environmental pollutants from spacecraft or aircraft has been developed. The instrument takes less than 3 min to generate an interferogram of the electromagnetic radiation in the 1.2–5.5 μ wavelength interval (8000–1800 cm^{-1}) which can be transformed into a spectrum displaying a resolution 0.2 cm^{-1}. The high speed with which the interferogram can be recorded is sufficient to

make the instrument usable in a 1000-km altitude polar orbiting satellite for a global survey of pollutants. The resolution capability and wavelength coverage is such that unequivocable identifications and concentration measurements can be made of many molecules such as CO, NO_2 and O_3 by the methods of high-resolution IR spectroscopy.

SCHUMACHER, L.

S04 Mariner Mars 1971 Attitude Control Subsystem Flight Performance

L. Schumacher

Technical Memorandum 33-600, March 15, 1973

This report describes the flight performance of the Mariner Mars 1971 Attitude Control Subsystem. Each phase of the mission is delineated and the attitude control subsystem performance is evaluated within the observed operational environment. Performance anomalies are introduced and discussed briefly within the context of general performance. More serious problems, such as the sun-sensor-interface incompatibility, gas-valve leaks, and scan-platform dynamic-coupling effects are given detailed analytical consideration. It is concluded that the Mariner Mars 1971 attitude control subsystem flight performance was satisfactory.

SHINOZUKA, M.

S05 On the First-Excursion Probability in Stationary Narrow-Band Random Vibration, II

J.-N. Yang and M. Shinozuka (Columbia University)

Trans. ASME, Ser. E: J. Appl. Mech., Vol. 39, No. 3, pp. 733–738, September 1972

For abstract, see Yang, J.-N.

SHOEMAKE, G. R.

S06 A Portable Self-Contained Gas Chromatograph

M. R. Stevens, C. E. Giffin, G. R. Shoemake, and P. G. Simmonds

Rev. Sci. Instr., Vol. 43, No. 10, pp. 1530–1534, October 1972

For abstract, see Stevens, M. R.

SHULMAN, G. P.

S07 Thermal Decomposition of Aliphatic Monoamino-Monocarboxylic Acids

P. G. Simmonds, E. E. Medley, M. A. Ratcliff, Jr., and G. P. Shulman

Anal. Chem., Vol. 44, No. 12, pp. 2060–2066, October 1972

For abstract, see Simmonds, P. G.

SHUMATE, M. S.

S08 3-D Multilateration: A Precision Geodetic Measurement System

P. R. Escobal, K. M. Ong, O. H. von Roos, M. S. Shumate, R. M. Jaffe, H. F. Fliegel, and P. M. Muller

Technical Memorandum 33-605, March 15, 1973

For abstract, see Escobal, P. R.

SIEGMETH, A. J.

S09 Tracking and Data System Support for the Pioneer Project: Pioneer 10—Prelaunch Planning Through Second Trajectory Correction: December 4, 1969 to April 1, 1972

A. J. Siegmeth, R. E. Purdue, and R. E. Ryan

Technical Memorandum 33-584, Vol. I, April 1, 1973

This report describes the Tracking and Data System support of the launch, near-Earth, and deep-space phases (through second trajectory correction) of the Pioneer 10 mission, which sent a Pioneer spacecraft into a flyby of Jupiter that would eventually allow the spacecraft to escape the solar system. During this period, scientific instruments aboard the spacecraft registered information about interplanetary particles and fields, and the radio metric data generated by the DSN continued to improve our knowledge of the celestial mechanics of the solar system. In addition to network-support activity detail, network performance and special support activities are covered.

SIMMONDS, P. G.

S10 Thermal Decomposition of Aliphatic Monoamino-Monocarboxylic Acids

P. G. Simmonds, E. E. Medley, M. A. Ratcliff, Jr., and G. P. Shulman

Anal. Chem., Vol. 44, No. 12, pp. 2060–2066, October 1972

Products from the thermal decompositions of a selected group of aliphatic monoamino-monocarboxylic acids have been analyzed by combined gas chromatography–mass spectrometry. Careful identification of both major and minor fragments suggests that, with the possible exception of glycine, amino acids of the aliphatic series decompose by a common reaction pathway. The primary decomposition is one of decarboxylation to yield an amine as the major product. Subsequent decomposition or reaction of the amine leads to the formation of nitriles and *N*-aklylaldimines as significant secondary products.

S11 A Portable Self-Contained Gas Chromatograph

M. R. Stevens, C. E. Giffin, G. R. Shoemake, and P. G. Simmonds

Rev. Sci. Instr., Vol. 43, No. 10, pp. 1530–1534, October 1972

For abstract, see Stevens, M. R.

SIMON, M. K.

S12 L-Orthogonal Signal Transmission and Detection

W. C. Lindsey (University of Southern California) and M. K. Simon

IEEE Trans. Commun., Vol. COM-20, No. 5, pp. 953–960, October 1972

For abstract, see Lindsey, W. C.

S13 On the Detection of Differentially Encoded Polyphase Signals

W. C. Lindsey (University of Southern California) and M. K. Simon

IEEE Trans. Commun., Vol. COM-20, No. 6, pp. 1121–1128, December 1972

For abstract, see Lindsey, W. C.

S14 **The Performance of a Noncoherent FSK Receiver Preceded by a Bandpass Limiter**

M. K. Simon and J. C. Springett

IEEE Trans. Commun., Vol. COM-20, No. 6, pp. 1128–1136, December 1972

Many applications of the bandpass limiter involve either coherent or noncoherent demodulation following the limiter. This article discusses the performance of a noncoherent frequency-shift keying receiver when it is preceded by a bandpass limiter. In particular, expressions for signal suppression factor, output signal-to-noise ratio, and error probability are obtained, from which one can assess the degradation in performance of the receiver due to the presence of the limiter. Both narrow-band and wide-band cases are treated, thus covering situations where no frequency uncertainty exists (i.e., known carrier frequency) as well as large-frequency uncertainties. Also discussed is the first-order signal plus noise probability density function following noncoherent demodulation.

SJOGREN, W. L.

S15 **Moon Model—An Offset Core**

G. A. Ransford and W. L. Sjogren

Nature, Vol. 238, No. 5362, pp. 260–262, August 4, 1972

For abstract, see Ransford, G. A.

SLEKYS, A.

S16 **DSN Progress Report for November–December 1972: A New Pulsar Timer**

A. Slekys

Technical Report 32-1526, Vol. XIII, pp. 133–138, February 15, 1973

The times-of-arrival of pulses of radiation from pulsating radio sources (pulsars) have been measured at the Venus Deep Space Station (DSS 13). This article describes a programmable high-speed timing source, designed to control the data sampling. A possible use of the timer, as part of a DSN navigation system, is to determine a spacecraft's position in inertial space. It is easily controllable by computer and is intended to be part of a demonstration of remote experiment operation in which the Sigma 5 computer at JPL will configure pulsar experiments at the Venus Deep Space Station.

SMITH, D. B.

S17 Low-Thrust Mission Risk Analysis, With Application to a 1980 Rendezvous With the Comet Encke

C. L. Yen and D. B. Smith

Technical Memorandum 33-593, March 15, 1973

For abstract, see Yen, C. L.

SMITH, J. G.

S18 On the Feasibility of Efficient Multiamplitude Communication

J. G. Smith

JPL Quarterly Technical Review, Vol. 2, No. 4, pp. 62–71, January 1973

Bandwidth constraints in Earth-satellite communication systems force consideration of uncoded M-ary modulation to obtain increased data rates. M-ary phase shift keying (MPSK) at first glance seems most promising because of the high transmitter efficiency achieved through Class C operation. Multiple phase-and-amplitude modulation candidates such as quadrature amplitude shift keying (QASK) appear less promising because the transmitter must operate at lower efficiency (in linear or multimode operation). However, initial studies indicate that QASK offers significant raw dc-power savings over MPSK, despite the reduced transmitter efficiency. For example, at S-band both solid-state and traveling-wave tube QASK transmitters can provide a 3-dB average dc-power savings over comparable 16-ary phase shift keying (PSK) for the same bit rate and error probability. The reason for this savings is that QASK requires a much smaller average signal-to-noise ratio than 16-ary PSK for the same error rate.

SNYDER, C. W.

S19 Solar Wind Observations on the Lunar Surface With the Apollo-12 ALSEP

M. Neugebauer, C. W. Snyder, D. R. Clay, and B. E. Goldstein

Planet. Space Sci., Vol. 20, No. 20, pp. 1577–1591, October 1972

For abstract, see Neugebauer, M.

SPRINGETT, J. C.

S20 The Performance of a Noncoherent FSK Receiver Preceded by a Bandpass Limiter

M. K. Simon and J. C. Springett

IEEE Trans. Commun., Vol. COM-20, No. 6, pp. 1128–1136, December 1972

For abstract, see Simon, M. K.

STAELIN, D. H.

S21 Microwave Emissivity of Ocean Foam and Its Effect on Nadiral Radiometric Measurements

P. W. Rosenkranz and D. H. Staelin (Massachusetts Institute of Technology)

J. Geophys. Res., Vol. 77, No. 33, pp. 6528–6538, November 20, 1972

For abstract, see Rosenkranz, P. W.

STELZRIED, C. T.

S22 Net-Field Polarization in a Magnetically Biased Plasma

W. V. T. Rusch (University of Southern California) and C. T. Stelzried

Radio Sci., Vol. 7, No. 12, pp. 1131–1141, December 1972

For abstract, see Rusch, W. V. T.

STEVENS, M. R.

S23 A Portable Self-Contained Gas Chromatograph

M. R. Stevens, C. E. Giffin, G. R. Shoemake, and P. G. Simmonds

Rev. Sci. Instr., Vol. 43, No. 10, pp. 1530–1534, October 1972

This article describes the design and fabrication of a completely portable, self-contained gas chromatograph. This instrument utilizes a closed-loop hydrogen carrier gas flow as maintained by a hydrogen generator–separator. It employs an auxiliary hydrogen generator to keep a positive flow of hydrogen through the detector. The detector is an ionization cross section detector. The only maintenance required is the addition of water (5–15 cc/day) to

the auxiliary hydrogen generator. Lower limit of detection for the present system is of the order of 1–10 ppm ethane.

STICKFORD, G. H., JR.

S24 Measurements of the Hβ Line Shape Using a Fiber Optics Slit System

G. H. Stickford, Jr.

AIAA J., Vol. 10, No. 10, pp. 1269–1270, October 1972

The presence of electrons and ions in a plasma has a large effect on the discrete or line emission from bound–bound atomic transitions. Stark broadening of the lines, due to electron and ion collisions, is the dominant broadening mechanism in singly ionized plasmas (10,000–20,000 K). Such broadening is strongly dependent on the electron density and nearly independent of the temperature. Thus it is an excellent monitor of the electron density. This article describes a procedure whereby the electron density of a transient plasma is measured by monitoring the emission of the hydrogen Hβ line. A fiber optics slit system, coupled with electronic phototubes, is used to measure the spectral shape and absolute magnitude of the Hβ emission with a time resolution of 0.1 μs.

TAUSWORTHE, R. C.

T01 DSN Progress Report for November–December 1972: Block IV Subcarrier Demodulator Assembly Acquisition Problem

R. B. Crow, J. K. Holmes, and R. C. Tausworthe

Technical Report 32-1526, Vol. XIII, pp. 42–47, February 15, 1973

For abstract, see Crow, R. B.

T02 Improvements in Deep-Space Tracking by Use of Third-Order Loops

R. C. Tausworthe and R. B. Crow

Proceedings of the 1972 International Telemetering Conference, Los Angeles, California, October 10–12, 1972, pp. 577–583

Third-order phase-locked receivers have not yet found wide application in deep-space communications systems because the second-order systems now used have performed adequately on past spacecraft missions. However, a survey of the doppler profiles for

future missions shows that an unaided second-order loop may be unable to perform within reasonable error bounds. This article discusses the characteristics of a simple third-order extension to present second-order systems that not only extends doppler-tracking capability, but widens the pull-in range and decreases pull-in time as well.

TOPS PROJECT

T03 Thermoelectric Outer Planets Spacecraft (TOPS) Advanced Systems Technology Project Final Report

TOPS Project

Technical Memorandum 33-589, April 1, 1973

A rare opportunity during the latter half of the 1970s to explore the planets beyond Mars prompted JPL in 1968 to initiate research and advanced development work on a ballistic-mode, outer-planet spacecraft using radioisotope-thermoelectric-generator (RTG) power. The resultant Thermoelectric Outer-Planet Spacecraft (TOPS) Project was established to provide the advanced systems technology that would allow the realistic estimates of performance, cost, reliability, and scheduling that are required for an actual flight mission. A system design of the complete RTG-powered outer-planet spacecraft was made; major technical innovations of certain hardware elements were designed, developed, and tested; and reliability and quality assurance concepts for long-life requirements were developed.

TRAJMAR, S.

T04 Electron Scattering by Molecules With and Without Vibrational Excitation—IV. Elastic Scattering and Excitation of the First Vibrational Level for N_2 and CO at 20 eV

D. G. Truhlar (University of Minnesota), S. Trajmar, and W. Williams

J. Chem. Phys., Vol. 57, No. 8, pp. 3250–3259, October 15, 1972

For abstract, see Truhlar, D. G.

T05 Electron Scattering by Molecules With and Without Vibrational Excitation—VI. Elastic Scattering by CO at 6–80 eV

D. G. Truhlar (University of Minnesota), W. Williams, and S. Trajmar

J. Chem. Phys., Vol. 57, No. 10, pp. 4307–4312, November 15, 1972

For abstract, see Truhlar, D. G.

TRUBERT, M. R.

T06 A Practical Approach to Spacecraft Structural Dynamics Problems

M. R. Trubert

J. Spacecraft Rockets, Vol. 9, No. 11, pp. 818–824, November 1972

This article discusses the system approach for structural dynamics. First, the concept of dynamic mass is presented. Second, the determination of a dynamic mass is given relative to the reaction forces and moments between two substructures in terms of the cantilever normal modes of one substructure. Third, it is shown how one can simply couple and uncouple substructures for dynamics problems. Fourth, an example is given for the digital simulation of a sine wave test for the purpose of calculating rotational response of the shaker. Fifth, forcing functions are mathematically determined from the measured responses of the space vehicle in flight. Finally, it is shown how one can perform a hybrid test simulation by combining a real-time analog computer with digitally determined structural characteristics, shaker properties, and actual control equipment in order to investigate the stability of the control loop.

TRUHLAR, D. G.

T07 Electron Scattering by Molecules With and Without Vibrational Excitation—IV. Elastic Scattering and Excitation of the First Vibrational Level for N_2 and CO at 20 eV

D. G. Truhlar (University of Minnesota), S. Trajmar, and W. Williams

J. Chem. Phys., Vol. 57, No. 8, pp. 3250–3259, October 15, 1972

Normalized experimental differential cross sections for scattering angles in the range 20–85 deg are presented for elastic scattering and excitation of the fundamental vibration of N_2 and CO by electrons with impact energy 20 eV. From three or four differential cross sections the integral cross sections are estimated. The elastic scattering cross sections are compared to the predictions of the polarized Born approximation, using five model potentials

(including polarization) which have been previously proposed for N_2 or CO, and other models. The vibrational excitation of both N_2 and CO appears to be dominated by resonance scattering.

T08 Electron Scattering by Molecules With and Without Vibrational Excitation—VI. Elastic Scattering by CO at 6–80 eV

D. G. Truhlar (University of Minnesota), W. Williams, and S. Trajmar

J. Chem. Phys., Vol. 57, No. 10, pp. 4307–4312, November 15, 1972

Elastic scattering differential cross sections in relative units for electron scattering from CO have been measured in the scattering angle range 15–85 deg and the impact energy range 10–80 eV. The experimental results are compared to the predictions of model polarized Born approximations, using five different model interaction potentials, and other models. Such a treatment is able to account for some of the features of the angle dependence of the differential cross sections. The largest discrepancies between theory and experiment are at 10 eV and at large scattering angles, and there are also smaller discrepancies at small scattering angles. Comparisons are also made to previous experimental studies.

UDLOCK, D. E.

U01 Formulating Propellants for Fully Case-Bonded End-Burning Motors

H. E. Marsh, Jr., and D. E. Udlock

J. Spacecraft Rockets, Vol. 9, No. 9, pp. 625–626, September 1972

For abstract, see Marsh, H. E., Jr.

VAN DILLEN, S. L.

V01 Mariner Jupiter/Saturn 1977—The Mission Frame

R. D. Bourke, R. F. Miles, Jr., P. A. Penzo, S. L. Van Dillen, and R. A. Wallace

Astronaut. Aeronaut., Vol. 10, No. 11, pp. 42–49, November 1972

For abstract, see Bourke, R. D.

VON ROOS, O. H.

V02 3-D Multilateration: A Precision Geodetic Measurement System

P. R. Escobal, K. M. Ong, O. H. von Roos, M. S. Shumate, R. M. Jaffe, H. F. Fliegel, and P. M. Muller

Technical Memorandum 33-605, March 15, 1973

For abstract, see Escobal, P. R.

WALLACE, C. J.

W01 Lipid-Absorbing Polymers

H. E. Marsh, Jr., and C. J. Wallace

JPL Quarterly Technical Review, Vol. 2, No. 4, pp. 1–6, January 1973

For abstract, see Marsh, H. E., Jr.

WALLACE, R. A.

W02 Mariner Jupiter/Saturn 1977—The Mission Frame

R. D. Bourke, R. F. Miles, Jr., P. A. Penzo, S. L. Van Dillen, and R. A. Wallace

Astronaut. Aeronaut., Vol. 10, No. 11, pp. 42–49, November 1972

For abstract, see Bourke, R. D.

WEBER, C. L.

W03 DSN Progress Report for November–December 1972: Convolutional Codes With a Frequency-Shift-Keying Modem

C. L. Weber

Technical Report 32-1526, Vol. XIII, pp. 114–126, February 15, 1973

This article presents an analytic approximation to the probability of error per bit for the Viterbi maximum-likelihood decoder of convolutional codes which employs an arbitrary modem. The effect of the decoder's limited path memory on performance is determined. The method is applied in particular to the quantized binary-frequency shift-keying modem. This may be useful for entry direct links.

WEBER, W. P.

W04 **Negative Ion Mass Spectrometry—A New Analytical Method for Detection of Trinitrotoluene**

J. Yinon, H. G. Boettger, and W. P. Weber (University of Southern California)

Anal. Chem., Vol. 44, No. 13, pp. 2235–2237, November 1972

For abstract, see Yinon, J.

WEETALL, H. H.

W05 **Behavior of Antidinitrophenyl Antigen–Antibody Complexes in Hydrochloric Acid and Guanidine**

N. Weliky and H. H. Weetall

Immunochemistry, Vol. 9, No. 11, pp. 1121–1127, November 1972

For abstract, see Weliky, N.

WELIKY, N.

W06 **Behavior of Antidinitrophenyl Antigen–Antibody Complexes in Hydrochloric Acid and Guanidine**

N. Weliky and H. H. Weetall

Immunochemistry, Vol. 9, No. 11, pp. 1121–1127, November 1972

Proteins, azophenylarsonate hapten and other ionizable antigens are completely dissociated from antibody at acidities below pH 3.0, or in 6*M* guanidine at pH 5.5. Complexes of antidinitrophenyl antibody and dinitrophenyl hapten coupled to bovine serum albumin, fibrinogen, or insoluble carboxymethylcellulose did not appreciably dissociate at these concentrations of acid or guanidine, indicating that the interaction of hydrocarbons in the specific interaction site was sufficient to prevent dissociation under conditions where antibody and hapten carrier protein ionic bonds are largely disrupted.

WIEBE, E.

W07 **DSN Progress Report for November–December 1972: Low-Noise Receivers: Microwave Maser Development**

E. Wiebe

Technical Report 32-1526, Vol. XIII, pp. 61–65, February 15, 1973

This article summarizes the operational status of the closed-cycle refrigerators (CCRs) used to cool traveling-wave masers in the DSN. The improved CCRs have now replaced virtually all the old Model 210s. The reliability of the new system has lived up to all expectations, but a continuing effort is being made to simplify the system in order to further improve its reliability. The second part of this article describes a simple way of eliminating the oil pump which is used to cool and lubricate the compressor.

WILCK, H. C.

W08 DSN Progress Report for November–December 1972: The LEAPSIG Sigma 5–Mac 16 Cross-Assembler

H. C. Wilck

Technical Report 32-1526, Vol. XIII, pp. 177–182, February 15, 1973

A cross-assembler, called LEAPSIG, has been developed to permit the Sigma 5 computer to assemble programs for the Mac 16 minicomputer. It was obtained by translating the Mac 16 assembler into a Sigma 5 program by means of Sigma 5 METASYMBOL "procedures." This article describes the LEAPSIG program, discusses the method by which it was generated, and presents information for using LEAPSIG on the Sigma 5.

WILLIAMS, H. E.

W09 Analysis of a Ring With a Hinged Cross Section

H. E. Williams (Harvey Mudd College)

J. Spacecraft Rockets, Vol. 9, No. 11, pp. 787–788, November 1972

In searching for a ring structure that could be folded and stored in minimum space, it has been proposed to construct a ring by lacing together three elements—the upper flange, lower flange, and a web—into a basic channel cross section. The resulting assembly constitutes a ring whose cross section may distort a limited amount. The ring assembly is analyzed in this article as an application of the principle of virtual work taken within the framework of small displacement theory.

WILLIAMS, W.

W10 **Electron Scattering by Molecules With and Without Vibrational Excitation—IV. Elastic Scattering and Excitation of the First Vibrational Level for N_2 and CO at 20 eV**

D. G. Truhlar (University of Minnesota), S. Trajmar, and W. Williams

J. Chem. Phys., Vol. 57, No. 8, pp. 3250–3259, October 15, 1972

For abstract, see Truhlar, D. G.

W11 **Electron Scattering by Molecules With and Without Vibrational Excitation—VI. Elastic Scattering by CO at 6–80 eV**

D. G. Truhlar (University of Minnesota), W. Williams, and S. Trajmar

J. Chem. Phys., Vol. 57, No. 10, pp. 4307–4312, November 15, 1972

For abstract, see Truhlar, D. G.

WOO, J.

W12 **DSN Progress Report for November–December 1972: DSS Command System Redesign**

J. Woo

Technical Report 32-1526, Vol. XIII, pp. 203–208, February 15, 1973

The existing DSN Command System cannot meet project requirements through the Viking era (1975). This article describes the DSN Command System redesign that will be used to support mission command requirements through 1975. Major areas of redesign include command-stack capacity and allocation of command-stack manipulating functions from the DSN computer to the Mission Control and Computing Center. This article describes the system configuration and the functional operation of the redesign.

WRIGHT, D. L.

W13 **The Mesa Arizona Pupil Tracking System**

D. L. Wright

JPL Quarterly Technical Review, Vol. 2, No. 4, pp. 87–92, January 1973

A computer-based pupil-tracking/teacher-monitoring system was designed for Mesa Public Schools, Mesa, Arizona. The established objectives of the system were to: (1) facilitate the economical collection and storage of student performance data necessary to objectively evaluate the relative effectiveness of teachers, instructional methods, materials, and applied concepts; and (2) identify, on a daily basis, those students requiring special attention in specific subject areas.

The system encompasses computer hardware/software and integrated curricula progression/administration devices. It provides daily evaluation and monitoring of performance as students progress at class or individualized rates. In the process, it notifies the student and collects information necessary to validate or invalidate subject presentation devices, methods, materials, and measurement devices in terms of direct benefit to the students. The system utilizes a small-scale computer (e.g., IBM 1130) to assure low-cost replicability, and may be used for many subjects of instruction.

WU, F. T.

W14 Ionization Processes in Mercury Discharges

F. T. Wu

Technical Memorandum 33-596, March 1, 1973

This report presents a summary of theoretical calculations of the ionization processes in mercury plasma. Various possible ionization processes are analyzed and discussed. It is found that the ionization due to excited-state interactions is dominant when the degree of ionization is small and that the ionization due to multistep electron impact is significant when the degree of ionization is high.

W15 Measurement of Electron Distribution Function in a Cesium Plasma

C. J. Chen, J. Wu (State University of New York), and F. T. Wu (State University of New York)

J. Appl. Phys., Vol. 43, No. 11, pp. 4570–4573, November 1972

For abstract, see Chen, C. J.

WU, J.

W16 Measurement of Electron Distribution Function in a Cesium Plasma

C. J. Chen, J. Wu (State University of New York), and F. T. Wu (State University of New York)

J. Appl. Phys., Vol. 43, No. 11, pp. 4570–4573, November 1972

For abstract, see Chen, C. J.

YANG, J.-N.

Y01 Probability of Stress-Corrosion Fracture Under Random Loading

J.-N. Yang

Eng. Fracture Mech., Vol. 4, No. 4, pp. 737–748, December 1972

A method is developed for predicting the probability of stress-corrosion fracture of structures under random loadings. The formulation is based on the cumulative damage hypothesis and the experimentally determined stress-corrosion characteristics. Under both stationary and nonstationary random loadings, the mean value and the variance of the cumulative damage are obtained. The probability of stress-corrosion fracture is then evaluated using the principle of maximum entropy. It is shown that, under stationary random loadings, the standard deviation of the cumulative damage increases in proportion to the square root of time, while the coefficient of variation (dispersion) decreases in inverse proportion to the square root of time. Numerical examples are worked out to illustrate the general results.

Y02 Nonstationary Envelope Process and First Excursion Probability

J.-N. Yang

Struct. Mech., Vol. 1, No. 2, pp. 231–248, 1972

An earlier definition of stationary random envelope is extended in this article to the envelope of nonstationary random processes possessing evolutionary power spectral densities. The density function, the joint density function, the moment function, and the crossing rate of a level of the nonstationary envelope process are derived. Based on the envelope statistics, approximate solutions to the first excursion probability of nonstationary random processes are obtained. In particular, applications of the first excursion

probability to the earthquake engineering problems are demonstrated in detail.

Y03 **On the First-Excursion Probability in Stationary Narrow-Band Random Vibration, II**

J.-N. Yang and M. Shinozuka (Columbia University)

Trans. ASME, Ser. E: J. Appl. Mech., Vol. 39, No. 3, pp. 733–738, September 1972

The first-excursion probability of a stationary narrow-band gaussian process with mean zero has been studied. Within the framework of point process approach, series approximations derived from the theory of random points and approximations based on the maximum entropy principle have been developed. With the aid of numerical examples, merits of the approximations proposed previously as well as of those developed in this article have been compared. The results indicate that the maximum entropy principle has not produced satisfactory approximations but the approximation based on nonapproaching random points is found to be the best among all the approximations proposed herein. A conclusion drawn from the present and the previous studies is that the point process approach produces a number of useful approximations for the first-excursion probability, particularly those based on the concepts of the Markov process, the clump-size, and the nonapproaching random points.

YANG, L. C.

Y04 **A High-Efficiency, Small, Solid-State Laser for Pyrotechnic Ignition**

L. C. Yang and V. J. Menichelli

JPL Quarterly Technical Review, Vol. 2, No. 4, pp. 29–37, January 1973

A completely self-contained, small, neodymium laser has been designed and demonstrated for use in a pyrotechnic ignition system. A nominal 16 J of laser energy (1.06-μm wavelength, 1-ms duration) was achieved in a rectangular 10.5- × 15.1- × 25.4-cm package weighing 5.14 kg. This high energy-to-weight ratio is encouraging for laser applications in which specific energy efficiency (energy per unit weight or volume) is important. This article describes the laser design concepts and presents some results on pyrotechnic ignition. Some details on a laser currently under construction, which will be 1/8 the size of the above laser, are included.

YEN, C. L.

Y05 Low-Thrust Mission Risk Analysis, With Application to a 1980 Rendezvous With the Comet Encke

C. L. Yen and D. B. Smith

Technical Memorandum 33-593, March 15, 1973

This memorandum presents a computerized, multistage failure-process simulation procedure used to evaluate the risk in a solar-electric space mission. The procedure uses currently available thrust-subsystem reliability data and performs approximate simulations of the thrust-subsystem burn operation, the system failure processes, and the retargeting operations. The method is applied to assess the risks in carrying out a 1980 rendezvous mission to the comet Encke. Analysis of the results and evaluation of the effects of various risk factors on the mission show that system component-failure rates are the limiting factors in attaining a high mission reliability. It is also shown that a well-designed trajectory and system-operation mode can be used effectively to compensate partially for unreliable thruster performance.

YINON, J.

Y06 Negative Ion Mass Spectrometry—A New Analytical Method for Detection of Trinitrotoluene

J. Yinon, H. G. Boettger, and W. P. Weber (University of Southern California)

Anal. Chem., Vol. 44, No. 13, pp. 2235–2237, November 1972

The detection of poly-nitro aromatic compounds concealed in airline baggage, such as trinitrotoluene (TNT), is an extremely relevant analytical problem which requires a highly sensitive as well as specific method for its solution. One of the most sensitive analytical devices available for the detection of trace quantities of material is the mass spectrometer. The use of positive ion mass spectrometry is difficult because it is approximately equally sensitive to all types of volatile organic compounds.

Negative ion mass spectrometry, on the other hand, is extremely selective in its sensitivity. With this thought in mind, the negative ion mass spectrum of TNT has been examined. This article presents some of the findings and proposals resulting from the examination.

Y07 **Modification of an AEI/GEC MS9 High-Resolution Mass Spectrometer for Electron Impact/Chemical Ionization Studies**

J. Yinon and H. G. Boettger

Chem. Instr., Vol. 4, No. 2, pp. 103–113, 1972

A double-focusing MS9 mass spectrometer has been modified to permit operation in both chemical ionization (CI) and electron impact (EI) modes. The modifications consist mainly of a closed ion chamber, a high capacity pumping system, a reactant gas inlet system, a new solid sample probe, and a source pressure measuring device. Changes have also been made in the electronic system and a new ion source power supply has been incorporated.

The new ion source can be operated in the CI mode at pressures up to 1 torr while the pressure in the analyzer is better then 10^{-7} torr. The new set-up has the ability to analyze solid, liquid, and gas samples in both CI and EI.

YOUNG, A. T.

Y08 **On the Temperature Distribution in a Planetary Atmosphere**

L. D. G. Young and A. T. Young

Astrophys. J., Vol. 176, No. 2, Pt. 1, pp. 533–554, September 1, 1972

For abstract, see Young, L. D. G.

YOUNG, L. D. G.

Y09 **On the Temperature Distribution in a Planetary Atmosphere**

L. D. G. Young and A. T. Young

Astrophys. J., Vol. 176, No. 2, Pt. 1, pp. 533–554, September 1, 1972

It has been suggested that a double maximum in one branch of a vibration-rotation band can yield information about the temperature distribution in a planetary atmosphere. Theoretical calculations indicate that a double maximum cannot occur in the intensity distribution of lines in either the *P*-branch or the *R*-branch of any diatomic or linear polyatomic molecule, unless the temperature ratio for two isothermal layers of gas exceeds ~9. A similar calculation predicts where double maxima can occur due to quantum-mechanical interactions.

This article presents a more sensitive method of estimating the range of temperature in the part of the atmosphere where spec-

tral lines are formed, from observations made in reflected sunlight. This method is applied to the best available spectroscopic observations of Venus made in the 7820 Å CO_2 band. Statistical tests suggest that we are not seeing an isothermal layer, based on these data. However, a 100°K temperature spread is near the limit of detection with present observational techniques.

YUEN, J. H.

Y10 A Double-Loop Tracking System

J. H. Yuen

IEEE Trans. Commun., Vol. COM-20, No. 6, pp. 1142–1150, December 1972

This article presents a nonlinear analysis which can be used to assess certain statistical characteristics of double-loop tracking systems. The analysis takes into account the mutual coupling effects of the loops in the system. Two approaches are taken to obtain steady-state probability density functions of the system phase errors, ϕ_1 and ϕ_2. From these probability density functions, important system performance statistics, e.g., the phase-error variances, can be calculated, thus illustrating the application and usefulness of the analysis. The analysis is applied to a satellite transponder as an example.

ZYGIELBAUM, A. I.

Z01 Near Sun Observations of the Solar Wind

P. S. Callahan, P. F. MacDoran, and A. I. Zygielbaum

Space Research XII, pp. 1529–1533, Akademie-Verlag, Berlin, 1972

For abstract, see Callahan, P. S.

Subject Index

Subject Categories

Subjects

Publication Index

Technical Reports

DSN Progress Reports for November–December 1972 (Technical Report 32-1526, Vol. XIII)

Technical Memorandums

JPL Quarterly Technical Review, Vol. 2, No. 4

Open Literature Reporting

NASA — JPL — Coml., L.A., Calif.